Technische Universität München
TUM School of Natural Sciences

Methods for Thermalization and Equilibration Dynamics in Quantum Many-Body Systems

Aslı Cebe

Vollständiger Abdruck der von der TUM School of Natural Sciences
der Technischen Universität München
zur Erlangung des akademischen Grades einer
Doktorin der Naturwissenschaften (Dr. rer. nat.)
genehmigten Dissertation.

Vorsitz: Prof. Dr. Stefan Filipp

Prüfer der Dissertation: 1. Hon.-Prof. Ignacio Cirac, Ph.D.
2. Prof. Dr. Michael Knap

Die Dissertation wurde am 09.01.2023 bei der Technischen Universität München eingereicht und durch die TUM School of Natural Sciences am 20.01.2023 angenommen.

Abstract

The focus of this thesis is on thermalization and equilibrium dynamics of one-dimensional quantum many-body systems. In particular, we develop effective numerical methods using the tensor network framework to explore their long time dynamics in novel ways. We investigate to which extent this allows us to numerically study fundamental problems in quantum statistical physics. Our methods are based on a Gaussian filter with a superoperator, which we dub *filtering technique*. The central topic of this thesis is the application of this filtering technique to different dynamical systems, particularly isolated time-independent and periodically driven systems. All in all this thesis aims to contribute to the understanding of the long time dynamics of many-body systems, as well as the study of thermal states beyond the conventional Gibbs ensemble.

First, we consider a generic time-independent Hamiltonian with non-degenerate spectrum, in which the long time averaged state is the diagonal ensemble. We approximate it by adapting a filtering technique with tensor networks. The filtering idea is based on the application of a Gaussian filter with Hamiltonian commutator to the initial density matrix. The result of this application converges to the diagonal ensemble in the limit of vanishing width. Numerically, we simulate the effect of this filter using Chebyshev expansions and provide numerical evidence that local observables in the filtered state indeed converge to the values that represent the long time average. Following the same idea of Gaussian filter, we construct an alternative procedure for our numerics, in which the Gaussian filter is approximated by a Cosine function. We demonstrate that the results are quantitatively in agreement with the former approach, moreover it leads us to further inquiries: we show that our filtering procedure can also be useful for the characterization of diagonal ensembles independent of models and the investigation of interesting intermediate-time dynamics beside long-time dynamics.

Second, we address many-body quantum systems described by time-periodic Hamiltonians, namely Floquet systems. We make use of the filtering technique to approximate the long stroboscopic-time average of local observables for isolated periodically driven quantum many-body systems, which gives the expectation value in the Floquet diagonal ensemble. Our numerical simulations detect that before converging to the infinite temperature state, the system relaxes to a quasi-stationary state, which can be interpreted as a prethermal regime. Our filtering procedure shows its sensitivity to the intermediate-time effects by capturing a clear signature of prethermalization in time-periodic systems as well.

Finally, we study the properties of an alternative thermodynamic ensemble to the Gibbs ensemble, which easily allows the computation of thermal expectation values with the use of tensor networks. We define the ensemble which maximizes Rényi entropic quantities and show that this idea provides a practical, numerical alternative to the Gibbs ensemble. We focus on a particular case which maximizes the 2-Rényi entropy for the same mean energy and reproduces the local observables of the corresponding Gibbs ensemble. We observe that this ensemble can be

efficiently represented by matrix product states and further employ variational algorithms to obtain efficient approximations to it, based on gradient descent optimization and non-linear evolution of the density operator.

Zusammenfassung

Der Schwerpunkt dieser Arbeit liegt auf der Thermalisierung und der Gleichgewichtsdynamik von eindimensionalen Quanten-Vielteilchensystemen. Insbesondere entwickeln wir mithilfe von Tensornetzwerken effektive numerische Methoden, um deren Langzeitdynamik auf neuartige Weise zu untersuchen. Wir untersuchen, inwieweit dies uns erlaubt, fundamentale Probleme der statistischen Quantenphysik numerisch zu erforschen. Unsere Methoden basieren auf einem Gauß-Filter mit einem Superoperator, welche wir als *Filtertechnik* bezeichnen. Das zentrale Thema dieser Arbeit ist die Anwendung dieser Filtertechnik auf verschiedene dynamische Systeme, insbesondere isolierte zeitunabhängige und periodisch getriebene Systeme. Insgesamt zielt diese Arbeit darauf ab, einen Beitrag zum Verständnis der Langzeitdynamik von Vielteilchensystemen sowie zur Untersuchung von thermischen Zuständen jenseits des herkömmlichen Gibbs-Ensembles zu leisten.

Zunächst betrachten wir einen generischen zeitunabhängigen Hamiltonoperator mit nicht entartetem Spektrum, bei dem der langzeitgemittelte Zustand das diagonale Ensemble ist. Wir approximieren ihn durch Anpassung einer Filtertechnik mit Tensornetzen. Die Idee der Filterung basiert auf der Anwendung eines Gauß-Filters mit einem Hamiltonschen Kommutator auf die anfängliche Dichtematrix. Das Ergebnis dieser Anwendung konvergiert im Grenzwert verschwindender Breite gegen das diagonale Ensemble. Numerisch simulieren wir die Wirkung dieses Filters mit Hilfe von Tschebyscheff-Entwicklungen und liefern numerische Beweise dafür, dass die lokalen Observablen im gefilterten Zustand tatsächlich gegen die Werte konvergieren, die den langfristigen Durchschnitt darstellen. In Anlehnung an die Idee des Gauß-Filters konstruieren wir ein alternatives Verfahren für unsere Numerik, bei dem der Gauß-Filter durch eine Cosinus-Funktion approximiert wird. Wir zeigen, dass die Ergebnisse quantitativ mit dem erstgenannten Ansatz übereinstimmen, darüber hinaus führt uns dies zu weiteren Forchungen: Wir zeigen, dass unser Filterverfahren auch für die Charakterisierung von modellunabhängigen diagonalen Ensembles und die Untersuchung interessanter Zwischenzeitdynamiken neben der Langzeitdynamik nützlich sein kann.

Zweitens befassen wir uns mit Vielteilchen-Quantensystemen, die durch zeitperiodische Hamiltonoperatoren beschrieben werden, nämlich Floquet-Systeme. Wir nutzen die Filtertechnik, um das lang-stroboskopische Zeitmittel lokaler Observablen für isolierte periodisch getriebene Quanten-Vielteilchensysteme zu approximieren, was den Erwartungswert im Floquet-Diagonalensemble ergibt. Unsere numerischen Simulationen zeigen, dass das System vor Erreichen des Zustands unendlicher Temperatur in einen quasistationären Zustand relaxiert, der als präthermischer Zustand interpretiert werden kann. Unser Filterverfahren zeigt seine Empfindlichkeit gegenüber den Zwischenzeiteffekten, indem es auch in zeitperiodischen Systemen eine klare Signatur der Präthermalisierung erfasst.

Schließlich untersuchen wir die Eigenschaften eines alternativen thermodynamischen Ensembles zum Gibbs-Ensemble, das auf einfache Weise die Berechnung thermischer Erwartungswerte mit Hilfe von Tensornetzen ermöglicht. Wir

definieren das Ensemble, das die Rényi-Entropien maximiert und zeigen, dass diese Idee eine praktische, numerische Alternative zum Gibbs-Ensemble darstellt. Wir konzentrieren uns auf einen speziellen Fall, der die 2-Rényi-Entropie für dieselbe mittlere Energie maximiert und die lokalen Observablen des entsprechenden Gibbs-Ensembles reproduziert. Wir stellen fest, dass dieses Ensemble effizient durch Matrixprodukt-Zustände dargestellt werden kann, und setzen Variationsalgorithmen ein, um effiziente Annäherungen an dieses Ensemble zu erhalten, die auf einem Gradientenverfahren und nichtlinearer Entwicklung des Dichteoperators basieren.

List of publications

This thesis is based on the following publications:

- *Approximating the long time average of the density operator: Diagonal ensemble*
  Aslı Çakan, J. lgnacio Cirac and Mari Carmen Bañuls.
  Phys. Rev. B 103, 115113 (2021).

- *Filtering for the Floquet diagonal ensemble*
  Sattwik Deb Mishra, Aslı Çakan, J. lgnacio Cirac and Mari Carmen Bañuls.
  Manuscript in preparation.

- *Variational Approximations of Thermal States for Tensor Networks*
  Giacomo Giudice, Aslı Çakan, J. lgnacio Cirac and Mari Carmen Bañuls.
  Phys. Rev. B 103, 205128 (2021).

Acknowledgements

First and foremost, I am deeply indebted to my co-supervisor and mentor Mari Carmen Bañuls whom I learned numerous invaluable things. I am grateful for kindly sparing her valuable times to introduce me MPS and numerical methods used in MPS simulations as well as for countless constructive suggestions concerning practical coding in my computations during my entire PhD. This thesis has greatly benefited from her attentive guidance, insights and extraordinary scientific knowledge. Without her understanding, encouragement and support, this thesis would not materialize.

I would like to express my deepest gratitude to my supervisor Ignacio Cirac, for his generous support, kindness and understanding throughout my graduate study. I cannot find any possible way to truly express my thanks to him for giving me a chance to work in his great group and interact with many unique scientists around the world.

I would like to thank my collaborators that I had the opportunity to work with during my PhD, Giacomo Giudice and Sattwik Deb Mishra for their productive collaboration, many inspiring discussions, and the opportunity to learn from them.

I am very thankful to all former and present members of the theory division for creating a unique and inspiring atmosphere in which I have always felt very fortunate in being able to discuss and learn from the others. I am grateful to all the things they have taught me and for the time we spent together. In particular, I would like to acknowledge with much appreciation Stefan Kühn for discussing many theoretical questions about MPS as well as in helping considerably with the technical issues.

I also would like to thank my former and present officemates Andras Molnar and Vanessa Paulisch for the numerous coffee breaks and some of the most memorable moments during my time at MPQ, Irene Papaefstathiou, David Castells and Sirui Lu for many valuable conversations not only about physics, and Caroline de Groot for her friendship and invaluable support. I also would like to thank Andrea Kluth for her great help in all administrative matters throughout my PhD. My special thanks to Anna Hackenbroich for her support and contributions to the various domains, I greatly value her unique friendship. My sincere thanks to my friends back home, Pınar Telli, Elif Cakan, Ozlem Yegrek and Olcay Turan for supporting me even in that distance.

Most importantly, I am indebted to my parents, Hatice and Kemal, my brother, Serhad, for their great help and support during my studies. This thesis would not have been possible without their support. I deeply appreciate them for encouraging me to follow my dreams and their belief in me.

Finally, I am very thankful to my son, Rodin, for his existence and love. I am grateful for his support by sleeping very well most of the time, and of course giving me his wonderful smile.

Contents

Part I

Introduction

Chapter 1

Motivation

Quantum statistical mechanics is one of the cornerstones of modern theoretical physics [1], and even today remains a field of active research. This field was born at the start of the 20$^{\text{th}}$ century, with a fundamental step taken by Gibbs [2] in his book *"Elementary principles in statistical mechanics"* published in 1902, where he introduced the concept of a *statistical ensemble* as:

> *"[...] imagine a great number of systems of the same nature, but differing in the configurations and velocities which they have at a given instant [...] we may set the problem, not to follow a particular system through its succession of configurations, but to determine how the whole number of systems will be distributed among the various conceivable configurations and velocities at any required time [...]"*

The realisation that collective dynamics, rather than individual trajectories of particles, may govern the behaviour of complex phenomena in physics, led Gibbs to define and calculate averages in statistical equilibrium. However, an outstanding question that to this day remains open is why the ensembles proposed capture the physics of thermodynamic equilibrium and why systems equilibrate.

Another fundamental realisation came from Jaynes [3, 4] in 1957, with the *maximum entropy principle*, taking a conceptually different path compared to Gibbs' approach. He introduced a postulate motivated by a subjective interpretation of probability. According to it, when sufficient information is lacking to make a definite prediction, then the best possible prediction is achieved by the distribution of a state which maximizes the entropy. Furthermore, Jaynes demonstrates in Ref. [3] that the *usual computational rules* as presented by Gibbs [2] are a consequence of the maximum entropy principle, providing the union of these two perspectives, as well as later the extension to particularly considering quantum systems [4].

Following this, significant efforts have been made to fundamentally understand how statistical mechanics can emerge in a quantum system, in particular, how the concepts of equilibration and thermalization appear at this fundamental level [5–11]. The study of the equilibration necessarily involves a system's non-equilibrium dynamics, which is called *thermalization*, and will be the main motivating topic behind this thesis.

One proposed framework of thermalization for a generic quantum many-body system is the eigenstate thermalization hypothesis (ETH), independently introduced by Deutsch [5] and Srednicki [6] at the beginning of the nineties. The ETH postulates a concrete form for the matrix elements of physical observables in the energy eigenbasis. One of the consequences of ETH is that, for generic non-integrable Hamiltonians, the value of any local observable in the long-time limit becomes equivalent to the thermal (Gibbs) ensemble, with differences that decrease with increasing system size, which is considered to be a sensible requirement for quantum states in thermal equilibrium.

The question of which quantum systems thermalize and how has been addressed for many different kinds of systems. Theoretical studies have concluded that non-integrable systems generally thermalize to ETH [9–16]. On the other hand, integrable systems retain dependencies on their initial state even in the long time limit due to an extensive number of conserved quantities. Therefore, they are not expected to thermalize, but are argued to equilibrate to the so-called Generalized Gibbs Ensemble (GGE) [9, 17–19]. Experimental studies have also considered non-equilibrium dynamics of quantum many-body systems, e.g. by sudden changes of the depth of an optical lattice [20–23] or by engineering specific initial states [24–30], in which the particular interest is whether observables, under near-unitary dynamics, relax to time independent thermal values which can be defined using traditional statistical mechanics.

However, these theoretical studies experience a fundamental limitation: although classical computers could, in principle, handle such systems exactly, simulating a general system of N spin-1/2 particles on a classical computer requires storing 2^N coefficients. Then any calculation performed for such a system (e.g., the computation of an observable) requires the execution of a number of operations that depends exponentially on the system size. In practice, rendering simulation of more than a few dozens of spins is not possible even on the largest super computers, and as a consequence, exact calculations with classical resources are limited to relatively small system sizes or short times.

Most recently, the growing interest in simulating large systems has necessitated developing powerful numerical methods. While integrable models which are exactly solvable provide instances for which the properties can be computed exactly even for large sizes [31], many systems of interest are non-integrable models which are not exactly solvable, and require the use of numerical algorithms. The foremost algorithms of this kind are tensor network methods [32] and the density-matrix renormalization group method [33], which have made possible to simulate the dynamics of large quantum many-body systems for relatively long times while methods for exact diagonalization have been brought to new levels [9, 16, 34], complemented by quantum Monte Carlo techniques [35–37]. Since these methods are very well-developed, their strengths have been identified as well as their limitations. Quantum Monte Carlo methods have been very successful, but suffer from a fundamental limitation, known as the sign problem [36], which commonly appears in the simulation of fermions or frustrated spin systems. The density matrix renormalization group algorithm has also enjoyed high success, in particular in one-dimensional quantum systems [38]. Furthermore, the understanding of this

algorithm in terms of tensor networks has provided remarkable insights about the local structure of quantum states [39] as well as efficient algorithms to study them [33].

The concept of tensor networks is very general and has led to significant algorithmic progress in many different areas, ranging from simulations of one-dimensional ground states [40, 41], thermal states [42–47] and time-evolution [42, 48–59] to higher-dimensional quantum systems, their variational optimization and computation of observables [50, 51, 60–71]. The success of these investigations as well as deeper mathematical understanding of TN [72] demonstrate the potential advantages of TN approach and, of novel algorithms to solve interesting problems in quantum many-body systems.

The work presented in this thesis has been motivated by the long-standing questions of non-equilibrium dynamics, equilibration and thermalization in quantum many-body systems, as well as the growing interest in employing TN. Towards this, we have developed novel methods harnessing the power of TN to tackle one-dimensional many-body systems in and out of thermal equilibrium. In particular, we describe isolated time-independent systems as well as periodically driven systems, with a particular kind of one-dimensional TN, the matrix product states, which we make use of in our computations both numerically and analytically.

Chapter 2

Basic Concepts

2.1 Tensor network basics

In this thesis, we make use of *matrix product states* (MPS), a particular kind of *tensor network* (TN) in one dimension, in order to study dynamics in and out of equilibrium of certain one-dimensional systems numerically. In this section we summarize the basic concepts of MPS, and also introduce *matrix product operators* (MPO) as a representation for operators such as the Hamiltonian describing the system and local observables. Subsequently, we review numerical methods, that are in particular efficient for simulating evolution of quantum systems with MPS. Further discussions of TN can be found throughout this thesis: in Chapter 4 and 5 their application to time-independent systems, in Chapter 6 their application to periodically driven systems and in Chapter 7 their application to the study of ensembles beyond Gibbs ensemble.

2.1.1 Matrix product states

Consider a quantum lattice system composed of N d-dimensional quantum systems. Any pure state of the system can then be written as

$$|\Psi\rangle = \sum_{i_1 \cdots i_N = 1}^{d} c_{i_1, \cdots i_N} |i_1\rangle \otimes \cdots \otimes |i_N\rangle \,, \tag{2.1}$$

with a tensor $c_{i_1,\cdots i_N}$ including d^N complex entries. The state is fully characterized by d^N complex numbers and storing those would require an exponential amount of memory. Matrix product states [48, 73, 74] are quantum states based on the idea of decomposing this tensor, $c_{i_1,\cdots i_N}$, into a network of contracted local tensors which construct the wave function. This decomposition is introduced in a graphical notation in Fig. 2.1, representing each tensor as a box and each index as a leg sticking out of the box. Links between the tensors correspond to a sum over the corresponding indices of the tensors. The dimension of the tensor indices which are contracted is called the bond dimension D.

The resulting tensor network representation is known as a *matrix product*

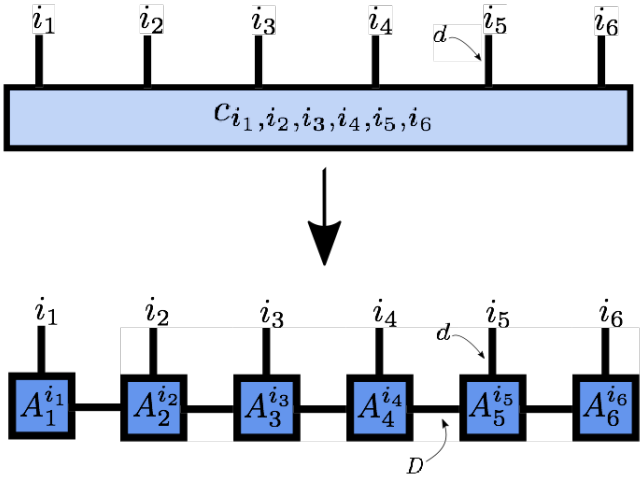

Figure 2.1: Illustration of the graphical notation described in the text, which demonstrates the decomposition of the general tensor $c_{i_1,\cdots i_N}$ representing the wavefunction (Eq. (2.1)) into a one-dimensional TN known as MPS (Eq. (2.2)) in open boundary conditions.

state [75] and this efficient ansatz for the many-body wave function $|\Psi\rangle$ is given by

$$|\Psi\rangle = \sum_{i_1 \cdots i_N = 1}^{d} A_1^{i_1} \cdots A_N^{i_N} \, |i_1\rangle \otimes \cdots \otimes |i_N\rangle \, . \tag{2.2}$$

In this expression, the $A_k^{i_k}$ are complex matrices $(D \times D)$ for $k = 2, \cdots, N-1$. $A_1^{i_1}$ and $A_N^{i_N}$ are D dimensional row and column vectors. Hence, the many-body coefficients of an MPS are obtained as a product of finite-dimensional matrices. Compared to the d^N complex numbers required to fully characterize a generic quantum state, this represents a huge simplification, as the number of parameters scales only polynomially with the system size [1] instead of exponentially.

An important property of MPS: They satisfy an area law [76]. A state is said to fulfill the area law if the entropy for a subsystem A, $S_A = \mathrm{Tr}\, \rho_A \log \rho_A$ – described by the reduced density matrix ρ_A – scales as the boundary, ∂A, of the subsystem $S_A = O(|\partial A|)$. Note that MPS fulfill the area law by construction since the entanglement entropy for a MPS with a fixed bond dimension D is upper bounded by $\log_2(D)$ [33]. This is constant, $S_A = O(1)$, i.e. independent of the subsystem size for one-dimensional case.

It has been proven in many cases the states of interest satisfy the area law, such as for models for which there is an energy gap between the ground state and the excited states in one dimension, i.e. for local, gapped Hamiltonians in 1D [77], and for such gapped models satisfying some spectral conditions in arbitrary dimension [78]. In particular, for the noted example in 1D above, one can show that the area law also implies that the Schmidt values decay fast, which shows that

[1] The number of parameters in the ansatz is given $O((N-2)\, dD^2 + 2Dd) = O\left(ND^2 d\right)$.

parametrization by MPS is a sensible and efficient way for one-dimensional ground states of local, gapped Hamiltonians. On the other side, it has been also shown that the thermal equilibrium states in any dimension can be efficiently approximated with MPS [45]. Additionally, it has been also proven for free bosonic and fermionic models [79, 80] as well as ground and thermal equilibrium states of frustration-free spin models [76].

In a more general setting, it has been also shown that *any quantum state* for which all Rényi entropies of order α for $0 < \alpha < 1$ fulfill the area law up to logarithmic corrections can be efficiently approximated by a MPS [56, 81]. In particular, these states also encompass ground states of critical systems [82, 83].

Matrix Product Operators

As any state can be cast into a MPS form in which the bond dimension necessary to do so scales in general exponentially in the system size [49], similar to a quantum state, it is also possible to represent any operator,

$$O = \sum_{i_1 \cdots i_N = 1}^{d} \sum_{j_1 \cdots j_N = 1}^{d} c_{i_1, \cdots i_N}^{j_1, \cdots j_N} \left| i_1 \right\rangle \left\langle j_1 \right| \otimes \cdots \otimes \left| i_N \right\rangle \left\langle j_N \right| \tag{2.3}$$

as a *matrix product operator* [42, 84], if one allows for matrices of exponential size in N,

$$O = \sum_{i_1 \cdots i_N = 1}^{d} \sum_{j_1 \cdots j_N = 1}^{d} M_1^{i_1, j_1} \cdots M_N^{i_N, j_N} \left| i_1 \right\rangle \left\langle j_1 \right| \otimes \cdots \otimes \left| i_N \right\rangle \left\langle j_N \right|, \tag{2.4}$$

where, $M_k^{i_k, j_k}$ are complex matrices and $M_1^{i_1, j_1}$ and $M_N^{i_N, j_N}$ are row and column vectors, respectively. In the graphical notation, a MPO is a MPS in a certain (operator) basis, hence, has an additional physical leg as shown in Fig. 2.2.(a).

One can always find a MPO representation for a Hamiltonian provided that is local [85, 86], as well as for certain types of long-range interactions [84]. In general, every operator of the form of Eq. (2.3) can be shown to correspond to a complex-weighted finite automaton which allows for finding the corresponding MPO representation with a bond dimension proportional to the number of internal states of the automaton [86] as it is valid for MPS and equivalent statement applies here for MPOs as well since MPOs are MPS in an operator basis.

In the MPS framework, one of the most important operations is the application of an MPO to an MPS. This application results in a MPS again, which is also shown in the graphical notation in Fig. 2.2.(b) by the direct application as regrouping the contractions such that the resulting MPS tensor can be obtained as a product of the individual site tensors. The bond dimension of the resulting MPS $\left| \phi \right\rangle = O \left| \Psi \right\rangle$ is given by the product of the bond dimension of the MPO and the initial MPS.

Alternatives to the direct application of an MPO to an MPS can be the variational optimization based on the same considerations, but variationally compressing a state towards a target state or the zip-up method [87], based on the truncation during the contraction process.

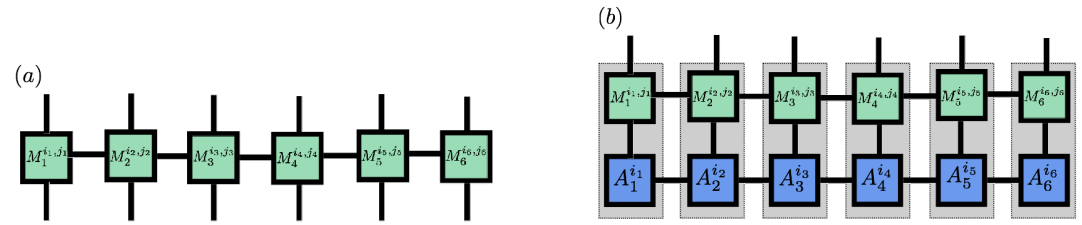

Figure 2.2: (a) Example of a MPO for a system with 6 sites. (b) Direct application of an MPO to an MPS yields a MPS again which is indicated with the tensors in grey dashed boxes.

2.2 Numerical Algorithms

The MPS family is a powerful theoretical tool, and additionally provides very efficient numerical approximations: to ground states [40, 41], thermal states [42–44, 46, 47] as well as time-evolution [42, 48–59], in which the computational cost of MPS algorithms for time-evolution scales as $O(ND^3)$ for N system sizes with open boundary conditions.

In particular, the Trotterized time-evolution of MPS combined powerful time-evolution schemes with the efficient truncation of the exponentially large Hilbert space, e.g. by the DMRG and the Time Evolved Block Decimation based methods [49–51, 54–57, 60, 88]. These numerical methods were started to be introduced around 2004, and since then, algorithms in particular for finite temperature [44, 51, 88] and real time-evolution [50, 60, 89] opened up the possibilities to improve the understanding of in and out of equilibrium dynamics of quantum many-body systems, which is the central interest of this thesis.

In this section, we briefly review these two aforementioned approaches for finite temperature and real time-evolution as well as one recent approach that we will make use of all throughout the rest of the thesis. First, we review two well-known methods, purification and trotterization that are based on an identical algorithm which we use for benchmarking while exploring systems in thermal equilibrium and far-from-equilibrium. Later, we review a different approach based on Chebyshev expansions, discuss how it is adapted into the quantum many-body context, hence make use of it to investigate dynamical behaviours of non-equilibrium systems in an alternative way to the conventional techniques. For details on other computational techniques and applications, we refer the interested reader to the review articles [32, 39, 48, 90–92].

2.2.1 Thermal states

From the point of view of thermodynamics, thermal states describe the equilibrium properties of a system. Given a Hamiltonian H, the Gibbs state

$$\rho_G = \frac{e^{-\beta H}}{\mathrm{tr} e^{-\beta H}}, \tag{2.5}$$

describes the state of the system at a given temperature $1/\beta$. On the other hand, thermal states arise from the principle of maximum entropy [3, 4]: for a given energy, the thermal ensemble is the one that maximizes the von Neumann entropy $S_G(\rho) = -\mathrm{tr}(\rho \log \rho)$.

In the quantum many-body context, numerical approaches to thermal equilibrium do resort to different methods to approximate Eq. (2.5). Monte Carlo methods use sampling to estimate very efficiently the physical properties from Eq.(2.5), but they face difficulties in scenarios where a sign problem appears, as discussed in Chapter 1.

In practice, TN are highly successful tools for studying thermal equilibrium [93–97] since thermal states for a local Hamiltonian obey an area law for the mutual information [45, 97] as discussed in the previous Section 2.1.1. In one spatial dimension, although MPS ansatz by default can only represent pure states, it can also be used to construct a representation of (mixed) Gibbs state with additional ingredients: one of the efficient approaches is given by purification, which is a purely mathematical procedure that allows to associate pure states with mixed states [98]. The procedure used to purify a mixed state ρ^a of a quantum system a is to define a pure state $|ap\rangle$, where another system p is introduced for the joint system ap such that $\rho^a = \mathrm{tr}_p(|ap\rangle \langle ap|)$. This pure state $|ap\rangle$ has the property that the reduced state on system a is equal to ρ^a.

Based on the procedure above, by doubling the Hilbert space, as physical and auxiliary degrees of freedom, $\mathcal{H} \to \mathcal{H}_p \otimes \mathcal{H}_a$, the density matrix is then represented by tracing over the auxiliary space of the purified quantum state $\Psi \in \mathcal{H}_p \otimes \mathcal{H}_a$:

$$\rho = \mathrm{tr}_a \, |\Psi\rangle \langle \Psi| \,, \tag{2.6}$$

only if $|\Psi\rangle$ is maximally entangled. To approximate the Gibbs state above in Eq. (2.5) at finite temperature β, the infinite temperature initial state is time evolved along the imaginary axis over $\beta/2$ as $|\Psi\rangle \propto e^{-\beta H/2} \sum_k |k\rangle |k\rangle$, where k label a basis of the system in the Hilbert space. Formally, this is an equivalent operation to a time-evolution, hence, thermal equilibrium states can be approximated using time-evolution techniques by writing a purification of Gibbs ensemble as above.

MPS family provides very powerful tools to explore dynamics in equilibrium, while the investigation of the dynamics out of equilibrium is a more challenging task as we will be discussing in the following section.

2.2.2 Time evolution

For a time-independent Hamiltonian, H, the time-evolution operator is $U = e^{-iHt}$, where $\hbar$ has been set to unity throughout this thesis. Even if one can efficiently represent the Hamiltonian as a MPO, it is generally not possible to find an efficient MPO representation for U directly. However, this is made tractable through the idea of breaking the total evolution time in small intervals [42, 48, 49, 53, 60] for which one can find an efficient MPO approximation for the time-evolution operator and compute the application of these operators to the initial MPS.

Explicitly, one can divide the time interval t in n intervals of size δ and can

compute the evolution as

$$|\Psi(t)\rangle = \left(e^{-iH\delta}\right)^n |\Psi(t=0)\rangle \,.$$

The most popular and versatile choice to approximate MPO for $e^{-iH\delta}$ is the Suzuki-Trotter [99] decomposition which was developed initially in the context of MPS [50, 51] and DMRG [60] in 2004 [2] and remained as a frequently referred time-evolution method in the ensuing years. One possible choice for $e^{-iH\delta}$ is a first-order Suzuki-Trotter decomposition as

$$e^{-iH\delta} = e^{-iH_{\text{even}}\delta} e^{-iH_{\text{odd}}\delta} + O\left(\delta^2\right), \tag{2.7}$$

for a nearest-neighbor H as $H = \sum_{i-1}^{N-1} h_{i,i+1}$, with $h_{i,i+1}$ acting on sites i and $i+1$. In the above expression, the Hamiltonian is divided in two parts, one containing the two-body terms starting at even sites, and the other one starting at odd sites, $H = H_{\text{odd}} + H_{\text{even}}$ with $H_{\text{odd}} = \sum_{i=1,3\ldots}^{N-1} h_{i,i+1}$ and $H_{\text{even}} = \sum_{i=2,4\ldots}^{N-1} h_{i,i+1}$. All the two-body terms in H_{odd} (H_{even}) mutually commute since $h_{i,i+1}$ has support on two sites only. Accordingly, we can write

$$U_{\text{odd}} = e^{-iH_{\text{odd}}\,\delta} = e^{-i\delta\sum_{i=1,3,\ldots}^{N-1} h_{i,i+1}} = \prod_{i=1,3,\ldots}^{N-1} e^{-ih_{i,i+1}\delta}$$

and similarly for $U_{\text{even}} = e^{-iH_{\text{even}}\delta}$. Hence, one obtains a MPO form for the entire operator after decomposing all the local terms appearing in U_{odd} and U_{even} [3]. In this case (first-order Suzuki-Trotter decomposition), the time step error is of order $O(\delta)$, which is controllable and can be estimated straightforwardly.

The time step error does not violate the unitarity of a real time-evolution since each of the constructed operators is unitary. However, in the case of large time step error, the energy and other conserved quantities are not necessarily expected to be constant. In order to minimize this error, one can choose a smaller time step size δ or higher-order decomposition formulas [99], which may nevertheless not be optimal choices for all cases, since they typically result in more MPOs to apply to the state sequentially for a single step. An alternative to higher-order decomposition could be the combination of large-scale Trotter decomposition with a small-scale Krylov-based approach [100].

Furthermore, the Trotter approach is not limited to the nearest-neighbor case and can also be generalized to longer range interactions. However, for those cases, the cost increases dramatically with the interaction range: in order to obtain sums of mutually commuting terms, one in general needs to split the Hamiltonian into more than two parts, which leads to a larger number of different MPOs to approximate the evolution operator to do a single step. For each of those MPOs, the bond dimension grows linearly with the range of the interactions in the corresponding

[2] In these papers, the method is introduced based on the application of quantum gates to individual state tensors, not based on MPO/MPS formalism. Here, for the implementations we use MPOs instead.

[3] Notice that this approach also applies to time-dependent Hamiltonians. One can simply take the Hamiltonian constant on every interval and proceed the same way as described above.

part of the Hamiltonian. To deal with long-range interactions directly, a different decomposition scheme for the time-evolution operator specifically engineered to construct an efficient representation as a MPO was introduced recently [101] which generates smaller MPOs than the Trotter approach. However, its drawback is that the time-evolution is not exactly unitary. Therefore, for practical numerical computations one is typically limited to local, short-ranged interactions.

All these aspects show that MPS techniques are very useful to explore dynamics close to equilibrium (as discussed in the previous section 2.2.1), but are fundamentally limited for out-of-equilibrium scenarios: the standard time-evolution of a MPS requires a computation with the evolution by repeatedly applying this trotterized MPO. It is pointed out in Section 2.1.1 as well that the application of a MPO onto a MPS results again in a MPS with a bond dimension given by the product of the bond dimension of the MPO and the initial MPS. Consequently, this brings an exponential growth of bond dimension with the number of steps.

There has been analytical and numerical efforts to render the computation feasible [33, 54–59, 102], in which the resulting MPS is approximated by another MPS with a smaller bond dimension using certain algorithms. The idea is more explicitly as follows: for a given MPS $|\Psi\rangle$ with bond dimension D, one wants to find a MPS $|\Psi'\rangle$ with bond dimension $D' < D$ which maximizes the overlap with the original MPS (or equivalently minimizing the norm distance). Based on this idea, the time-evolution for an initially given MPS $|\Psi(t=0)\rangle$ can be computed as a sequence of applying the MPOs approximating $e^{-iH\delta}$, and subsequently truncating the result after a certain number of steps to a MPS of smaller bond dimension D'.

A crucial question is how large D' should be considered to be able to find a good approximation. The answer depends on the entanglement growth during the evolution, and recall that the entanglement is upper bounded by $\log_2(D')$ [33] for a MPS with bond dimension D', as it is stated in Section 2.1.1. While the method is expected to work well with moderate D' as long as the system stays close to the ground state [56], however, in far-from-equilibrium scenarios, the entanglement can grow linearly in time [54, 56, 103], hence in this case, D' would need to grow exponentially. Although there exist improved algorithms for these scenarios [102], only short-time scales are available.

Addressing these consequences and limitations will form the motivation for this thesis. Instead of simulating standard time-evolution, we will introduce novel methods to address long-time dynamics and thermal properties of quantum systems.

2.3 Chebyshev Expansions

One of the recent approaches to simulate the evolution of quantum systems is given by Chebyshev expansions of the exponential operators. In the context of many-body numerics, they can be implemented in combination with *any method* that is able to efficiently apply a Hamiltonian to a state [104]. Exact diagonalization [105, 106] and Monte Carlo [107] methods have been pursued within this context as well as its combination with tensor network states [108–115]. In particular, it has been shown that Chebyshev expansions combined with TN applications offer

efficient representations to study e.g. one-dimensional spectral functions [108], time-evolution [109, 110, 112], density of states [114] as well as controlling the entanglement with energy variance [115].

Let us start by summarizing the properties of Chebyshev polynomials of the first kind, $T_n(x)$, which are defined by the following recurrence relations

$$T_{m+1}(x) = 2xT_m(x) - T_{m-1}(x), \quad m > 0 \tag{2.8}$$

$$T_0(x) = 1, \quad T_1(x) = x. \tag{2.9}$$

Any piecewise continuous function $f(x)$ for $-1 \leq x \leq 1$ can be expanded as

$$f(x) = \sum_m p_m T_m(x),$$

using orthogonality properties of the polynomials, in which the coefficients can be calculated as

$$p_m = C_m^{-1} \int dx w(x) f(x) T_m(x),$$

over a weight function $w(x) = (\pi\sqrt{(1-x)^2})^{-1}$, and C_m are the normalization factors $C_m = \int_{-1}^{1} dx w(x) f(x) T_m(x)^2$. Accordingly, the Chebyshev expansion can be given as

$$f(x) \quad = \quad = \frac{1}{\pi\sqrt{1-x^2}} \left[\mu_0 + 2\sum_{m=1}^{\infty} \mu_m T_m(x) \right] \tag{2.10}$$

where μ_m are called *Chebyshev moments* and given by $\mu_m = \int_{-1}^{1} dx f(x) T_m(x)$.

Making a cut-off at a finite number M of Chebyshev terms, in general, would introduce artificial oscillations of period $1/M$, called Gibbs oscillations. In this case, the use of kernel polynomial method (KPM) [116] suppresses these oscillations by introducing kernels and improves the convergence of the truncated series by multiplying the coefficients with specific factors, γ_m^M, e.g. the Jackson kernel which is used throughout this thesis:

$$\gamma_k^M = \frac{(M-n+1)\cos\frac{\pi n}{M+1} + \sin\frac{\pi n}{M+1}\cos\frac{\pi}{M+1}}{M+1}. \tag{2.11}$$

It puts most of the weight on the smallest order terms, and the actual number of terms that contribute to the final result is much smaller than M. Within this factor, the expansion in Eq. (2.10) is rewritten as,

$$f(x) \quad = \quad \frac{1}{\pi\sqrt{1-x^2}} \left[\gamma_0\mu_0 + 2\sum_{n=1}^{\infty} \gamma_n\mu_n T_n(x) \right]. \tag{2.12}$$

The idea behind of this numerical strategy in simulating the evolution of quantum many-body systems is based on the expansion of the Dirac delta function in terms of Chebyshev polynomials, and the choice of Jackson kernel polynomial

method (JKPM) leads the expansion in Eq. (2.12) to approximate Dirac delta function $\delta(x-a)$ sitting at $-1 < a < 1$, in which all coefficients for odd polynomials vanish, and the $M-th$ order approximation reads,

$$f(x) \approx \sum_{m=0}^{M/2} (-1)^m \frac{2-\delta_{m0}}{\pi} \gamma_{2m}^{M} T_{2m}(x). \tag{2.13}$$

The M order expansion of the function at $x = 0$ results in a broadened peak of width $\sigma = \pi/M$, while near boundaries, it is $\sigma = \pi/M^{3/2}$. This peak indeed provides a good approximation to a Gaussian. Thus, the truncated sum above in Eq. (2.13) can be used to approximate a Gaussian with $\sigma \sim \pi/M$:

$$f(x) \approx \frac{1}{\sqrt{2\pi\sigma^2}} e^{-x^2/2\sigma^2}. \tag{2.14}$$

In the context of quantum many-body systems, the same truncated series in Eq. (2.13) can be made use of in order to approximate a Gaussian (as in Eq. (2.14)) of any Hamiltonian H by rescaling it, $\tilde{H}$, such that the energy spectrum is contained in $[-1, 1]$:

$$e^{-H^2/2\sigma^2} \approx \sum_{m=0}^{M/2} (-1)^m \frac{2-\delta_{m0}}{\pi} \gamma_{2m}^{M} T_{2m}(\tilde{H}). \tag{2.15}$$

The main element in this expansion which needed to be constructed for numerics is $T_m(\tilde{H})$. In the MPS framework [39], fixed bond dimension MPO approximations to the polynomials $T_m^{(D)}(\tilde{H}) \simeq T_m^{(}\tilde{H})$ can be constructed for any Hamiltonian H that can be represented as an MPO [51, 84, 88]. Thus, starting by the first two Chebyshev polynomials in Eq. (2.10), which can be given by the exact MPOs [84] with small bond dimension; $T_0(\tilde{H}) = \mathbb{1}$ and $T_1(\tilde{H}) = \tilde{H}$, one can apply the recurrence relation between Chebyshev polynomials as given in Eq. (2.8).

In order to find a MPS approximation for the action of a Gaussian operator on a given initial state $|\Psi_0\rangle$, one can recurrently apply each polynomial in the sum of Eq. (2.15) to the initial MPS instead of acting with the full polynomials $T_m(\tilde{H})$ as in [108–110, 112, 114, 115] since this leads to lower computational effort, allowing to operate directly with MPS instead of working with more costly operators.

Based on the same conceptual and technical details, we will make use of the Chebyshev expansions in combination with MPS techniques, in order to approximate the diagonal ensembles in one-dimensional isolated quantum systems with the purpose of exploring the long-time dynamics. Complementary discussions can be found in Chapter 4.

Chapter 3

Thermalization and Equilibration Dynamics

In this chapter, before diving into the details, we will briefly outline the main concepts discussed throughout this thesis, which are thermalization and equilibration dynamics in isolated time-independent and periodically driven systems.

3.1 Time-independent systems

When an isolated quantum system is initialized in a pure state out of equilibrium, the unitary character of the evolution ensures that the state remains pure at any later times. However, if observations are restricted to a subsystem, thermalization may occur, that is, the rest of the system can act as a bath for the observed region [5, 9]. More explicitly, if expectation values reach and remain close to a certain value for an extended period of time, one talks about equilibration [7, 10, 11]. And thermalization occurs if those values correspond to the expectation values at the thermal equilibrium state consistent with the energy of the system [5, 6, 8, 9].

Let us consider a system governed by a (local) Hamiltonian H, and an initial state $|\Psi(0)\rangle = \sum_k c_k |E_k\rangle$ in energy eigenbasis (where $c_k = \langle E_k| \Psi(0)\rangle$), which evolves unitarily under the Hamiltonian as

$$|\Psi(t)\rangle = e^{-iHt} |\Psi(0)\rangle . \tag{3.1}$$

The corresponding density operator is given as

$$\rho(t) = |\Psi(t)\rangle \langle\Psi(t)| .$$

If equilibration happens, then it happens towards its time-averaged state which is a mixed state given by

$$\begin{aligned}
\lim_{T\to\infty} \frac{1}{T} \int_0^T \rho(t) dt &= \lim_{T\to\infty} \frac{1}{T} \int_0^T \sum_{k,l} c_k c_l^* e^{-it(E_k - E_l)} |E_k\rangle \langle E_l| \, dt \\
&= \lim_{T\to\infty} \frac{1}{T} \sum_{k,l, E_k = E_l} c_k c_l^* |E_k\rangle \langle E_l| \, T \\
&+ \lim_{T\to\infty} \frac{1}{T} \sum_{k,l, E_k \neq E_l} c_k c_l^* |E_k\rangle \langle E_l| \frac{1}{-i(E_k - E_l)} \left(e^{-iT(E_k - E_l)} - 1 \right) .
\end{aligned}$$

The terms in the second sum become smaller as T grows, and in the limit of infinitely long time the second sum will vanish and the long time-averaged state will be given by only the first sum in the above.

For a generic Hamiltonian with non-degenerate spectrum, the long time limit of time-averaged observables corresponds to the expectation value in the diagonal ensemble [17], which is,

$$\lim_{T\to\infty} \frac{1}{T} \int_0^T \rho(t)dt = \sum_k |c_k|^2 \, |E_k\rangle \langle E_k| \, . \tag{3.2}$$

To decide whether the system can thermalize it is thus enough to compare the expectation values of any local observable O in the diagonal ensemble to those in thermal equilibrium (as given in Eq. (2.5)) at the same energy:

$$\langle O\rangle_{\mathrm{D}} := \sum_k |c_k|^2 \, \langle E_k|O|E_k\rangle \, . \tag{3.3}$$

But while the thermal state of a local Hamiltonian can be efficiently approximated using tensor networks [93, 95, 97], simulating the out-of-equilibrium dynamics, and thus directly constructing the diagonal ensemble, is a much harder problem [55, 56]. We notice that some numerical methods have been developed that can approximate the diagonal ensemble with some restrictions, such as exact diagonalization (limited to small systems) or the numerical linked cluster expansion [117–119] (for which the expansion may fail to converge for some parameter choices, or initial states).

Generally speaking, integrable systems, due to their extensive number of conserved local quantities, do not thermalize but are instead argued to relax or equilibrate to the so-called generalized Gibbs ensemble (GGE) [9, 17–19], compatible with all the constraints. In contrast, non-integrable systems are typically expected to thermalize [9, 11–16]. It is thus especially interesting to identify non-integrable systems that fail to do so, as the current interest in systems with many-body localization [120–122], quantum scars [123] or disorder-free localization [124–126] makes evident. Nevertheless, the (absence of) thermalization of non-integrable systems is hard to determine, since the applicability of analytical tools for such models is limited, and numerical simulations of out of equilibrium dynamics are restricted to small systems or short times.

Necessity of new tools has motivated the work presented in Part II of this thesis. Part II is dedicated to improve the understanding on thermalization and equilibration dynamics by taking a different route with the use of a *filtering technique*. The concept of *filtering* in the MPS framework was first introduced in the recent work [115] which focuses on understanding the connection between entanglement resources and their energy variances for a local Hamiltonian in one-dimensional spin chains by using the filtering technique (a Gaussian filter) with different numerical strategies based on Chebyshev expansions [1] and Cosine functions. Later, these filtering strategies applied to density of states calculations [114, 127]

[1] Notice that as discussed in Section 2.3, Chebyshev-based approaches combination with the MPS techniques were suggested earlier in [108–113] with the purpose of exploring different problems.

and quantum algorithms which compute physical observables in a state where an energy filter is applied [128].

3.2 Floquet systems

Many-body quantum systems governed by time-periodic Hamiltonians i.e., a period T exists such that $H(t+T) = H(t)$ possess a particular case of dynamics [129–146]. The Floquet theorem [147, 148] guarantees the presence in the Hilbert space of a complete basis of solutions of the time-dependent Schrödinger equation which are periodic, such that,

$$|\Phi_{\mathrm{F}\alpha}(t)\rangle = \mathrm{e}^{-i\varepsilon_\alpha t}\,|\Phi_{\mathrm{P}\alpha}(t)\rangle\,, \tag{3.4}$$

where $|\Phi_{\mathrm{P}\alpha}(t)\rangle = |\Phi_{\mathrm{P}\alpha}(t+T)\rangle$ is known as Floquet mode and the ε_α is the eigenenergy, known as Floquet quasienergy. Eq. (3.4) is reminiscent of the time-independent case which is discussed in the previous section. The difference is the state $|\Phi_{\mathrm{P}\alpha}(t)\rangle$ which is now periodic in time rather than a time-independent eigenstate of the Hamiltonian. If we expand a general initial state as

$$|\Phi(0)\rangle = \sum_\alpha |\Phi_{\mathrm{P}\alpha}(0)\rangle\,\langle\Phi_{\mathrm{P}\alpha}(0)\mid\Phi(0)\rangle\,,$$

then the time-evolution can be written, in a form that is similar to the time-independent case (given in Eq. (3.1)),

$$|\Phi(t)\rangle = \underbrace{\sum_\alpha \mathrm{e}^{-i\varepsilon_\alpha t}\,|\Phi_{\mathrm{P}\alpha}(t)\rangle\,\langle\Phi_{\mathrm{P}\alpha}(0)}_{U(t)}\,|\Phi(0)\rangle,$$

where the time-evolution operator is $U(t) = \sum_\alpha \mathrm{e}^{-i\varepsilon_\alpha t}\,|\Phi_{\mathrm{P}\alpha}(t)\rangle\,\langle\Phi_{\mathrm{P}\alpha}(0)|$. For an evolution from $t = 0$ to $t = T$, the elements of a complete orthonormal set of eigenstates of $U(T)$ are the Floquet states $|\varepsilon_\alpha\rangle$.

According to the Floquet theory [147], the Floquet Hamiltonian H_F is given by

$$e^{-iH_F T} \coloneqq \mathcal{T}\left(e^{-i\int_0^T dtH(t)}\right), \tag{3.5}$$

where $H(t)$ is the Hamiltonian of the system which is periodic in time $H(t) = H(t+T)$ and $\mathcal{T}$ is the time-ordering operator. Calculating the Floquet Hamiltonian is one of the non-trivial problems [149–152] in periodically driven systems since it contains the full information about their thermodynamic properties.

A possible method for calculating the Floquet Hamiltonian is to expand it with respect to the period T: this is the Floquet Magnus (FM) expansion [153, 154]:

$$H_F = \sum_{n=0}^{\infty} T^n \Omega_n, \tag{3.6}$$

where

$$\begin{aligned}\Omega_n \;=\; & \sum_\sigma \frac{(-1)^{n-\theta[\sigma]}\theta[\sigma]!(n-\theta[\sigma])!}{i^n(n+1)^2 n! T^{n+1}} \int_0^T dt_{n+1}\cdots \\ & \times \int_0^{t_2} dt_1 \left[H\left(t_{\sigma(n+1)}\right), \left[H\left(t_{\sigma(n)}\right), \ldots, \left[H\left(t_{\sigma(2)}\right), H\left(t_{\sigma(1)}\right)\right]\ldots\right]\right],\end{aligned}$$

where σ is a permutation and $\theta[\sigma] = \sum_{i=1}^{n} \theta(\sigma(i+1) - \sigma(i))$ with $\theta(\cdot)$ is the step function. The FM expansion is useful particularly for the high frequency $\omega = 2\pi/T$ limit in finite system sizes, in which the higher order contribution is negligible. However, it has been noticed that the FM expansion is not a convergent series expansion in general [149, 154]. Due to the divergence problem, a technique of truncation in the FM expansion has been recently developed for describing the Floquet Hamiltonian in particular for transient time scales [155, 156]. Accordingly, the truncated Magnus expansion to approximate the transient dynamics has been given as,

$$H_F^{(n)} = \sum_{m=0}^{n} T^m \Omega_m, \qquad \text{for} \quad e^{-iH_F^{(n)}T} \simeq e^{-iH_F T}. \tag{3.7}$$

$H_F^{(n)}$ is the nth order truncated Floquet Hamiltonian and for example the first two terms in the expansion read as,

$$\begin{aligned} H_F^{(0)} &= \frac{1}{T}\int_0^T dt H(t) \\ H_F^{(1)} &= \frac{1}{2iT^2}\int_0^T dt_1 \int_0^{t_1} dt_2 [H(t_1), H(t_2)]. \end{aligned}$$

Several studies have demonstrated that the time-evolution of the truncated Floquet Hamiltonian is reliable up to a certain long-time: for high-frequency driving [149], for the Friedrichs model on the continuous space [157], and for lattice systems when driving is local [155] as well as when interactions are short-ranged [155, 158, 159].

Periodic driving can be used to engineer desirable interaction Hamiltonians for analog quantum simulations [135, 160–174]. Furthermore, digital quantum simulators employing Trotterization can be interpreted as Floquet systems [175, 176]. Periodically driven quantum systems can also serve as a platform for realizing interesting phases of matter like discrete time crystals [146, 177–185] and Floquet topological phases [186–192]. Periodic driving has also been used for opening gaps in graphene [193–195], controlling magnetic exchange interactions in solids [152, 196–199], realizing artificial gauge fields in cold atoms [200, 201], and stabilizing or inducing superconductivity [202–204]. These applications of Floquet systems necessitate an understanding of their long-time dynamics.

At long times, the diagonal ensemble in Floquet systems is defined in terms of the overlap of the initial state of the system and the Floquet states, similar to the time-independent case as given in Eq. (3.2):

$$\rho = \sum_{\alpha} |\langle \Phi(0)|\varepsilon_\alpha\rangle|^2 |\varepsilon_\alpha\rangle\langle\varepsilon_\alpha|. \tag{3.8}$$

The expectation value of a local observable in a Floquet quantum system is expected to equilibriate, in average, to its expectation value in the Floquet diagonal ensemble (FDE) [140, 205, 206], which is given by

$$\langle O\rangle_{\mathrm{D}} = \sum_{\alpha} |\langle \Phi(0)|\varepsilon_\alpha\rangle|^2 \langle\varepsilon_\alpha|O|\varepsilon_\alpha\rangle\,. \tag{3.9}$$

Although exceptions like many-body localized [142, 207–215] and other non-ergodic systems [216–224] exist, generic non-integrable Floquet many-body systems have been predicted to absorb energy from the periodic driving, rendering the diagonal ensemble equivalent to an infinite temperature state for local observables; this is the Floquet version of the eigenstate thermalization hypothesis, and is called Floquet ETH [209, 225–230]. This is indeed a consequence from the analogy of ETH in non-driven systems [9]. The ETH postulates that each energy eigenstate is not distinguishable from the microcanonical ensemble for the same energy. In periodically driven systems, the energy is not conserved anymore and hence the extension of ETH to the driven case shows that the steady state is a state of infinite temperature (i.e., a random state). Thus, the information reflected from the system is not visible in the infinite-time scale due to the heating effect.

However, the experiments on many-body quantum systems do not focus on the long-time limit; rather, they are interested in the transient dynamics for the experimental time scale. The transient-time behavior of generic Floquet systems can be less trivial, exhibiting interesting dynamical behaviours, such as prethermalization [149, 155, 158, 181, 182, 231–244], where the system relaxes to a long-lived quasi-stationary state before reaching the infinite temperature state. This can be due to the emergence of an effective, static Hamiltonian that is quasi-conserved [150, 170, 174, 181, 200, 245–247], slowing the heating rate. Due to the suppressed heating, the prethermal window can be used for applications like quantum simulation and preparation of non-equilibrium phases of matter by engineering the effective Hamiltonian [149, 170, 181–183].

Motivated by the burgeoning applications of Floquet systems as discussed above, the work presented in Chapter 6 aims to explore whether the application of the filter algorithms to the Floquet scenario contributes to the understanding of the dynamics in intermediate time regimes.

Part II

Thermalization and Equilibration in Isolated Quantum Many-Body Systems

Chapter 4

Approximating the diagonal ensemble

Most of the content of this chapter is contained in:

- *"Approximating the long time average of the density operator: Diagonal ensemble"*
  Aslı Çakan, J. lgnacio Cirac and Mari Carmen Bañuls
  Phys. Rev. B 103, 115113 (2021)

In this chapter, we are interested in exploring long-time dynamics of isolated generic quantum systems out of equilibrium, in which the long-time average of observables is given by the diagonal ensemble as discussed in Chapter 3. Here, we present an alternative method to approximate the diagonal ensemble instead of simulating the standard real time evolution. We introduce a *filtering technique*, and show how it can filter out the off-diagonal components of a density operator with respect to the energy basis, thus approximate the diagonal ensemble without resourcing to the explicit simulation of the dynamics.

In the first part of this chapter, we review our filtering procedure explicitly, where we apply to the initial density matrix a Gaussian with a superoperator that filters out off-diagonal matrix elements in the energy eigenbasis. In the limit of vanishing width of the Gaussian, the result will converge to the diagonal ensemble, in the most generic case, when there are no degeneracies in the spectrum. If there were degenerate energy levels, the procedure would leave untouched the coherences in the corresponding energy subspace, and thus would still lead to the correct limit of the time-averaged density operator.

In the second part of this chapter, we describe the main elements of our numerical simulations, in which we make use of MPS techniques: as described in Chapter 2.3, a Gaussian can be approximated as a sum of Chebyshev polynomials, and its application to an initial vector can be numerically simulated using MPS [33, 39] methods, at least for moderate widths. Here we carry out these simulations for a spin chain in the non-integrable regime, and investigate how the values of local observables converge towards the thermal equilibrium. Moreover, we analyze the behaviour of operator space entanglement entropy and examine how it depends on the Gaussian filter width. Later, we also discuss the distinct behavior of an

integrable instance: for comparison, we consider an integrable case of the same model, for which the observables may converge to different non-thermal values, depending on the initial state. Finally, we summarize our findings and discuss potential extensions of our work.

4.1 Filtering the diagonal ensemble

Let us consider a system of size N governed by a (local) Hamiltonian H, and a pure initial state, which can be written in the energy eigenbasis as

$$|\Psi_0\rangle = \sum_k c_k |E_k\rangle ,$$

with the normalization condition $\sum_k |c_k|^2 = 1$ (where the sum runs over the energy basis). We are interested in the long time average properties of the evolved state, i.e. given any physical observable $O = \sum_{k,l} O_{kl} |E_k\rangle \langle E_l|$, we want to compute

$$\lim_{T\to\infty} \frac{1}{T} \int dt \, \langle \Psi(t)| O |\Psi(t)\rangle = \sum_k |c_k|^2 O_{kk} = \mathrm{tr}[\rho_D(\Psi_0) O] \tag{4.1}$$

where the first equality holds under the generic condition, which we assume in the following, that the spectrum is non-degenerate [1], and in the second one we have used the definition of the diagonal ensemble

$$\rho_D(\Psi_0) = \sum_n |c_k|^2 |E_k\rangle \langle E_k| . \tag{4.2}$$

If the system thermalizes, the diagonal expectation value $\langle O \rangle_D := \mathrm{tr}\,(\rho_D O)$ will be equal to the expectation value in the thermal equilibrium state,

$$\rho_{th}(\beta) = \frac{e^{-\beta H}}{\mathrm{tr}(e^{-\beta H})},$$

that corresponds to the mean energy of the initial state, $\mathrm{tr}(H\rho_{th}(\beta)) = \langle \Psi_0| H |\Psi_0\rangle$. Thus, an approximation to the diagonal ensemble would allow us to probe whether a given state thermalizes or not.

In the energy eigenbasis, the density matrix for the initial state can be written as

$$\rho_0 = \sum_{k,l} c_k c_l^* |E_k\rangle \langle E_l| .$$

Filtering out the off-diagonal matrix elements in this basis will result in the diagonal ensemble (4.2). We thus define an (unnormalized) Gaussian filter which acts on the mixed state as a superoperator

$$F_\sigma[\rho] := e^{-\hat{H}_C^2/2\sigma^2}[\rho], \tag{4.3}$$

[1] If this condition is not fulfilled, ρ_D should be replaced by a block-diagonal operator, where each block corresponds to a different energy subspace, with the same matrix elements as in the initial state.

where $\hat{H}_C$ is the commutator with the Hamiltonian, i.e. $\hat{H}_C[\rho] = H\rho - \rho H$. Notice that F_σ is a completely positive trace preserving map, i.e. a quantum channel. The effect of this filter is to suppress the off-diagonal matrix elements corresponding to pairs of states with different energies. As the width σ is reduced, and for a generic, non-degenerate, Hamiltonian, the application of the filter will converge to the desired result

$$F_\sigma[\rho_0] \underset{\sigma\to 0}{\longrightarrow} \rho_D(\Psi_0).$$

Notice that the filter would not affect the density operator components in a degenerate energy subspace. Thus, if the Hamiltonian has degenerate levels, the limit of the procedure is block diagonal, corresponding to the long time limit of the time-average of the evolved state.

Mapping the basis operators to vectors [248] as $|E_k\rangle\langle E_l| \to |E_k E_l\rangle$, we can write the density matrix as a vector of dimension 2^{2N}, on which the filter acts as a linear operator, and the problem becomes formally analogous to the energy filters used in [113–115, 249].

In this representation, the commutator corresponds to the linear operator

$$\hat{H}_C = H \otimes \mathbb{1} - \mathbb{1} \otimes H^T,$$

which, if H is local, is also a local Hamiltonian with eigenvectors $|E_k E_l\rangle$ and corresponding eigenvalues $E_k - E_l$, for $k, l = 1 \dots 2^N$. We can then apply the filtering procedure for reducing the energy variance from a state with given mean energy as described in 3. For a product initial state $|\Psi_0\rangle$, the (vectorized) initial density matrix $|\rho_0\rangle = |\Psi_0\rangle \otimes |\Psi_0\rangle$ is also a product.

With respect to the Hamiltonian $\hat{H}_C$, any physical state has mean value

$$\langle\rho_0|\,\hat{H}_C\,|\rho_0\rangle = \mathrm{tr}\left(\rho_0^\dagger\,[H,\rho_0]\right) = 0.$$

The filter (4.3) preserves this property of the initial state while it reduces the corresponding (effective energy) variance, $\langle\rho|\,\hat{H}_C^2\,|\rho\rangle = -\mathrm{tr}\left([H,\rho]^2\right)$, which measures precisely the off-diagonal part of the density operator in the energy basis.

4.1.1 Chebyshev approximation of the filter

Formally, this filtering procedure is analogous to the one described in [115], and some of the properties can be directly translated to the current case. In particular, the Gaussian filter F_σ can be approximated by a series of Chebyshev polynomials.

As discussed in Section 2.3, any piece-wise continuous function $f(x)$ defined in the interval $x \in [-1, 1]$ can be approximated by a linear combination of the M lowest-degree Chebyshev polynomials [116]. In particular, the corresponding series for the delta function truncated to order M (and improved using the kernel polynomial method) is known to approximate a Gaussian of width $\sqrt{\pi}/M$. We can thus use such series to order $M \propto N/\sigma$ to approximate the Gaussian filter F_σ. As discussed in Section 2.3, this sum has the form as Eq. (2.12) and we apply the same truncated series to the Hamiltonian commutator $\hat{H}_C$,

$$Q_M := \sum_{m=0}^{\lfloor M/2 \rfloor} (-1)^m \frac{2-\delta_{m0}}{\pi} \gamma_{2m}^M T_{2m}(\alpha \hat{H}_C), \tag{4.4}$$

where α is a rescaling constant to ensure that the spectrum of $\alpha\hat{H}_C$ lies strictly within the interval $[-1, 1]$. We use $H_C = \alpha\hat{H}_C$ for the rescaled Hamiltonian commutator in the rest of the Chapter.

As in [108, 110, 114, 115, 250, 251], we can then take advantage of the fact that we do not need the full polynomials $T_m(H_C)$, which in our case are operators acting on a 2^{2N} dimensional vector space, but only the vectors resulting from their action on the initial state $T_m(H_C)|\rho_0\rangle$. The latter satisfy the same recurrence relation as the polynomials and can be computed with lower computational cost.

We will denote the result of applying the series expansion to order M as

$$|\rho_M\rangle := Q_M |\rho_0\rangle , \tag{4.5}$$

and its norm is given as

$$\langle \rho_M | \rho_M \rangle \sim \frac{1}{\sigma\sqrt{N}}.$$

Notice that this vector has a different normalization than $|\rho_\sigma\rangle$, because the sum in Q_M approximates a normalized Gaussian distribution, unlike F_σ from (4.3), which we will be discussing in the following Section 4.1.3 and Section 4.3.1.

The off-diagonal width of the operator ρ_M is determined by the corresponding variance of H_C as

$$\delta^2 := \frac{\langle \rho_M | H_C^2 | \rho_M \rangle}{\langle \rho_M | \rho_M \rangle}, \tag{4.6}$$

since $\langle \rho_M | H_C | \rho_M \rangle = 0$.

4.1.2 Properties of the diagonal filter

Notice that the filtering procedure described so far is general, as it does not make any assumption on the spatial dimension of the problem. In the following we will focus on a one-dimensional problem, for which we can use tensor networks in order to obtain numerical approximations.

As in [115], we can use matrix product state (MPS) techniques [33, 39] to simulate the application of this filter to an initial state. In this way we construct a matrix product operator (MPO) [51, 88, 252] approximation to the filtered ensemble. One of the essential results obtained in [115] is that for large system sizes and narrow filters, the required bond dimension for the approximation can be bounded as $D \lesssim c'\sqrt{N} D_0^{1/\delta}$, where c' and D_0 are $O(1)$ constants. Accordingly, the expression for the entanglement entropy,

$$\mathcal{S} \lesssim k/\delta + \log\sqrt{N} + \text{const} \tag{4.7}$$

corresponds here to a bound for the operator space entanglement entropy (OSEE) [253].

The spectrum of H_C exhibits however an exponential degeneracy in the subspace of eigenvalue zero, which imposes a significant difference. For each eigenstate $|E_n\rangle$

of H, $|E_n E_n\rangle$ is eigenstate of H_C with zero eigenvalue. Thus, even if the spectrum of H is non-degenerate and even if it fulfills the stronger assumption of non-degenerate gaps, the "zero energy" subspace of H_C is always exponentially degenerate.

Hence the target diagonal ensemble states could in principle have arbitrarily small OSEE, even with vanishing width σ (an extreme case would be the maximally mixed state, with zero OSSE). This is in contrast to the Hamiltonian filtering, where the limit would generically have thermal (i.e. volume law) entanglement. Even if we expect that the general relations between energy fluctuations and entropy or bond dimension demonstrated in [115] still hold during the main part of the filtering procedure, eventually, as the width becomes negligible and the procedure converges to the diagonal ensemble, the OSSE can converge to a non-generic value that will depend on the initial state.

The scenario we discuss here also exhibits another fundamental difference regarding physical observables. For a local operator O, the expectation value is computed as

$$\frac{\mathrm{tr}\,(O\rho)}{\mathrm{tr}\rho} = \frac{\langle O|\,\rho\rangle}{\langle \mathbb{1}|\,\rho\rangle}, \tag{4.8}$$

where $|O\rangle$ and $|\mathbb{1}\rangle$ are respectively the vectorized observable and identity operators [2].

As an overlap between two vectors, this is a global quantity, and no longer local in space. Therefore, the considerations in [115] about the minimal entanglement of a subregion required for local observables to converge to thermal values do not immediately apply here. More explicitly, one of the conclusions in Ref. [115] is that decreasing the energy variance as $\delta \sim 1/\log(N)$ by keeping a polynomial scaling in bond dimension is sufficient to reach convergence in the thermodynamic limit, which is not necessarily expected to apply our case since we do not have the same local structure here.

4.1.3 Convergence of the off-diagonal components

The pure initial state is given by a physical density operator, normalized in trace, $\mathrm{tr}\rho_0 = 1$, and also Frobenius norm, $\langle \rho_0|\,\rho_0\rangle = \mathrm{tr}\rho_0^2 = 1$. The filter (4.3) preserves the former, but not the latter. Instead, the Frobenius norm of the filtered vector $|\rho_\sigma\rangle$ indicates the magnitude of the remaining off-diagonal components.

The state resulting from the application of the original Gaussian filter F_σ on ρ_0 can be written as a sum of two mutually orthogonal components,

$$|\rho_\sigma\rangle = |\rho_\mathrm{D}\rangle + \sum_{n,m\neq n} c_n c_m^* e^{-(E_n-E_m)^2/(2\sigma^2)}\,|E_n E_m\rangle\,. \tag{4.9}$$

The first term is precisely the diagonal ensemble, and the second one includes all off-diagonal components of the density operator. Denoting them by $|\Delta\rho\rangle := |\rho_\sigma\rangle - |\rho_\mathrm{D}\rangle$, the (Frobenius) norm of the off-diagonal components is

$$\langle \Delta\rho|\,\Delta\rho\rangle = \sum_{n,m\neq n} |c_n|^2 |c_m|^2 e^{-(E_n-E_m)^2/\sigma^2}. \tag{4.10}$$

[2] Notation for operators $\langle A|\,B\rangle := \mathrm{tr}(A^\dagger B)$.

The magnitude of these components may be estimated using simple arguments. We consider as initial state ρ_0 a pure product state, for which the energy distribution, given by $|c_n|^2$, is peaked around the mean energy $E_{\rho_0} = \mathrm{tr}(H\rho_0)$, and has variance $O(N)$. For large systems, this distribution behaves as a Gaussian [254] and we can approximate the norm of the vector $|\rho_\sigma\rangle$ by a double integral over energies, from which we obtain

$$\langle \rho_\sigma | \, \rho_\sigma \rangle \sim \frac{\sigma}{\sqrt{N}}. \tag{4.11}$$

The norm of the diagonal component, equivalent to the inverse participation ratio of the initial state, $\langle \rho_D | \, \rho_D \rangle = \sum_n |c_n|^4$ is independent of σ.

Typically, the number of energy eigenstates contributing to the sum will be exponentially large in the system size, unless the mean energy of the initial state E_ρ corresponds to a region of exponentially small density of states. To see this, we can take again into account the aforementioned distribution of the weights for our initial states, and the fact that for large systems the density of states approaches also a Gaussian distribution [254, 255]. The inverse participation ratio then decreases exponentially with the system size,

$$\langle \rho_\mathrm{D} | \, \rho_\mathrm{D} \rangle \sim 2^{-N}. \tag{4.12}$$

Unless the width of the filter is exponentially small in N, the norm of the filtered state is dominated by the off-diagonal component, and we expect both of them to decrease proportionally to the width, for fixed size N, according to (4.11). Notice nevertheless that a bound on the (Frobenius) norm of $|\Delta\rho\rangle$ is not enough to extract conclusions about the convergence of physical observables, a question that we explore numerically in section 4.3.

4.2 Setup for the numerical simulations

We use numerical simulations to explore some of the questions in the previous section. In particular, we investigate whether the diagonal ensemble can be approximated by a MPO, and how the physical observables approach the diagonal expectation values as we filter out the off-diagonal matrix elements of the density matrix.

4.2.1 MPS approximation of the ensemble

We use matrix product operators (MPO) [51, 84, 88] to represent the density operators corresponding to the initial and filtered states. Once vectorized, they are represented by MPS with double physical indices, which can be manipulated using standard tensor network methods [33, 39, 73, 256].

We find a MPS approximation for the action of the filter Eq. (4.4) on a given initial state. The method is completely analogous to the one presented in [115] for filtering out energy fluctuations (as explained in Section 2.3), with the only difference that here the effective Hamiltonian is the commutator superoperator

H_C acting on the vectorized density matrices. For a local Hamiltonian H, the commutator H_C can also be written as a MPO.

4.2.2 Model and initial states

We focus our study in the Ising spin chain with both longitudinal and transverse fields,

$$H_{\text{Ising}} = J \sum_i \sigma_z^{[i]} \sigma_z^{[i+1]} + g \sum_i \sigma_x^{[i]} + h \sum_i \sigma_z^{[i]}. \tag{4.13}$$

If either $g = 0$ or $h = 0$, the model becomes exactly solvable. For the remaining of this section we focus on the generic, non-integrable case. We choose parameters $(J, g, h) = (1, -1.05, 0.5)$, far from the integrability limit.

As initial states we consider product states in which all spins are aligned in the same direction. We denote such states by the direction in which the spins are aligned, e.g. $|X\pm\rangle = 2^{-N/2} \left(|0\rangle \pm |1\rangle\right)^{\otimes N}$, $|Y\pm\rangle = 2^{-N/2} \left(|0\rangle \pm i\,|1\rangle\right)^{\otimes N}$, $|Z+\rangle = |0\rangle^{\otimes N}$ and $|Z-\rangle = |1\rangle^{\otimes N}$.

4.3 Numerical Results

We have applied the procedure described in the previous section to system sizes $20 \leq N \leq 60$, using MPS with bond dimensions $100 \leq D \leq 1000$. Additionally, we cross-check results for small system sizes $N \leq 20$ which can be explored with exact diagonalization.

4.3.1 Scaling

We expect the off-diagonal width δ of our simulations to follow the scaling predicted in Ref. [115], namely $\delta^2 \propto 1/M^2$, for large enough number of terms in the approximation of the filter, and provided that the truncation error is not significant. Thus, the decrease of the width with M provides us with a check that our simulations are in the expected regime. Figure 4.1 shows that this is indeed the case. The figure shows that for all system sizes, the converged data are well described by a power law fit $\delta^2 \propto M^{-\alpha}$ (dotted lines) with exponents $-2.13, -1.98, -1.97, -1.95, -1.96$ for $N = 20, 30, 40, 50, 60$, respectively.

A further check is provided by the norm of the filtered state $|\rho_\sigma\rangle$. As described in section 4.1.3, $\langle\rho_\sigma|\,\rho_\sigma\rangle$ should decrease as the inverse off-diagonal width. Since our algorithm applies the normalized filter (4.4), $Q_M \sim \frac{1}{\sqrt{2\pi\sigma^2}} F_\sigma$, we expect, for the proper values of M and σ,

$$\langle\rho_M|\,\rho_M\rangle \sim \frac{1}{\sigma\sqrt{N}}. \tag{4.14}$$

To directly probe this relation, we plot the vector norm of our resulting state in figure 4.2, for system sizes $N = 20 - 60$, and find that our data agrees well with this prediction, except for the smallest values of M.

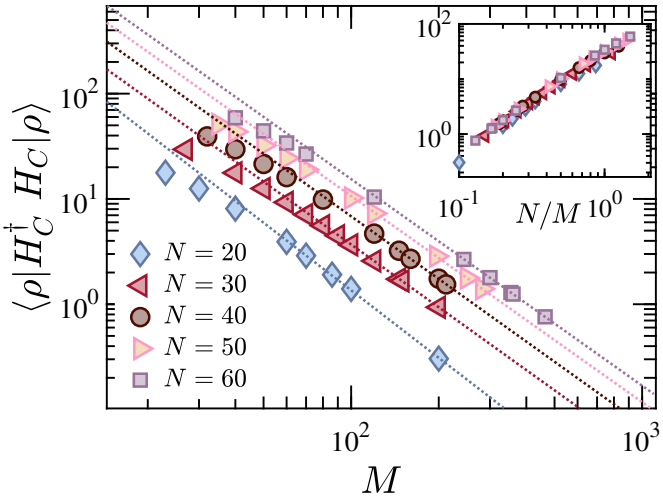

Figure 4.1: Scaling of the variance $\delta^2 = \langle\rho_M|H_C^\dagger H_C|\rho_M\rangle$, as a function of the Chebyshev truncation parameter M for different system sizes $N = 20 - 60$ with bond dimension $D = 1000$ and initial state $|X+\rangle$. Except for the smallest values of M, we find that our results scale with the expected [115] $\delta^2 \propto 1/M^2$.

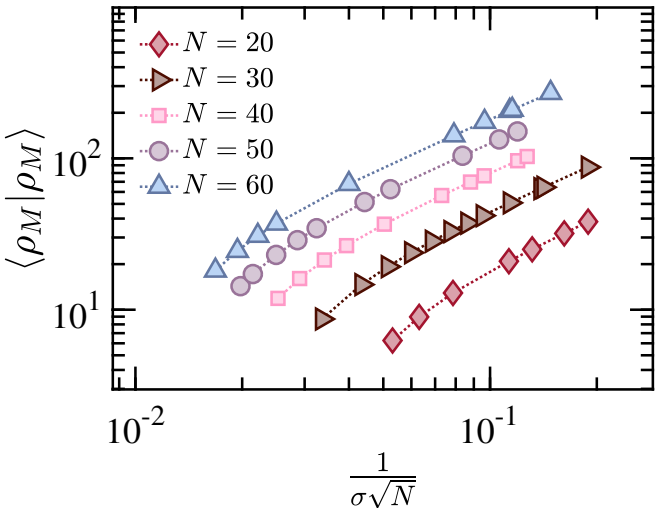

Figure 4.2: Relation between vector norm of off-diagonal components and inverse off-diagonal width as explained in the text and given in Eq. (4.14) for system sizes $N = 20 - 60$ and bond dimension, $D = 1000$, starting with initial state $|X+\rangle$, where the slopes of all are ~ 1.

4.3.2 Convergence of local observables

As the filtered state approaches the diagonal ensemble, so will the values of physical observables. If the state thermalizes, such limit will agree with the thermal value corresponding to the initial energy, and thus comparing this to the converged

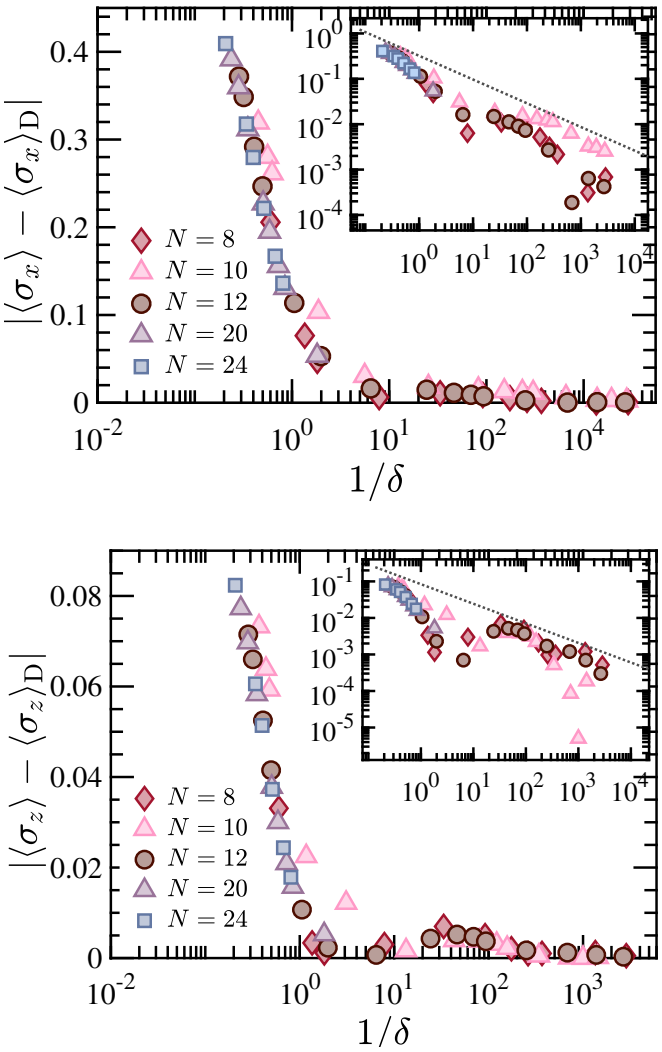

Figure 4.3: Absolute error in local observables σ_x (upper) and σ_z (lower figure) between exact diagonal ensemble values and exact Chebyshev filter results as a function of inverse off-diagonal width for system sizes $N = 8, 10, 12, 20$ and 24 with the initial state $|X+\rangle$. The insets indicate the log-log plot of the corresponding figures, which we show the upper bounds with the straight dotted lines. The slope for σ_x is -0.52 and it is -0.53 for σ_z.

values can be used to probe thermalization of the system. Here we are interested in the rate of convergence of the physical expectation values.

For the problem of reducing the energy variance of a pure state, it has been predicted that for chaotic systems [257] a polynomial decrease of the variance with the system size is sufficient for all local observables to converge to their thermal values. In Ref. [115] it was numerically observed for model (4.13) that an energy variance decreasing as $1/\log N$ or faster was sufficient for convergence in the thermodynamic limit. But as discussed in section 4.1, these conclusions do not need to apply in our case, because the expectation value in the mixed state does

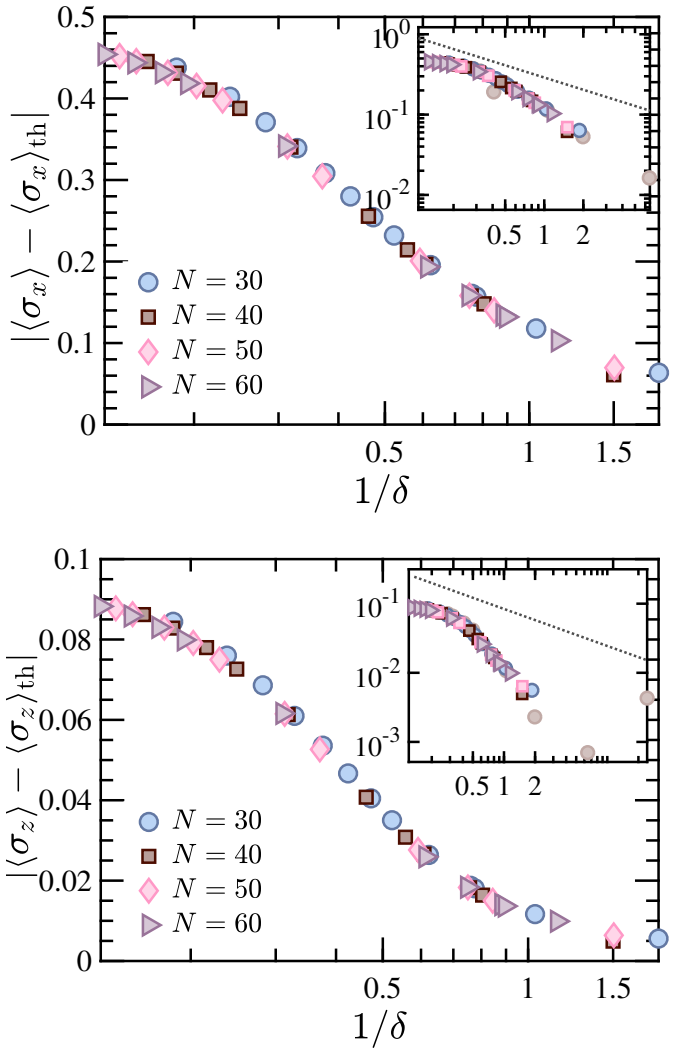

Figure 4.4: Absolute error in local observables σ_x (upper) and σ_z (lower figure) between thermal values and numerical results based on Chebyshev filter as a function of inverse off-diagonal width for system sizes $N = 30 - 60$ with the initial state $|X+\rangle$. The insets indicate the log-log plot of the corresponding figures, where we add the upper bounds with the dotted lines and the data points belong to $N = 12$ with lighter color as reference values taken from figure 4.3.

not have the same local structure. We thus explore this question numerically by studying the local x and z magnetizations in the middle of the chain, $\mathcal{O} = \sigma_{x,z}^{\lfloor N/2 \rfloor}$, and analyzing how the expectation values vary as the width of the filter decreases. For systems of size $N \leq 12$ we can compute the action of the filter exactly for any width, while for larger systems, up to $N \leq 60$, we run MPS simulations up to the narrowest filter widths that we can reliably reach with a maximum bond dimension $D = 1000$.

For small systems, $N \leq 24$, we can compare the filtered values with the exact computation of magnetizations in the diagonal ensemble. For larger systems we

do not have access to either the evolved state at long times or the exact diagonal ensemble, but we can approximate the thermal ensemble corresponding to the initial energy using MPO [51, 88, 258]. For the cases we study, there are analytical and numerical arguments in favor of thermalization [114, 259], such that the thermal expectation values should be very close to the diagonal ones. Thus, for our analysis it is enough to use the thermal value as reference. However, our simulations for large systems do not seem to reach full convergence (see subsection 4.3.4 for a more detailed discussion of the numerical errors).

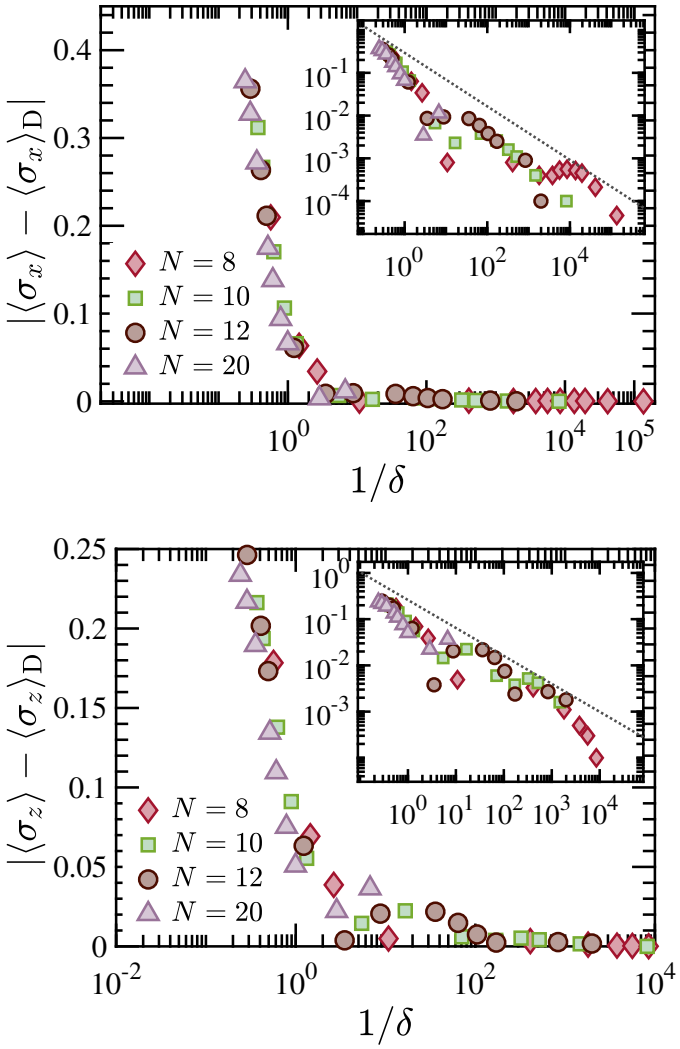

Figure 4.5: Absolute error in local observables σ_x (upper) and σ_z (lower figure) between exact diagonal ensemble values and Chebyshev filter results, as a function of inverse off-diagonal width for system sizes $N = 8, 10, 12$ and 20 with the initial state $|Z+\rangle$. The insets indicate the log-log plot of the corresponding figures, which we show the upper bounds with the grey dotted lines. Slopes for σ_x is -0.62(63) and it is -0.60(47) for σ_z.

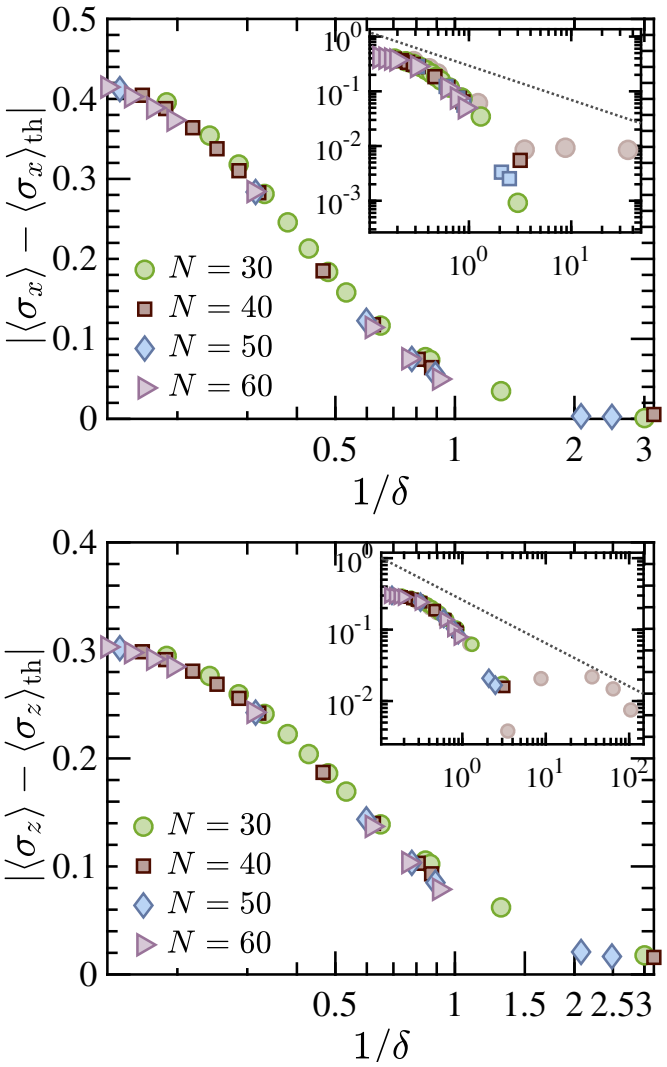

Figure 4.6: Absolute error in local observables σ_x (upper) and σ_z (lower figure) between thermal values and numerical results based on Chebyshev filter as a function of inverse off-diagonal width for system sizes $N = 30 - 60$ with the initial state $|Z+\rangle$. The insets indicate the log-log plot of the corresponding figures, where we put the upper bounds with the dotted lines and the data points belong to $N = 12$ with lighter color as reference values taken from figure 4.5.

We plot the results for small and large system sizes in figures 4.3 and 4.4 for initial state $|X+\rangle$, and in figures 4.5 and 4.6 for initial state $|Z+\rangle$. In all cases we represent the absolute value of the difference between the expectation values in $|\rho_M\rangle$ and the diagonal (thermal, for large systems) values as a function of the off-diagonal width δ. In all cases, i.e. for the different initial states and different sizes, we observe that this absolute error, which is given exclusively by the off-diagonal part of ρ_M, decreases at least as fast as $1/\sqrt{\delta}$ (see insets). Moreover, the figures show that curves for different system sizes practically collapse on top of each other.

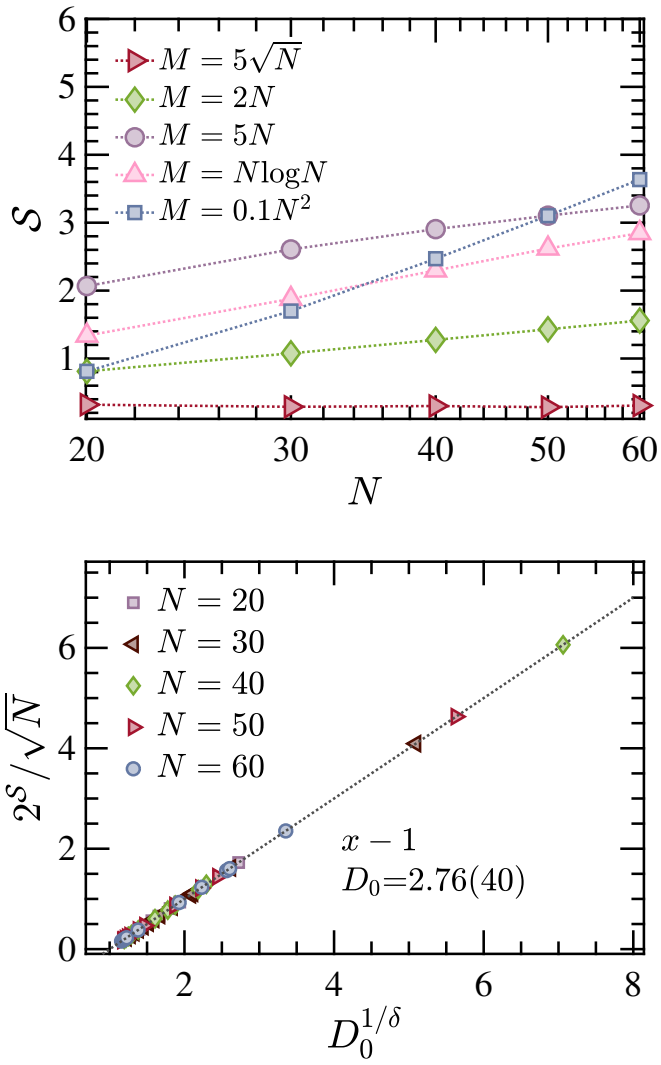

Figure 4.7: Upper figure: Operator space entanglement entropy of the half chain as a function of logarithm of the system size, N, with different truncation numbers of Chebyshev filter, $M = f(N)$ and bond dimension, D=1000 for initial state $|X+\rangle$. Our data show that the entropy grows with $\log N$ in all cases except that the line for $M = 5\sqrt{N}$ stays constant. Lower figure: Behavior of the exponential of the entropy as predicted by Ref. [115] that we have explained in the text and shown in Eq. (4.7). The dotted line indicates the linear fit where all data points locate on the same line as expected for large system sizes. D_0 from fitting the data for all system size is 2.76(40) and the slope of the fit is 1.

4.3.3 Entropy

Since we start with a product state $|\rho_0\rangle$ and evolve it with a local Hamiltonian H_C, the same arguments used in the case of pure states [115, 260] then imply that the OSEE can be bounded as a function of the off-diagonal width and the system size as given in Eq. (4.7). Here we check whether it is similarly bounded.

Figure 4.7 (upper panel) shows that indeed, the evolution of the OSEE while filtering out the off-diagonal components of the state satisfies a similar bound. The plot shows the OSEE corresponding to the middle cut of the approximate filtered state ρ_M, as a function of the system size, for simulations in which the number of Chebyshev terms was chosen as different functions of the size $M = f(N)$, corresponding to a width $\delta(N) \propto 1/M$. We observe that for $M \propto \sqrt{N}$, which corresponds to $\delta \propto \sqrt{N}$, the OSEE does not grow with the system size, while for $M \propto N$ or $M \propto N \log N$ (correspondingly $\delta \sim$ const or $\delta \propto 1/\log N$), it increases as $\log N$. For faster growing $M \propto N^2$, also the increase in entropy is faster (compatible with it growing at most as N^2, as predicted by the argument in [115]).

The asymptotic universal scaling of the entropy can be appreciated more explicitly in figure 4.7 (lower), which shows that

$$2^{\mathcal{S}} \propto \sqrt{N}(D_0^{1/\delta} - 1)$$

for all system sizes $N \geq 20$ with a constant $D_0 = 2.76$.

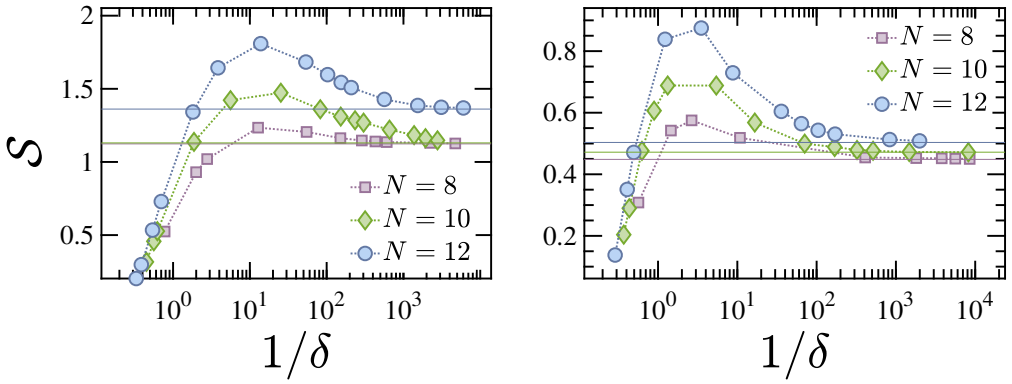

Figure 4.8: Relation between entropy and logarithm of $1/\delta$ based on exact calculation for $N = 8, 10, 12$ with initial state, $|X+\rangle$ (left) and $|Z+\rangle$ (right figure). Purple, green and blue horizontal lines indicate the exact entropy values in the diagonal ensemble for the same system sizes $N = 8, 10, 12$ respectively, belonging to the same color map in the legend.

The limit of the filtering procedure when the width vanishes is a mixed state in the exponentially degenerate null space of H_C. This subspace supports states with zero OSEE (e.g. the maximally mixed state), and thus the final OSEE is not generic, but will be determined by the initial state, in contrast to the case of pure state filtering, where we could generically expect that the entanglement entropy converged to a thermal volume law.

We can explore how the limit value is approached during the filtering by analyzing the results for small systems, as shown in figure 4.8. As illustrated in the figure for different initial states and sizes $N \leq 12$, the entropy grows with $1/\delta$ for moderate widths, but it reaches a maximum after a certain point, and then decreases towards the diagonal value. If we examine how this final value depends

on the system size, we observe, that in all the cases studied the diagonal OSEE increases almost linearly with the size, although the values change considerably from one state to another, where the slope of each initial states are $0.0678, 0.8917, 0.0237$ for $|X+\rangle, |Y+\rangle, |Z+\rangle$, respectively.

4.3.4 Error Analysis

In our strategy, for a fixed order M of the Chebyshev expansion, the main source of error is the truncation error, namely approximating the action of each Chebyshev polynomial on the initial state by a MPS with limited bond dimension. We can quantify this error for a given order m using as reference the best approximation found for the corresponding term $T_m(H_C)\,|\rho_0\rangle$ (in our case, with $D = 1000$) and comparing it to its truncated versions with smaller bond dimensions. In this way we can extract the bond dimension required for fixed precision.

In previous works that used MPS approximations of Chebyshev series [108, 110, 114, 250, 251] it was observed that the required bond dimension for such terms increases polynomially with the degree m. Our results, illustrated in figure 4.9, seem to agree with such behavior, except for the smallest values of m. We have also observed, as in the recent work [114], that for fixed m the bond dimension required to maintain constant truncation error in $T_m(H_C)\,|\rho_0\rangle$ gets smaller for larger system sizes. Notice, however, that for larger systems, also polynomials of higher degree will be required to attain a constant width δ, since, as discussed in Section. 4.1.1, the order of the expansion scales as $M \propto N/\delta$, which will be also checked in the following chapter 5.

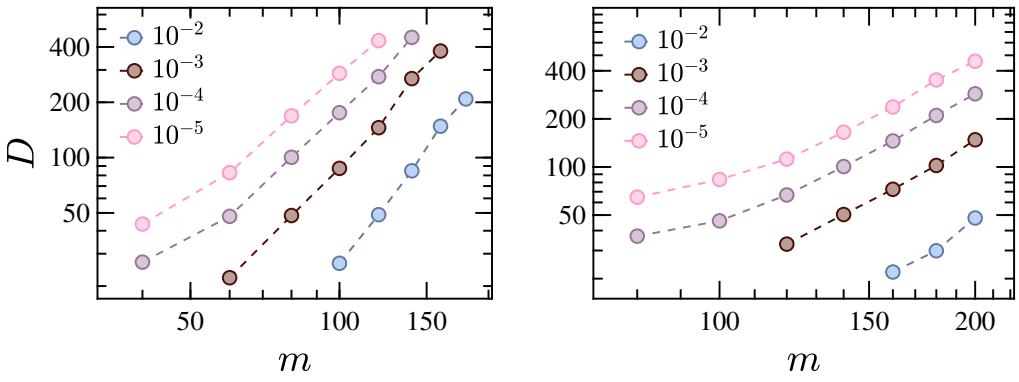

Figure 4.9: Scaling of the bond dimension required to keep a constant precision in the MPS approximation of $T_m(H_C)\,|\rho_0\rangle$, as a function of the degree m for various values of the truncation error, $10^{-2}, 10^{-3}, 10^{-4}, 10^{-5}$ and system sizes $N = 20$ (left) and $N = 30$ (right) for which we take $D = 500$ as a reference.

4.4 Integrable case

The results in section 4.3.2 are consistent with the generic expectation that for non-integrable cases, the values of local observables in the diagonal ensemble agree with those in thermal equilibrium. But the presence of local conserved quantities imposes constrains on the equilibration of observables. Thus for integrable models, long time averages are not expected to agree with the thermal ensemble. Instead, the system could in such cases converge to a generalized Gibbs ensemble [17] compatible with all conserved quantities.

We expect that, as the width of the filter decreases, our method approximates the actual time averaged state in the limit of infinite time. Hence local observables can converge to values that differ from thermal equilibrium. In order to probe this case, we have applied the method to an integrable choice of parameters in Eq. (4.13), namely $(J, g, h) = (1, 1.05, 0.)$, for various translationally invariant product states. We have simulated system sizes up to $N = 50$, with bond dimension up to $D = 1000$.

The scaling of variance and entropy with the filter width in the integrable case does not substantially differ from those described in subsections 4.3.1 and 4.3.3. However, local observables can exhibit qualitative differences, as illustrated in figures 4.10.

Figure 4.10 shows the convergence of a local observable $\langle \sigma_x \rangle$ at the middle of the chain as a function of the inverse width $1/\delta$, for two different initial states $|X+\rangle$ and $|Z+\rangle$. In both cases, the limit of the time averaged observable noticeably differs from the thermal value, as we have checked using exact diagonalization for system sizes $N \leq 20$. Applying our algorithm to these and also larger system sizes, indeed suggests convergence of the observable to values that are distinct from thermal equilibrium (indicated by dashed horizontal lines).

4.5 Discussion

We have presented a method to approximate the diagonal ensemble corresponding to a quantum many-body state. By applying a Gaussian filter to the density operator, the off-diagonal components in the energy basis are suppressed and, in the limit of vanishing filter width, the result converges to the ensemble that represents the long time average of the time evolved state. For a Hamiltonian with non-degenerate spectrum, this is the diagonal ensemble.

Numerically, the filter can be approximated by a Chebyshev polynomial series, and applied using MPS standard techniques, in an analogous manner to what was already described in Ref. [115] for an energy filter. In our case, we obtain a MPO approximation to the filtered ensemble.

The method allows us to treat larger systems than exact diagonalization. However our results for small systems indicate that the operator space entanglement entropy of the diagonal ensemble scales as a volume law, which limits the system sizes for which the MPO can provide a reliable approximation. Still, we are able to simulate the effect of filters with moderate off-diagonal width and to analyze the convergence of local observables towards the thermal equilibrium.

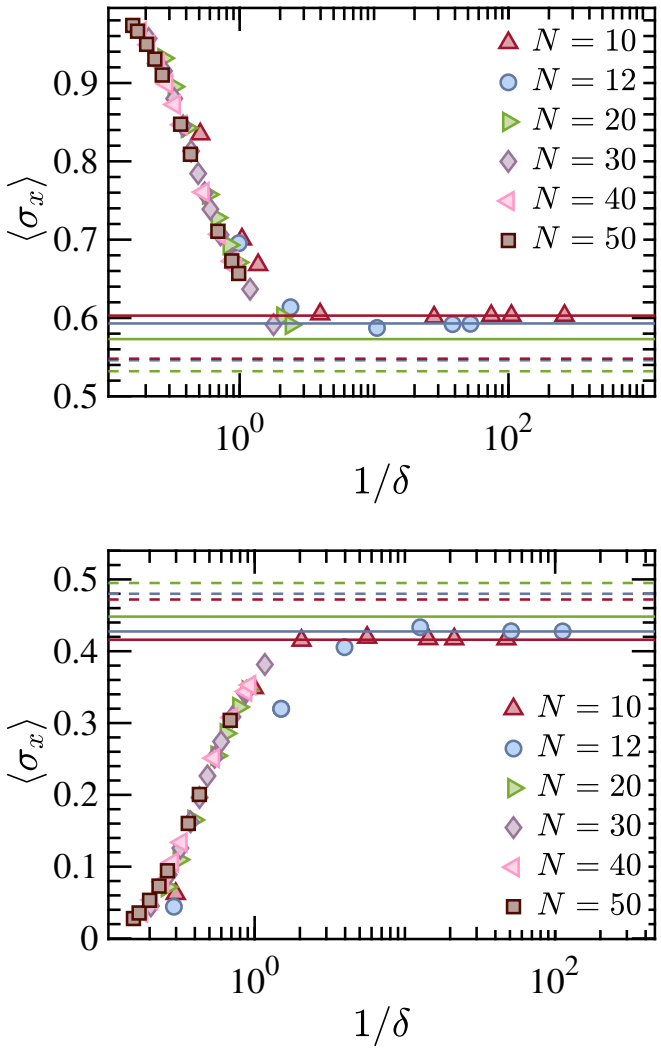

Figure 4.10: Expectation value of local observables σ_x at the middle of the chain based on Chebyshev filter simulations for initial states $|X+\rangle$ (upper) and $|Z+\rangle$ (lower figure) as a function of inverse off-diagonal width for system sizes $N = 10 - 50$. Red, blue and green solid lines indicate the long time average values for $N = 10, 12, 20$ respectively. Red, blue and green dashed lines indicate the thermal values for the same system sizes $N = 10, 12, 20$ respectively, belonging to the same color map in the legend.

We have applied this method to a non-integrable spin chain and several out of equilibrium product initial states for system sizes up to $N = 60$. We have numerically observed that local observables converge towards their thermal values as a power of the inverse off-diagonal width. Remarkably, this behavior is mostly independent of the system size. Even for moderate off-diagonal widths, the method provides in this way insight beyond exact diagonalization. In the future, it can be thus used to explore other one-dimensional models.

It is worth noticing that our procedure does not directly target the diagonal

ensemble, but the limit of the time-averaged state. In an integrable case this can be a generalized Gibbs ensemble, and differ considerably from the thermal equilibrium one (see e.g. [117, 118, 261]). For an integrable instance of the model, we have explicitly shown how local observables in the filtered state can indeed converge to values far from thermal equilibrium. A detailed analysis of integrable cases requires however more precise simulations than the ones shown here, which we will be presenting the further analysis in the following Chapter 5.

Chapter 5

Filtering with alternative tools

This chapter contains our unpublished work in which we study the dynamics of out-of-equilibrium systems, approximating the expectation values in the diagonal ensemble with the use of another novel method to perform the numerical simulations efficiently. In addition, we discuss whether this approach gives advantages for further investigations of relevant questions such as, how to characterize the diagonal ensembles independent of models. We include our preliminary studies in this regard, in which many of the results are work in progress, and have been tested for small system sizes, benchmarks and initial investigations, hoping that they can be useful for further inquiries.

In the first part of this chapter, we present another tool which can be employed as an alternative approach to the Chebyshev method used in our previous work [262] which we introduced in Chapter 4, with the purpose of computing the expectation values by explicitly constructing a MPO description for diagonal ensemble. Here, instead of obtaining a tensor network approximation of the diagonal ensemble, we make use of a more efficient way which only targets the expectation value of observables. More precisely, we take a Gaussian filter as before, but numerically approximate this filter by different means than Chebyshev expansions. Inspired by recent works [115, 128], we use the Cosine filter to approximate the effect of the Gaussian filter, which allows for computations that directly focuses on the expectation values using the same filtering idea. We analyze the convergence of local observables to their steady state values, in order to study the thermalization of different systems. Compared to the standard time-evolution and our previous approach by Chebyshev expansions (see Chapter 4), this alternative approach promises cheaper computational cost in the numerics in particular for calculation of expectation values.

In the second part of this chapter, we make use of this efficient method to explore certain questions, in particular, how to distinguish the diagonal ensemble in generic and non-ergodic scenarios. Moreover, we evaluate whether their interesting short-time dynamics are detectable by our filtering procedures. We finalize this part by providing our initial investigations and benchmarks, which should be explored further in future.

5.1 Approximation by the Cosine filter

The approach we present here is based on the one described in Chapter 4, with the combination of the Cosine filter approach which is also considered by the recent works [115, 128]. First, we consider a Gaussian filter of the Hamiltonian commutator, $H_C[\rho] = H\rho - \rho H$, as formerly in Sec. 4.1. We apply the filter on the initial density matrix, in order to suppress the off-diagonal elements, which results in the diagonal ensemble given in Eq. 4.2,

$$F(H_C;\delta)[\rho] := e^{-H_C^2/2\delta^2}[\rho]. \tag{5.1}$$

Second, in order to approximate this Gaussian filter above (Eq. 5.1), we consider the Cosine filter as an alternative to the Chebyshev expansions. The idea of the Cosine filter uses the fact that

$$e^{-MX^2/2} \simeq \cos^M(X),$$

for $|X| < 1$ and even number of M, which can be further approximated, as in [113], by the expansion

$$\cos^M(X) \simeq \sum_{m=-M}^{M} c_m e^{-i2mX} \simeq \sum_{m=-\lfloor x\sqrt{M}\rfloor}^{\lfloor x\sqrt{M}\rfloor} c_m e^{-i2mX}, \tag{5.2}$$

where x is a real constant and the coefficients c_m are given by

$$c_m = \frac{1}{2^M}\begin{pmatrix} M \\ M/2 - m \end{pmatrix}.$$

The sum above can be restricted to $-\lfloor x\sqrt{M}\rfloor \leq m \leq \lfloor x\sqrt{M}\rfloor$ as written in Eq. 5.2 where $\lfloor\cdots\rfloor$ gives the closest even integer with the error scaling as a Gaussian function of x. With a suitable choice of $x = O(1)$, the error can be made arbitrarily small. Then, the Gaussian filter in our case as given in Eq. 5.1 can be approximated by adapting $X = H_C/\alpha$ in Eq. 5.2,

$$F(H_C;\delta) \simeq \cos\left[H_C/\alpha\right]^M \simeq \sum_{m=-R}^{R} c_m e^{-i2mH_C/\alpha}, \tag{5.3}$$

where $\alpha = O(N)$ that rescales the Hamiltonian commutator such that its spectrum lies in one period $(\pi/2)$ of the Cosine function [1], $M = \alpha^2/\delta^2$ and $R = x\alpha/\delta$. The difference between our application of Cosine filter with the reference works [115, 128] enters here, where we take $X = H_C/\alpha$, instead of $X = (H - E)/\alpha$, since we use a Gaussian filter with Hamiltonian commutator as indicated in Eq. 5.1 instead of filtering over only the Hamiltonian by itself. Then, the Cosine filter in Eq. 5.3 can be expressed in terms of the evolution operator $e^{-iH_C t}$ for certain times t,

$$\sum_{m=-R}^{R} c_m e^{-i2mH_C/\alpha} \simeq \sum_{m=-R}^{R} c_m e^{-iH_C t_m} = P_\delta, \tag{5.4}$$

[1] The approximation holds in fact for the range beyond that too, see reference [128] for details.

where $t_m = 2m/\alpha$ with a time step $2/\alpha$.

Thus, we denote the result of applying the filter (Eq. 5.4) to a vectorized initial density matrix $|\rho_0\rangle = |\Psi_0\rangle \otimes |\overline{\Psi}_0\rangle$ as

$$|\rho_\delta\rangle := P_\delta \, |\rho_0\rangle \,, \tag{5.5}$$

which can be written more explicitly as

$$\begin{aligned} |\rho_\delta\rangle &= \sum_{m=-R}^{R} c_m e^{-iH_C t_m} \, |\rho_0\rangle = \sum_{m=-R}^{R} c_m e^{-i(H\otimes\mathbb{1}-\mathbb{1}\otimes H^T)t_m} \, |\Psi_0\rangle \otimes |\overline{\Psi}_0\rangle \\ &= \sum_{m=-R}^{R} c_m (e^{-iHt_m} \, |\Psi_0\rangle \otimes e^{iH^T t_m} \, |\overline{\Psi}_0\rangle) \\ &= \sum_{m=-R}^{R} c_m (e^{-i2mH/\alpha} \, |\Psi_0\rangle \otimes e^{i2mH^T/\alpha} \, |\overline{\Psi}_0\rangle). \end{aligned} \tag{5.6}$$

This expression (Eq. 5.6) reveals the key difference from the previous approximation by Chebyshev expansions, which we will discuss in the following section in detail.

5.1.1 Computation of local observables

We now consider how the calculation of the expectation value of local observables differs from the former approach based on the Chebyshev expansions. The Gaussian filter which needs to be approximated is essentially the same for both procedures with Chebyshev and Cosine filters as they share the fundamental properties [115] attaining the similar scaling $\delta \propto N/M$. However, approximating the Gaussian of Hamiltonian commutator with Cosine filter provides more efficient computations since it leads to simpler terms and allows evolving a pure state (see Eq. 5.6) in contrast to the Chebyshev filter, in which the diagonal ensemble is described by an MPO and the expectation value of local observables are computed by the contraction of the vectorized form of filtered density operator and observables (see Section 4.1.2 and Eq. 4.8).

Here, the expectation value of local observables of the filtered state are computed by applying Eq. 5.6, which gives

$$\mathrm{tr}\,(OP_\delta[\rho_0]) = \sum_{m=-R}^{R} c_m \langle\Psi_0| \, e^{i2mH/\alpha} O e^{-i2mH/\alpha} \, |\Psi_0\rangle. \tag{5.7}$$

We will denote

$$b_{O,m} = \langle\Psi_0| \, e^{i2mH/\alpha} O e^{-i2mH/\alpha} \, |\Psi_0\rangle.$$

Summing over all m provides the final expectation value of observables

$$\langle O\rangle_\delta = \frac{\mathrm{tr}(OP_\delta[\rho_0])}{\mathrm{tr}(P_\delta[\rho_0])} = \frac{\sum_m c_m b_{O,m}}{\sum_m c_m}, \tag{5.8}$$

where the normalization factor is simply the sum of c_m coefficients, because the filtering operation is trace preserving.

5.1.2 Numerical results

The advantage of the result of Cosine filter given in Eq. 5.8 is that it describes the evolution of pure states only. In the previous construction, the Chebyshev polynomials $T_m(H_C)$ with commutator superoperator H_C are acting on the vectorized (i.e., with double physical indices) density matrices (also see Section 4.1.1 and 4.2.1). On the other hand, the Cosine filter gives a 2^N reduction in problem complexity via evolution of pure states. Thus, this new construction allows us to represent the evolution operator directly with the system's Hamiltonian as a MPO [51, 84, 88] and represent the initial state using standard MPS methods [39, 48] in order to simulate the evolution as above, giving a computational advantage.

In the following, we compare the exact and numerical results based on Chebyshev and Cosine filters comparatively, make cross-checks for both non-integrable and integrable cases, starting with all initial states considered before in Section 4.2.2.

Non-integrable case: Ising chain

We present one particular case here in Fig. 5.1, for the non-integrable Ising model which is also considered in the previous chapter for Chebyshev filter based calculations:

$$H_{\text{Ising}} = J \sum_i \sigma_z^{[i]} \sigma_z^{[i+1]} + g \sum_i \sigma_x^{[i]} + h \sum_i \sigma_z^{[i]}. \tag{5.9}$$

with the same parameter choice $(J, g, h) = (1, -1.05, 0.5)$ to compare one-to-one with Chebyshev filter calculations. We analyze the convergence of local observable σ_x at the middle of the chain with decreasing width δ, starting from the initial state $|X+\rangle$. Comparison of our former data set based on Chebyshev filter (light colors) with the one discussed here with Cosine filter (colors) is given in Fig. 5.1, showing that we reproduce exactly the same evolution as in Fig. 4.3 for small systems and Fig. 4.4 for large system sizes.

Here we take notice of a couple of points on the results of Chebyshev and Cosine filters. First, the computational cost of the Cosine filter is lower than the previous method based on Chebyshev expansions due to the fact that here we start from pure states instead of starting from mixed states. Hence the computations here require 2^N dimensional vector space in exact results instead of 2^{2N} which is demanded by the Chebyshev approach.

Second, both filters are expected to give quantitatively the same results which we have also illustrated in Fig. 5.1, since they are not two different filter strategies, but two different approximations of the same Gaussian filter which suppresses the off-diagonal terms and converges to the diagonal ensemble. In addition to reproducing the previous results, we show that one can go beyond the former data (lighter data points in Fig. 5.1) and analyze the regime for much smaller δ values with less computational effort (clear data points in Fig. 5.1).

Furthermore, we have here the same interesting observation as given by the Chebyshev results that the local observable values for all system sizes fall on top of each other, converging all to their thermal values as the inverse off-diagonal width increases.

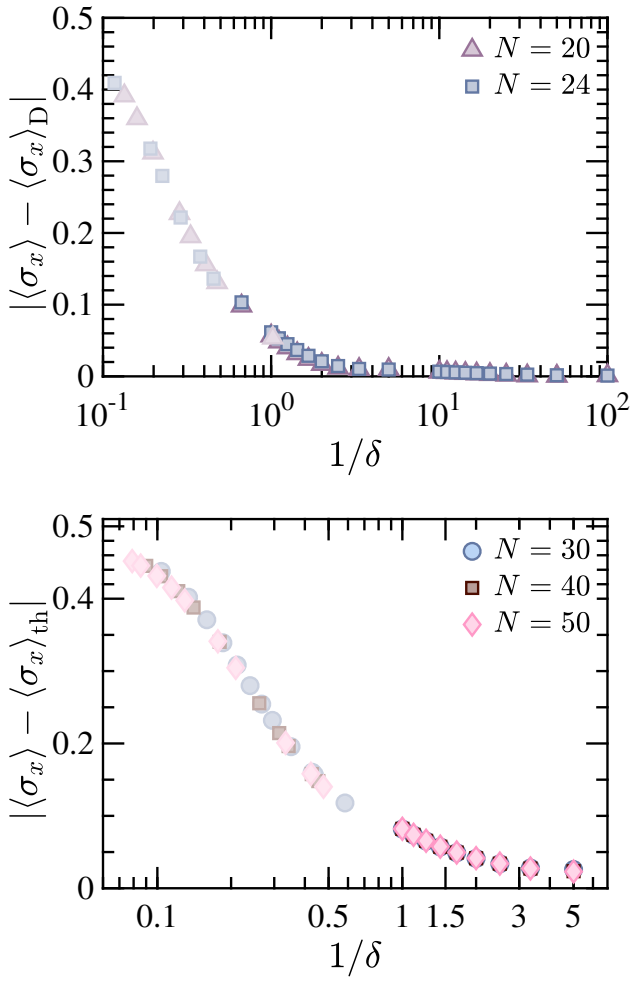

Figure 5.1: Absolute error in expectation value of local observables σ_x between filtered results and exact diagonal ensemble values for small system sizes in the upper figure and thermal values for larger system sizes in the lower figure as a function of inverse off-diagonal width, starting with initial state $|X+\rangle$. The color map and lighter colored data points are exactly the same as the ones introduced in upper Fig. 4.3 and Fig. 4.4 in Section 4.3.2. The same but non-transparent colors indicate our new results with Cosine filter, which is seen that we can draw beyond the previous data set since the new approach allows us to analyze further with lower computational cost.

As discussed in detail in Section 4.3.2, it is possible to reach the exact values for system sizes $N \leq 24$ and we can compute the absolute errors between the filtered and diagonal values (upper Fig. 5.1). However, there is no such access to the corresponding diagonal values for larger system sizes. Nevertheless, we can compute the variation of the expectation values taking the thermal values as reference since the thermal expectation values are expected to be very close to the diagonal ones in non-integrable models (lower Fig. 5.1). For large systems, although our simulations with both approximations do not seem to reach full

convergence, we show that it is possible to improve and reach to much narrower widths with Cosine filter where the absolute error is considerably small.

Integrable case: XXZ chain

Here we consider an integrable instance of the XXZ chain and illustrate our results in Fig. 5.2. The addition of this study to the preivous study of the non-integrable case provides a more conclusive test of our method since in this model, the diagonal ensemble results do not agree with the thermal ones, but converge to the corresponding GGE values [117, 118, 263]. Note that our filtering technique targets the long time limit, and this limit can be a GGE in the case of an integrable model. Therefore, integrable models can also be studied with our procedures.

Compared to the integrable case of Ising model which we have studied in the previous chapter (in Section 4.4), we include here some of our results for a more complicated integrable model and a different initial state as studied in [263]. This corresponds to the Hamiltonian,

$$H_{\mathrm{XYZ}} = \sum_i \left(J_x \sigma_x^{[i]} \sigma_x^{[i+1]} + J_y \sigma_y^{[i]} \sigma_y^{[i+1]} + \Delta \sigma_z^{[i]} \sigma_z^{[i+1]} \right) + h \sum_i \sigma_z^{[i]}. \tag{5.10}$$

We choose for our comparison the same range of parameters as studied in [263]. In particular, Fig. 2 of [263] explicitly shows results of local, nearest neighbor correlations, $\sigma_z^{[i]}\sigma_z^{[i+1]}$, and next-nearest neighbor correlations, $\sigma_z^{[i]}\sigma_z^{[i+2]}$, for Hamiltonian parameters $(J_x, J_y, \Delta, h) = (1, 1, [1, 2, 4, 8], 0)$, and initial state

$$\left(|\uparrow\downarrow\uparrow\downarrow \ldots\rangle + |\downarrow\uparrow\downarrow\uparrow \ldots\rangle \right) / \sqrt{2} \tag{5.11}$$

For this particular set of parameters, the long time average of the expectation value of these correlators was shown to converge to the Bethe ansatz predictions as the system size increases for all Δ values.

Fig. 5.2 shows the results of our simulations for the same case with solid dots. We observe that our filter results agree with the exact diagonalization results approaching to the Bethe ansatz predictions for both local correlations with increasing system size and they are quantitatively in agreement with those in Fig. 2 in Ref. [263].

Based on our numerical experiments for several different models and initial states, we conclude that the alternative approach introduced in this chapter can allow us to conduct more detailed analyses of other interesting and more complex models as well. Further preliminary research in this regard is given in the following section.

5.2 Characterization of the diagonal ensemble using filters

Two different filtering approaches have been presented by now with the motivation to find efficient tensor network approximations, targeting thermalization and

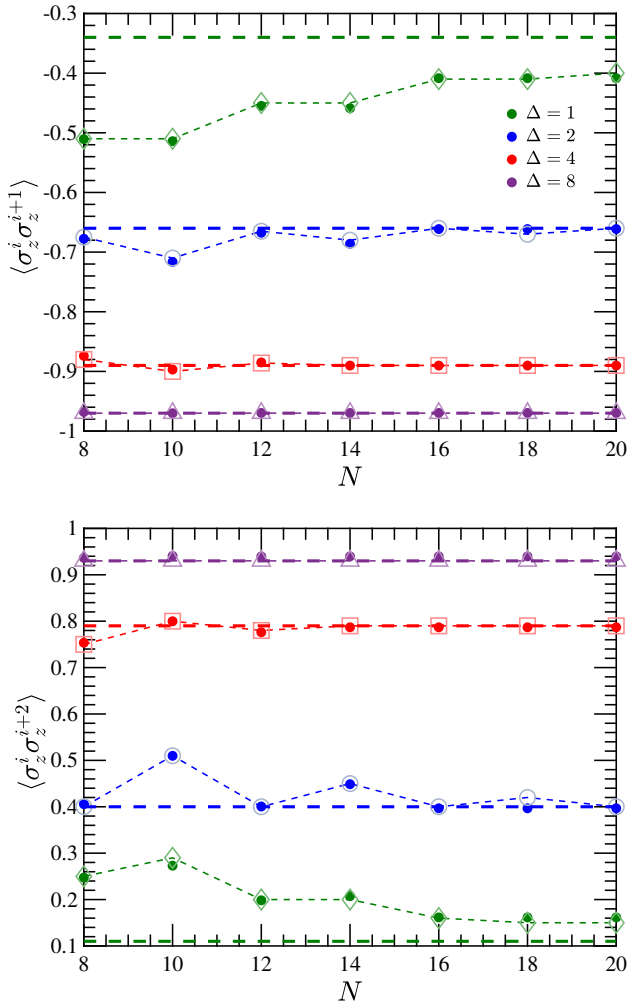

Figure 5.2: Local (two-site), nearest neighbor, $\sigma_z^i \sigma_z^{i+1}$, and next-nearest neighbor correlators, $\sigma_z^i \sigma_z^{i+2}$, as a function of system size, N, for different anisotropy parameters $\Delta = 1, 2, 4$ and 8, starting with a particular superposition state, as in the ref. work [263]. Our filter results are shown with solid dots while the exact diagonalization (empty symbols) and GGE (dashed lines) data are based on the results in Ref. [263].

equilibration dynamics. Accordingly, we have analyzed both nonintegrable and integrable regimes. Primarily, we have been concerned with the most generic case, when there are no degeneracies in the spectrum (i.e., the nonintegrable case). However, we have also noted that our filtering procedures lead us to the correct limit even if there are degeneracies, since the coherences in the corresponding energy subspace will remain untouched by the filtering.

At this point, the natural follow-up question is whether one can characterize these degeneracies with the help of the filtering technique, and hence distinguish the generic and non-ergodic scenarios.

Another question that follows is, in addition to exploring thermalization to the

Gibbs ensemble in nonintegrable models and equilibrium to the GGE's in integrable models, whether the filtering procedure we introduced is sensitive enough to detect interesting dynamical behaviours of different systems as well.

5.2.1 Incoherent and Coherent Averages

The purpose of this section is to give preliminary insights on these questions. First we start by introducing the expectation value of local observables in *coherent* and *incoherent averages* using our filtering idea which are convenient for formulating general Hamiltonian dynamics independent from the model. After briefly discussing these approaches, we test and compare them with the Cosine filter, also called *direct filter* since the Cosine filter is diagonal in energy eigenbasis and directly converges to the diagonal ensemble in the limit of vanishing width. Finally, we provide some of our preliminary results for a near-integrable Ising model and a PXP model.

Let us start by considering a system governed by a (local) Hamiltonian H, and a pure initial state $|\psi\rangle$ for which we are interested in approximating the long-time averaged expectation value of a given physical observable O,

$$\begin{aligned}\overline{O} &= \lim_{T\to\infty}\frac{1}{T}\int_0^T dt\langle\psi(t)|O|\psi(t)\rangle \\ &= \lim_{T\to\infty}\frac{1}{T}\int_0^T dt\sum_{k,k'} c_k c_{k'}^* e^{iE_{k'}t}e^{-iE_k t}\langle k'|\,O\,|k\rangle \\ &= \sum_{k,k',E_k'=E_k} c_k c_{k'}^*\langle k'|\,O\,|k\rangle\,, \end{aligned} \tag{5.12}$$

where k indexes are the energy eigenbasis. Here, we propose approximating this long-time averaged value with the following definitions which are targeting the degeneracies in the system, and are computable with the help of filtering techniques:

1. Incoherent Average

If there are no degeneracies in the spectrum (i.e., in the generic case), the long-time averaged expectation value above (Eq. 5.12) is given by the expectation value in the diagonal ensemble:

$$\overline{O} = O_\psi^{DE} \equiv \sum_k \langle k|\,O\,|k\rangle\,|\,\langle k|\,\psi\rangle|^2 \tag{5.13}$$

with $\langle k|\,O\,|k\rangle = O(E_k)$, and can be approximated by the use of the filtering idea as follows:

$$O_{\psi,\delta}^{DE} = \int dE \frac{\mathrm{tr}\left(OP_\delta^{(H)}(E)\right)}{\mathrm{tr}\left(P_\delta^{(H)}(E)\right)} \quad \langle\psi|P_\delta^{(H)}(E)|\psi\rangle, \tag{5.14}$$

where,

$$P_\delta^{(H)}(E) = \sum_{m=-R}^{R} c_m e^{-i(H-E)t_m}. \tag{5.15}$$

Note that the evolution operator in Eq. 5.15 is not defined with Hamiltonian commutator as formerly used in our filter. Instead, the Gaussian filter here is taken directly with Hamiltonian of the system $F(E;\delta) := e^{-(H-E)^2/2\delta^2}$ as introduced in [114, 115, 249], and Eq. 5.15 is the consequence of approximating this Gaussian by the Cosine filter in a similar way as introduced in the previous section (see Section 5.1).

The first term in the above integral (Eq. 5.14) gives the average expectation value of O over all states with the same energy $^{\mathrm{tr}\left(OP_\delta^{(H)}(E)\right)}/_{\mathrm{tr}\left(P_\delta^{(H)}(E)\right)} = O(E)$ and the second term gives the weight $\langle\psi|P_\delta^{(H)}(E)|\psi\rangle = \sum_{k,E_k=E}|c_k|^2$ in the $\delta \to 0$ limit, which are equivalent to the terms in the expectation value in diagonal ensemble in Eq. 5.13. The result converges to the exact diagonal value as $\delta \to 0$. We call this expression (Eq. 5.14) the *Incoherent Average*, which coincides with the diagonal ensemble when there is no degeneracy in the spectrum, i.e., sensible for the nonintegrable models. However, if there were degeneracies, then this expression would give something different: it would be the average over $\langle E_n|\,O\,|E_n\rangle$ for each energy, multiplying by the total weight at that energy $\sim \sum_{k,E_k=E}|\,\langle\psi|\,E_k\rangle|^2$.

2. Coherent Average

If the spectrum is degenerate, using the same filter above (Eq. 5.15) we can estimate the long-time averaged limit of expectation values which is also discussed in Ref. [114] based on Chebyshev filter. Similarly, in the $\delta \to 0$ limit, the time-averaged expectation value of O in the degenerate case can then be approximated by the following expression using the filter as

$$O_{\psi,\delta} = \frac{\int dE\langle\psi|P_\delta^{(H)}(E)OP_\delta^{(H)}(E)|\psi\rangle}{\int dE\ \langle\psi|{P_\delta^{(H)}}^2(E)|\psi\rangle} \equiv \int dE\bar{O}(E). \tag{5.16}$$

Here, the *coherent average* (Eq. 5.16) is expected to converge to the true long time limit as $\delta \to 0$ in any case:

$$\begin{aligned}\lim_{\delta\to 0}\langle\psi|P_\delta^{(H)}(E)OP_\delta^{(H)}(E)|\psi\rangle &= \sum_{k,k'}\sum_{E_k=E_{k'}=E}\langle\psi\,|E_k\rangle\,\langle E_{k'}|\,\psi\rangle\,\langle k|\,O\,|k'\rangle \\ &= \sum_{k,k'} c_k c_{k'}^* O_{kk'}\end{aligned}$$

If there was no degeneracy, then it would result in the diagonal ensemble form $(\sum_k |c_k|^2 O_{kk})$ which is also obtained from the incoherent average (Eq. 5.14) in the limit of vanishing width.

3. Comparison to true long-time limit

Our purpose here is to compare incoherent and coherent averages, which are introduced in the previous subsections, with the true long-time limit. To do so, we recall the Cosine filter we studied in the previous section which applies the

Gaussian filter with Hamiltonian commutator, and converges to the *true* diagonal value as $\delta \to 0$:

$$O_\delta = \frac{\mathrm{tr}(OP_\delta[\rho_0])}{\mathrm{tr}(P_\delta[\rho_0])}. \tag{5.17}$$

In the limit of vanishing width, Eq. 5.17 should agree with the coherent average value given in Eq. 5.16, while they are not necessarily expected to agree for larger δ values: consider the initial state $|\psi\rangle = \sum_k c_k |k\rangle$ in its energy eigenbasis with the normalization condition $\sum_k |c_k|^2 = 1$, and for a given any physical observable $O = \sum_{k,l} O_{kl} |k\rangle \langle l|$, the following relation holds for direct filter:

$$\mathrm{tr}(OP_\delta[\rho_0]) = \sum_{k,l} c_k c_l^* O_{kl} e^{-(E_k - E_l)^2/2\delta^2}. \tag{5.18}$$

As for the coherent average case from Eq. 5.16:

$$\int dE \langle\psi|P_\delta^{(H)}(E) O P_\delta^{(H)}(E)|\psi\rangle = \sum_{k,l} \int dE\ c_k c_l O_{kl} e^{-(E_k - E)^2/2\delta^2} e^{-(E_l - E)^2/2\delta^2}.$$

By changing the variable $E' := E_l - E$:

$$\int dE \langle\psi|P_\delta^{(H)}(E) O P_\delta^{(H)}(E)|\psi\rangle = \sum_{k,l} \int dE'\ c_k c_l^* O_{kl} e^{-(E' - (E_k - E_l))^2/2\delta^2} e^{-E'/2\delta^2}. \tag{5.19}$$

Eq. 5.18 and Eq. 5.19 do not result in the same quantity, however they converge to the same value (true long time) in the limit of $\delta \to 0$.

5.2.2 Models and Results

Here, we numerically investigate how all three quantities listed above differ at finite δ, which we can compute with the same effort using the exact filter. We test these quantities with our filters not only in the generic scenarios, but also non-ergodic (non-thermalizing) scenarios. Thus, in this part we present our study on different models including the PXP model and near-integrable Ising model to analyze whether our filters can distinguish and capture their interesting dynamical behaviours e.g. prethermalization and scars beyond the direct thermalization and equilibrium dynamics on a single time scale.

PXP model

Here we start with the PXP model,

$$H_{\mathrm{PXP}} = \sum_{i=2}^{N-1} P_{i-1} \sigma_x^{[i]} P_{i+1} + \sigma_x^{[1]} P_2 + P_{N-1} \sigma_x^{[N]}, \tag{5.20}$$

which is a constrained model in a Rydberg chain realized in a recent experiment [264] and its non-thermal eigenstates have been dubbed *quantum scars*.

It has been observed in this experiment [264] that PXP dynamics reveal unexpected behaviours depending on the initial states. While some specific initial

states showed relaxation to thermal ensembles, as expected in an ergodic system, some other states exhibited periodic revivals.

Similarly, in the recent numerical studies of the quench dynamics, such revivals of the wave function and local observables have been demonstrated when the system is quenched from initial $|Z_2\rangle \equiv |\uparrow\downarrow\uparrow\downarrow\ldots\rangle$ and $|Z_3\rangle \equiv |\uparrow\downarrow\downarrow\uparrow\downarrow\downarrow\ldots\rangle$ states [265, 266], contrary to the other initial states, such as $|0\rangle \equiv |\downarrow\downarrow\downarrow\ldots\rangle$ and $|Z_4\rangle \equiv |\uparrow\downarrow\downarrow\downarrow\uparrow\ldots\rangle$, which exhibit fast relaxation without revivals [123]. Furthermore, it has been postulated [123, 259, 267] that the large overlap of these $|Z_2\rangle$ and $|Z_3\rangle$ states with scar states causes the slow dynamics, and these states sit in the middle of the spectrum ($E = 0$) which has an exponentially large degeneracy. In this case, the incoherent average (Eq. 5.14) might not necessarily be a good estimation of long time limit.

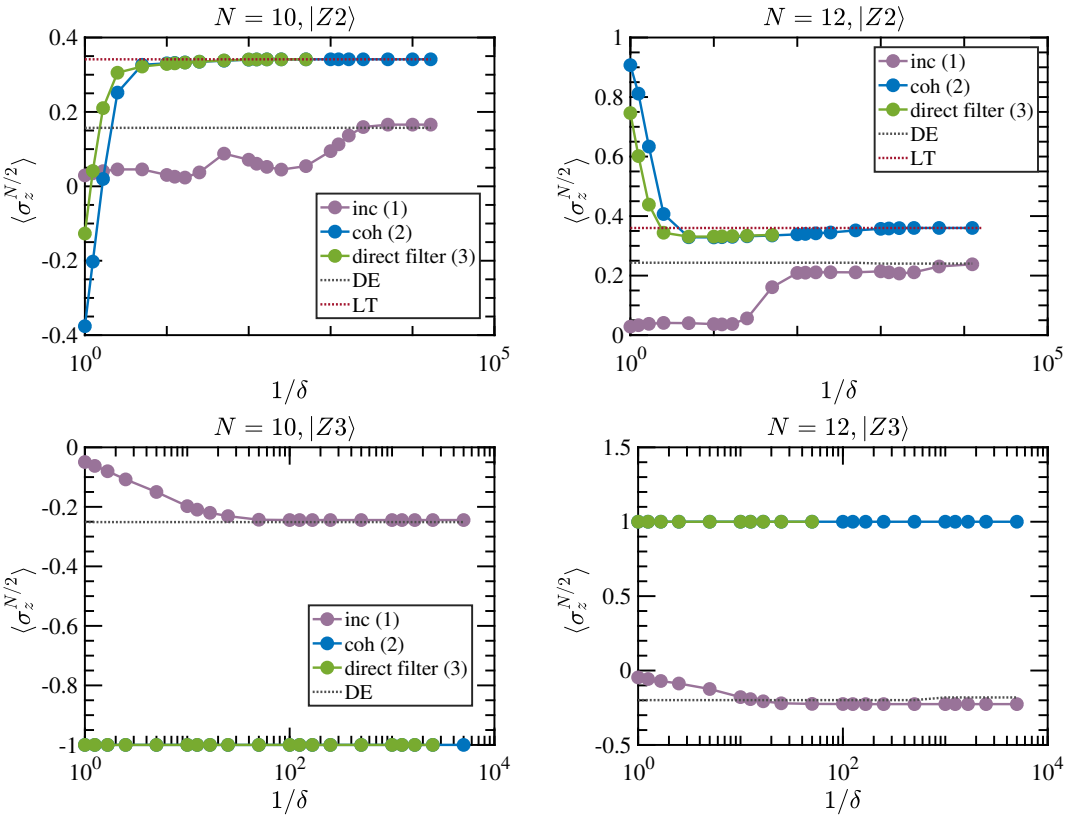

Figure 5.3: **PXP model:** the expectation value of local observables σ_z in the middle of the chain as a function of the inverse width for system size $N = 10$ and $N = 12$, starting with initial states $|Z_2\rangle$ (upper) and $|Z_3\rangle$ (lower figures). Purple colors represent the incoherent average results (Eq. 5.14 in itemize 1), blue colors indicate the coherent average (Eq. 5.16 in itemize 2) while green ones show the direct filter (Eq. 5.17 in itemize 3) results. Red dashed lines indicate the corresponding long time average values and grey dashed lines represent the corresponding exact diagonal ensemble values.

Therefore, here we consider these two special initial states $|Z_2\rangle$ and $|Z_3\rangle$, to test and benchmark our approaches. In Fig. 5.3, we illustrate all the expectation

values which are itemized above in Section 5.2 as *incoherent average* (itemize 1: purple data), *coherent average* (itemize 2: blue data) and *direct filter* (itemize 3: green data) for system sizes $N = 10, 12$ and initial states $|Z_2\rangle$ (upper) and $|Z_3\rangle$ (lower figures) together with the long time average (red dashed) and exact diagonal ensemble values (grey dashed lines).

For both initial states, the results of coherent (blue) and direct filter (green) converge to the long time average value (red dashed) as expected (see Eq. 5.18 and Eq. 5.19), while the incoherent diagonal ensemble results are converging to the diagonal value (grey dashed lines). When there are degeneracies in the spectrum, the coherent average values (blue) are expected to converge to a value different from incoherent values (purple), which is observed in our calculations.

The results belonging to the initial state $|Z_2\rangle$ do not reach the full convergence even for $N = 12$ (upper right figure), and it seems that it takes extraordinarily long by starting to converge at around $1/\delta \sim 10^4$ compared to the initial state $|Z_3\rangle$. In the case of larger systems, this will take even longer, and we cannot expect to reach those times with MPS simulations. On the other hand, the results of the initial state $|Z_3\rangle$ converge relatively faster (lower figures), and MPS simulations for this case seem more feasible.

However, we believe that the difference should not only be the system size or initial state, and further checks such as spectral decompositions are needed to be monitored which may give more hint about the dynamics. We leave further investigations for future research, hoping that our preliminary study provides an initial insight and motivation.

Near-integrable case: Ising Model

Next we consider an instance of isolated near-integrable quantum many-body systems, in which dynamics have been studied extensively in experiments [24, 30, 243, 268–274]. In particular, a recurring subject has been the prethermalization phenomenon and its stability to perturbations [268, 273].

These experiments provided a new insight to test theoretical concepts. It has been postulated that in the presence of quasi-conserved quantities, an isolated system is expected to exhibit a two-step relaxation: before reaching thermal equilibrium, it is first expected to relax to a quasi-stationary state described by a GGE [15, 244, 275–279]. In the context of near-integrable systems, this behavior has been related to prethermalization [268]. After this intermediate relaxation, a slower relaxation to the thermal equilibrium is expected to happen [280].

This two-step relaxation in the dynamics can occur if the system's Hamiltonian consists of an unperturbed term and a perturbative term. The initial evolution is controlled by the unperturbed Hamiltonian and the prethermal state is defined by its equilibrium state. The perturbation leads to a subsequent slow relaxation to the thermal equilibrium of the perturbed Hamiltonian. However, it cannot be expected that every perturbation will result in a two-step relaxation process since splitting any Hamiltonian into two parts as unperturbed and perturbative is possible in arbitrary ways. Therefore, the unperturbed Hamiltonian should have a distinctive feature that clearly distinguishes it from the system's total

(perturbed) Hamiltonian, so that the prethermal and thermal relaxation regimes become qualitatively different [15, 244, 276, 281–283].

One of the well-studied setups to understand the prethermalization phenomenon in near-integrable systems is when the unperturbed Hamiltonian is given by an integrable model, while the perturbative term is expressed by an integrability-breaking perturbation [15, 244, 276, 281–283]. In this case, the prethermal state is not a thermal state due to the extensive set of conserved quantities of integrable (unperturbed) Hamiltonian, but it is described by a GGE [17, 59, 120, 272]. The perturbation with the integrability breaking causes a slow relaxation from the GGE to the thermal equilibrium of total Hamiltonian [19, 274, 280, 281, 284].

Here we use the Ising chain with both longitudinal and transverse fields, which we studied in Section 4.2.2 (Eq. 4.13) and Section 5.1 (Eq. 5.9)

$$H_{\text{Ising}} = J \sum_i \sigma_z^{[i]} \sigma_z^{[i+1]} + g \sum_i \sigma_x^{[i]} + h \sum_i \sigma_z^{[i]}, \tag{5.21}$$

now with a different parameter choice such that it fits into the category defined above: we consider the unperturbed Hamiltonian, i.e., integrable model by taking the parameters as $(J, g, h) = (-1, 0.8, 0)$, and the perturbative term with the integrability breaking with a weak perturbation in longitudinal field h as $(J, g, h) = (-1, 0.8, 0.08)$.

In Fig. 5.4, we use the same color map as shown in PXP model, in order to illustrate all the expectation values computed by *incoherent average* (purple), *coherent average* (blue) and *direct filter* (green data) for system sizes $N = 10$ (upper) and $N = 12$ (lower figure) together with the long time average values for integrable (upper dashed lines) and near-integrable case (lower dashed lines). We observe that the results belong to the coherent average (blue) and direct filter (green) are slightly different for large δ values, and start agreeing as δ decreases as expected (given by the derivation in Eq. 5.18 and Eq. 5.19), while incoherent average values are converging slower to the long time limit, choosing a different path from the other two.

In addition, the coherent average (blue) seems to detect the intermediate regime showing a prethermal plateau, together with direct filter (green), which can be seen more clearly in the insets. We see that both values seem to relax to the long time limit of the integrable case $(J, g, h) = (-1, 0.8, 0)$ for a while (upper dashed lines in the insets) before reaching to the long time value of near-integrable case $(J, g, h) = (-1, 0.8, 0.08)$ (lower dashed lines in the insets). In contrast, the incoherent diagonal ensemble does not seem to capture the prethermal window. This is plausible since the incoherent average (given by Eq. 5.14) is expected to apply for the cases with non-degenerate spectrum by definition.

Our preliminary results show the filters' potential capabilities to answer different questions and detect interesting dynamics. While here we leave further analysis and numerical simulations for future works, in the following chapter we will be discussing how to adapt the filtering technique to the time-dependent systems with the purpose of exploring the prethermalization phenomenon there as well.

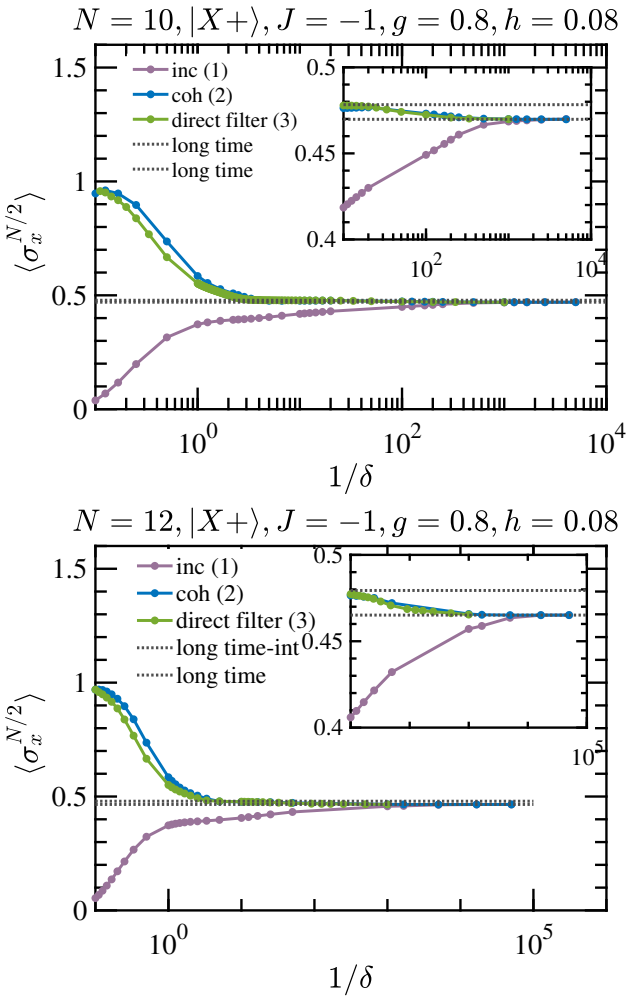

Figure 5.4: **Near-integrable Ising model:** expectation value of local observables σ_x at the middle of the chain as a function of the inverse width for system sizes $N = 10$ (upper) and $N = 12$ (lower figure), starting with initial state $|X+\rangle$. Purple colors represent the incoherent average results (Eq. 5.14 in itemize-1), blue colors indicate the coherent average (Eq. 5.16 in itemize-2) while green ones show the direct filter (Eq. 5.17 in itemize-3) results. Grey dashed lines belong to the long time average values of corresponding integrable case with parameters $(J, g, h) = (-1, 0.8, 0)$ (upper dashed) and near-integable case by a small perturbation with longitudinal field $(J, g, h) = (-1, 0.8, 0.08)$ (lower dashed line).

5.3 Outlook

We have presented an alternative way of approximating the expectation values in the diagonal ensemble by unifying two recent ideas given in [262] and [115, 128]: staying with the idea of the Gaussian filter with Hamiltonian commutator which was previously studied in Chapter 4, we have used another tool for our numerics to approximate the effect of Gaussian filter which provides more efficient computations,

allowing us to improve our understanding on thermalization and equilibration dynamics in different system.

First, we have presented the promise of replacing the previous approximation by Chebyshev polynomial series with the Cosine filter, in order to approximate the Gaussian filter and simulate for the similar Ising model to cross-check. Even if it is obvious that both approaches are expected to give quantitatively the same results, the new approach has improved our algorithm efficiency by replacing the evolution from mixed states to pure states. We have clearly demonstrated that this improvement allows one to simulate further regimes with the latter procedure (see Fig. 5.1).

Furthermore, we have tested this approach on a XXZ scenario, which has a higher computational cost than the Ising chain and requires even more computational effort in the former algorithm (Chebyshev filter). Additionally, we have preliminarily performed computations for different instances such as a near-integrable Ising and PXP model and concluded that this new tool allows us to examine other interesting models as well.

Later, we have discussed whether this method can be utilized to find answers for further questions. These questions have been related to characterizing diagonal ensembles and noticing interesting behaviours in the long time limit such as prethermalization and quantum scars concepts besides thermalization to Gibbs ensemble for nonintegrable models or equilibration to GGE's for integrable models. Accordingly, we have studied two different models in isolated systems which reflect different kinds of dynamics: prethermalization when breaking the integrability and quantum scars in PXP model. Our preliminary results have given hints that different dynamical behaviours in different models can indeed be detected by our filtering procedures, which considerably ease the numerical implementation with standard MPS techniques to treat and perform efficient simulations for larger systems.

Moreover, although all our results are computed for one-dimensional spin chains, these filtering procedures can in principle be applied to higher dimensions since they do not make any assumption on the spatial dimension of the problem.

We leave more detailed analyses for future works. Also, we hope that this inspires the search for other interesting approaches, that promise faster, but lower computational effort.

Part III

Prethermalization in Periodically Driven Systems

Chapter 6

Filtering for the Floquet diagonal ensemble

Most of the content of this chapter is being prepared for a publication:

- *"Filtering for the Floquet diagonal ensemble"*
  Sattwik Deb Mishra*, Aslı Çakan*, J. lgnacio Cirac and Mari Carmen Bañuls

In this chapter, our aim is to apply the efficient filtering technique, which is formerly introduced in Chapter 4 to approximate the diagonal ensemble and made use of in Chapter 5 for further investigations in time-independent systems, now to a time-periodic setting. The main motivation is to explore the filter's use to probe non-equilibrium dynamics of time-periodic systems by approximating the expectation values in *Floquet* version of diagonal ensemble which is previously outlined in Chapter 3.2.

In the first part of this chapter, we present a route how the filtering idea of the construction with the Hamiltonian commutator can be extended to the case of a periodic time-dependent system. We could in principle proceed analogously as introduced in Chapter 4, where the filtered state was explicitly constructed to obtain a tensor network approximation of the diagonal ensemble. Instead, we proceed with the more efficient approach which only targets observable expectation values as we discussed in Chapter 5, where we also examined its potential capabilities to answer different questions, including interesting short-time dynamics such as prethermalization. We adapt here a periodic version of a Gaussian filter and, using a Fourier transformation [1] of the filter, show that in the case of Floquet systems, expectation values at stroboscopic times (i.e., multiples of the time period of the Hamiltonian) can be used to approach the Floquet diagonal ensemble.

In the second part of this chapter, focusing on a non-integrable time-periodic system that exhibits Floquet ETH and prethermalization, we analyze how the filtered expectation value tends to the value in the diagonal ensemble as the filter width is decreased, and whether the convergence behavior of the filtered expectation value reveals a signature of the Floquet dynamical phenomenon of

[1] We notice that Fourier transform-based implementations of general functions of time-independent Hamiltonians to approximate their ground states have been studied before [285–287].

prethermalization. Finally, we conclude this part by summarizing our results and discussing potential extensions of our work.

6.1 Filtering for periodically driven systems

As outlined in Chapter 3.2, for a system described by a time-periodic Hamiltonian $H(t)$ with period T, the Floquet operator, i.e., the propagator over one time period T starting from $t = 0$, is defined as

$$U_T \coloneqq \mathcal{T} \exp\left(-i \int_0^T dt' H(t')\right), \tag{6.1}$$

and the Floquet Hamiltonian H_F is defined as the logarithm of the Floquet operator U_T,

$$\exp(-iH_F T) \coloneqq U_T. \tag{6.2}$$

Let $|\varepsilon_\alpha\rangle$ be the Floquet states — the eigenstates of the Floquet operator U_T with corresponding eigenvalues $e^{-i\varepsilon_\alpha T}$. The Floquet Hamiltonian H_F has the same eigenstates as U_T but its eigenvalues are not specified uniquely by Eq. (6.2); the eigenvalue of H_F corresponding to $|\varepsilon_\alpha\rangle$ can be $\varepsilon_\alpha + 2n\pi/T$, $\forall n \in \mathbb{Z}$. We consider the eigenvalues of the Floquet Hamiltonian, called the quasienergies, to lie in $[-\pi/T, \pi/T)$ with the understanding that the spectrum can be considered as having a period of $2\pi/T$.

For time-independent Hamiltonians, as described in Chapter 3.1 and Chapter 4, the diagonal ensemble for a given initial state is a density operator, diagonal in the Hamiltonian eigenbasis, with the same probability as the initial state for each energy eigenstate. Similarly, as described in Chapter 3.2 as well, the Floquet diagonal ensemble is defined in terms of the overlap of the initial state of the system $|\psi_0\rangle$ with the Floquet states $|\varepsilon_\alpha\rangle$ (as given by Eq. (3.8)),

$$\rho_\mathrm{DE} = \sum_\alpha |\langle\psi_0|\varepsilon_\alpha\rangle|^2 |\varepsilon_\alpha\rangle\langle\varepsilon_\alpha|. \tag{6.3}$$

In order to find efficient tensor network approximations for the expectation values in the diagonal ensemble, we have employed two different filtering procedures by now: the first procedure has been introduced in Chapter 4 to obtain an MPO approximation to the diagonal ensemble of a time-independent system, by applying a Gaussian filter of the Hamiltonian commutator to the initial density operator, to suppress the off-diagonal elements as

$$f(H_C; \delta) = e^{-\frac{H_C^2}{2\delta^2}}, \tag{6.4}$$

where $H_C \coloneqq [H, .]$ is the superoperator representing commutation with H. The effect of this filter is approximated by a series of Chebyshev polynomials, constructed

from the MPO representation of the Hamiltonian. The second procedure has been introduced in Chapter 5 in which the same Gaussian filter above in Eq. (6.4) is made use of but approximated by Cosine filter which leads to the computation that directly targets the expectation value of (local) observables. Here, for the Floquet scenario, we follow the same idea with the second procedure as we will be arguing in the following subsection, since it allows us to perform a similar filtering using only the well-defined evolution operator (see Section 5.1.1).

Based on the latter idea explained above, the expectation value of an observable O in the Floquet diagonal ensemble (given in Eq. (6.3)) can then be approximated by a similar way as explicitly given in Chapter 5.1, which results in the following quantity,

$$\langle O\rangle_\delta = \sum_{m=-\infty}^{\infty} c_m \langle\psi_0| U_T^{\dagger m} O U_T^m |\psi_0\rangle , \tag{6.5}$$

which is analogous of expression Eq. (5.7) in Chapter 5.1. In the expression above Eq. (6.5), c_m are Fourier series coefficients of a function $f_P(x;\delta)$ which is a $\frac{2\pi}{T}-$periodic summation of Gaussians of width δ:

$$\begin{aligned} &f_{\mathrm{P}}(x;\delta) \coloneqq \\ &\sum_{n=-\infty}^{\infty} e^{-\frac{(x-2n\pi/T)^2}{2\delta^2}} \mathcal{I}\left(\frac{(2n-1)\pi}{T} \le x < \frac{(2n+1)\pi}{T}\right) \\ &= \sum_{m=-\infty}^{\infty} c_m e^{-imTx}, \end{aligned} \tag{6.6}$$

where $\mathcal{I}(.)$ is the indicator function which is unity if its argument is true and zero otherwise.

6.1.1 Computation of local observables

To demonstrate the expectation value of local observables in Floquet case as given in Eq. (6.5) more explicitly, let us start by introducing the filtered state obtained by acting on the initial state with the following filtering superoperator,

$$\rho_\delta = f_P(H_{\mathrm{F,C}};\delta)\,[\rho_0] , \tag{6.7}$$

where $H_{F,C} \coloneqq [H_{\mathrm{F}}, .]$ is the Floquet Hamiltonian commutator, in which the filter construction here is reminiscent of the construction that we had in Chapter 5 (Section 5.1.1) with the difference that the filter function here is periodic in the first argument.

As $H_{\mathrm{F,C}}$ has eigenoperators $|\varepsilon_\alpha\rangle\langle\varepsilon_\beta|$ with corresponding eigenvalues $\varepsilon_\alpha - \varepsilon_\beta$, the filtered state can be written in the basis of Floquet states as,

$$\rho_\delta = \sum_{\alpha,\beta} f_P(\varepsilon_\alpha - \varepsilon_\beta;\delta)\langle\varepsilon_\alpha|\psi_0\rangle\langle\psi_0|\varepsilon_\beta\rangle|\varepsilon_\alpha\rangle\langle\varepsilon_\beta| . \tag{6.8}$$

The differences of quasienergies lie in the open range $(-2\pi/T, 2\pi/T)$, so the action of the filter Eq. (6.7) is to suppress terms in the sum above Eq. (6.8) that don't satisfy $\varepsilon_\alpha - \varepsilon_\beta \approx 0, \pm 2\pi/T$. Even though the Gaussian filter in here has extra peaks at $\pm 2\pi/T$ (as shown in Fig. 6.1), their contribution to the filtered state vanishes in the limit of vanishing width δ. The remaining effect is that of the central peak which precisely selects the diagonal terms and suppresses the off-diagonal ones.

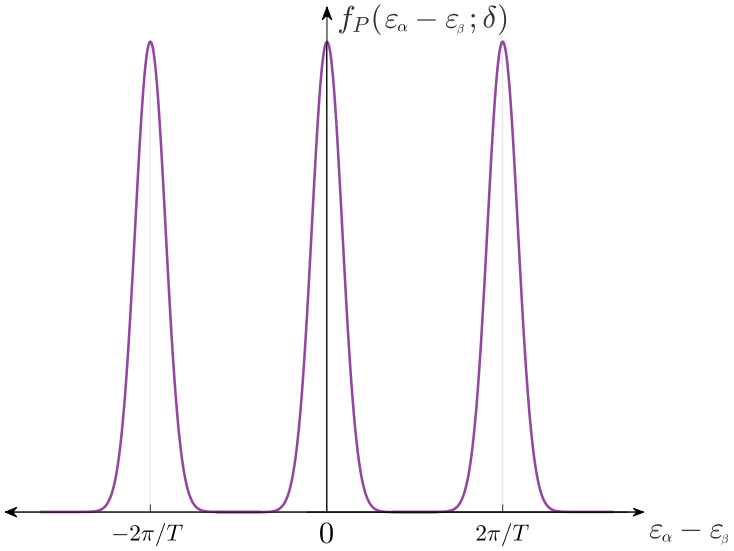

Figure 6.1: Periodic Gaussian filter function (Eq. (6.6)) of the superoperator $H_{\mathrm{F,C}} = [H_{\mathrm{F}}, .]$. $H_{\mathrm{F,C}}$ has eigenoperators $|\varepsilon_\alpha\rangle \langle\varepsilon_\beta|$ with corresponding eigenvalues $\varepsilon_\alpha - \varepsilon_\beta \in (-2\pi/T, 2\pi/T)$.

We now consider computing the expectation value of an observable in the filtered state. Using the action of the exponential of the commutator,

$$e^{-iH_{\mathrm{F,C}}mT}\rho = e^{iH_{\mathrm{F}}mT}\rho e^{-iH_{\mathrm{F}}mT}, \tag{6.9}$$

and the fact that the filtering operation is trace-preserving as in the time-independent case shown in Chapter 5.1, we obtain,

$$\begin{aligned}
\langle O\rangle_\delta &= \mathrm{Tr}\, O f_P(H_{\mathrm{F,C}}; \delta)\,[\rho_0] && (6.10)\\
&= \sum_{m=-\infty}^{\infty} c_m \langle\psi_0| e^{iH_{\mathrm{F}}mT} O e^{-iH_{\mathrm{F}}mT} |\psi_0\rangle\,, && (6.11)\\
&= \sum_{m=-\infty}^{\infty} c_m \langle\psi_0| U_T^{\dagger m} O U_T^m |\psi_0\rangle\,. && (6.12)
\end{aligned}$$

Thus, expectation values in the state filtered by the periodic version of the Gaussian filter can be calculated from the Floquet stroboscopic dynamics. As in Chapter 5.1, the calculation of expectation values in the filtered state can be done by just classical post-processing if each of the expectation values in the sum in Eq. (6.12) can be obtained from a quantum simulation.

As in the time-independent case, the expression above in Eq. (6.12) can be approximated well by truncating the sum to $-R \leq m \leq R$:

$$\langle O \rangle_\delta = \sum_{m=-R}^{R} c_m \langle \psi_0 | U_T^{\dagger m} O U_T^m | \psi_0 \rangle . \tag{6.13}$$

where the coefficients c_m are given by the same expression as formerly described in Chapter 5.1

$$c_m = \frac{1}{2^M} \begin{pmatrix} M \\ M/2 - m \end{pmatrix} . \tag{6.14}$$

Here, $M = 1/T^2\delta^2$, $R = x/T\delta$ and x is a real constant. The runtime of a quantum simulation to obtain the stroboscopic expectation values would be $2R$ steps [2], illustrating the tradeoff between runtime and filter width. Similar runtime-width dependencies have been studied in the case of time-independent systems in Chapter 5.1 as well as in the use of cosine filters in Refs. [288–290].

We point out here that in the time-independent case in Chapter 5.1, the Hamiltonian commutator in the Gaussian filter is rescaled by a factor α such that its spectrum is contained in one fixed period of the filter, while here in time-periodic case, the period is fixed by T and cannot be changed.

6.2 Numerical results

6.2.1 Model

We consider a periodically kicked Ising spin-chain [231, 291],

$$H(t) = \sum_{i=1}^{N} \boldsymbol{B}_i(t) \cdot \boldsymbol{\sigma}_i + \sum_{i<j}^{N} \sum_{\alpha,\gamma=x,y,z} J_{ij}^{\alpha\gamma}(t) \sigma_i^\alpha \sigma_j^\gamma, \tag{6.15}$$

where $\sigma_i = (\sigma_i^x, \sigma_i^y, \sigma_i^z)$ is the Pauli matrix of the ith spin, $\boldsymbol{B}_i(t)$ is the local magnetic field at the ith site, and $J_{ij}^{\alpha\gamma}(t)$ indicates the interaction between the ith and jth spins. Here we focus on one particular case which is studied in [231] with period T where the first half of the period is governed by $H(t) = H_z$ and the second half of the period is governed by $H(t) = H_x$. Explicitly, H_z and H_x are defined as follows,

$$H_z = \sum_{i=1}^{N} \left[-J\sigma_i^z \sigma_{i+1}^z + B_z \sigma_i^z \right] , \tag{6.16}$$

$$H_x = B_x \sum_{i=1}^{N} \sigma_i^x . \tag{6.17}$$

We choose Hamiltonian parameters as $(J, B_x, B_z) = (1, 0.9045, 0.809)$ for our calculations, where this model is robustly non-integrable, and we assume open

[2] Notice that $2R$ is the number of evolution and measurements while the runtime R is for the largest one only.

boundary conditions. 12 specific choice of periods in range $0.81 \leq T \leq 1.51$ is considered to scan a region at around $T \sim 1$, where the transition from prethermal to fully thermalizing regime has been observed [231]. Further, for $T \geq 1$, the transient dynamics have been shown to be well approximated by a technique in Floquet Magnus expansion (that we introduced in Chapter 3.2 with Eq. (3.7) and will be further arguing below). Therefore, in this case, the Floquet operator, as defined in Eq. (6.1), is

$$U_T = \exp(-iH_xT/2)\exp(-iH_zT/2). \tag{6.18}$$

For this particular choice of parameters, it has been shown that this model is non-integrable and exhibits Floquet ETH [227, 231]. As discussed in Chapter 3.2, one of the consequences of Floquet ETH is that generic non-integrable periodically driven many-body systems are expected to heat up to infinite temperature in the long-time limit since it postulates that all of the Floquet eigenstates are identical, and indistinguishable from the infinite-temperature state, although several exceptions exist which are listed in Chapter 3.2. Therefore, for local observables, the Floquet diagonal ensemble in this case is indistinguishable from the maximally mixed ensemble. In our simulations, we consider the same local observable σ_1^z as in Ref. [231]—the z-component of the first spin on the lattice for which we thus expect zero expectation value in the long-time limit.

6.2.2 Results

We numerically simulate the Floquet dynamics of the model described in Eq. (6.15) with a particular choice of driving for system sizes $N \in \{20, 50\}$, using MPS techniques. In addition, we cross-check results for small system sizes $N \leq 20$ which can be explored with exact diagonalization. We include here our results for system sizes, $N = 20$ and $N = 50$. For $N = 20$, we compute the state at stroboscopic times by approximating Floquet operator Eq. (6.18) using a Krylov-subspace method (hereafter referred to as Arnoldi method) [292–294], which approximates the action of U_T onto the state directly. For the larger size ($N = 50$), we represent the Floquet operator, U_T Eq. (6.18), as a matrix product operator [51, 84, 88]. To calculate the time-evolution from the initial state, we represent the state of the system as a matrix product state [39, 48] that is truncated to a fixed bond dimension after an application of the MPO representation of the Floquet propagator U_T (see Chapter 2.1 for detailed explanation). Here we carry out our numerical simulations with bond dimensions $100 \leq D \leq 400$ and observe that our results converge in bond dimension $D = 400$.

In Fig. 6.2 we show the stroboscopic dynamics of the observable σ_1^z for two different system sizes, $N = 20$ (left column), and $N = 50$ (right column, MPS simulations with bond dimension $D = 400$), calculated for two different time periods $T = 1.02$ and $T = 1.15$, each starting from the initial product state $|Z-\rangle$ where all the spins are pointing down. For both the time periods shown, we observe that the expectation value relaxes and plateaus first before increasing to the infinite temperature value — this transient dynamical phenomenon has been called prethermalization [231, 239].

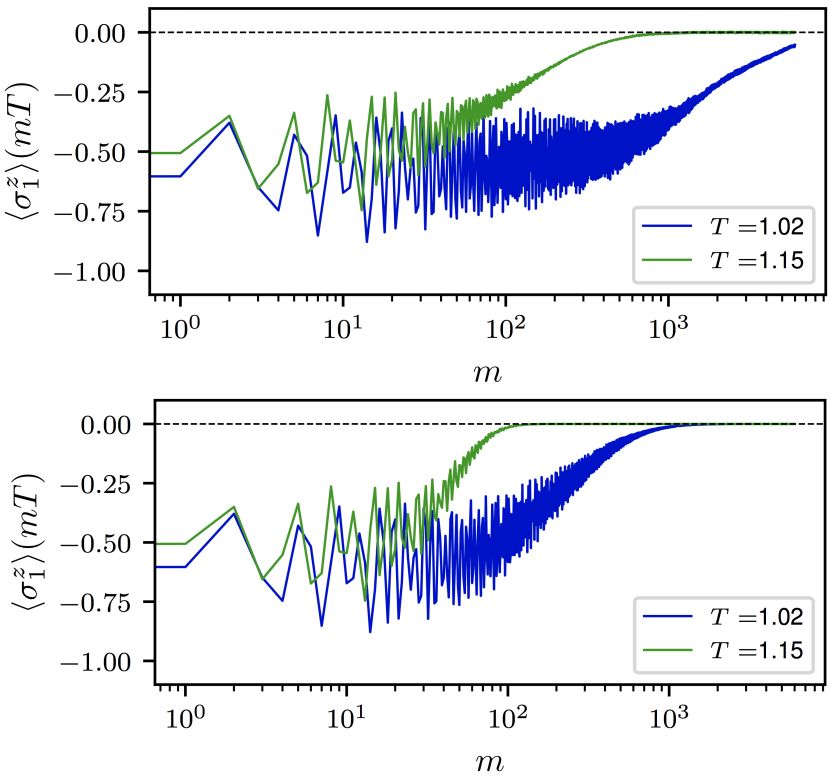

Figure 6.2: Expectation value of local observable σ_1^z at stroboscopic times $t = mT$, $m \in \{0, 1, \ldots, 6 \times 10^3\}$) starting from initial state $|Z-\rangle = |1\rangle^{\otimes N}$ as taken in Ref. [231], for system sizes $N = 20$ (left column, computed by the Arnoldi method) and $N = 50$ (right column, MPS simulations with bond dimension $D = 400$) for different time periods $T = 1.02$ and $T = 1.15$ in a kicked Ising chain given by Eq. (6.15). Here we show that prethermalization can be seen in the transient-time dynamics same as observed in Ref. work [231]– $\langle\sigma_1^z\rangle(mT)$ relaxes initially and oscillates around a prethermal value before completely relaxing to the infinite temperature value of zero.

The dynamical simulations described above allow us to approximate each of the expectation value terms in the sum in Eq. (6.12) which we then multiply with the filter coefficients to obtain the filtered expectation value. This procedure is a classical simulation of a quantum algorithm as the stroboscopic time expectation values could alternatively be obtained from a quantum simulator as proposed in [289] (see also [290]).

In Fig. 6.3, we illustrate the action of the Gaussian periodic filter for the model described above for the two system sizes $N = 20$ (left column) and $N = 50$ (right column, MPS simulations with bond dimension $D = 400$). It can be seen from the plots in the top row that, as expected, the filtered expectation value converges to the expectation value in the infinite temperature ensemble (indicated by a black dashed line) as the filter width δ decreases. Due to finite size effects for small time periods (e.g. $T = 0.81$ for $N = 20$) the system does not satisfy Floquet ETH, i.e., it does not completely thermalize to the infinite temperature ensemble [295] and

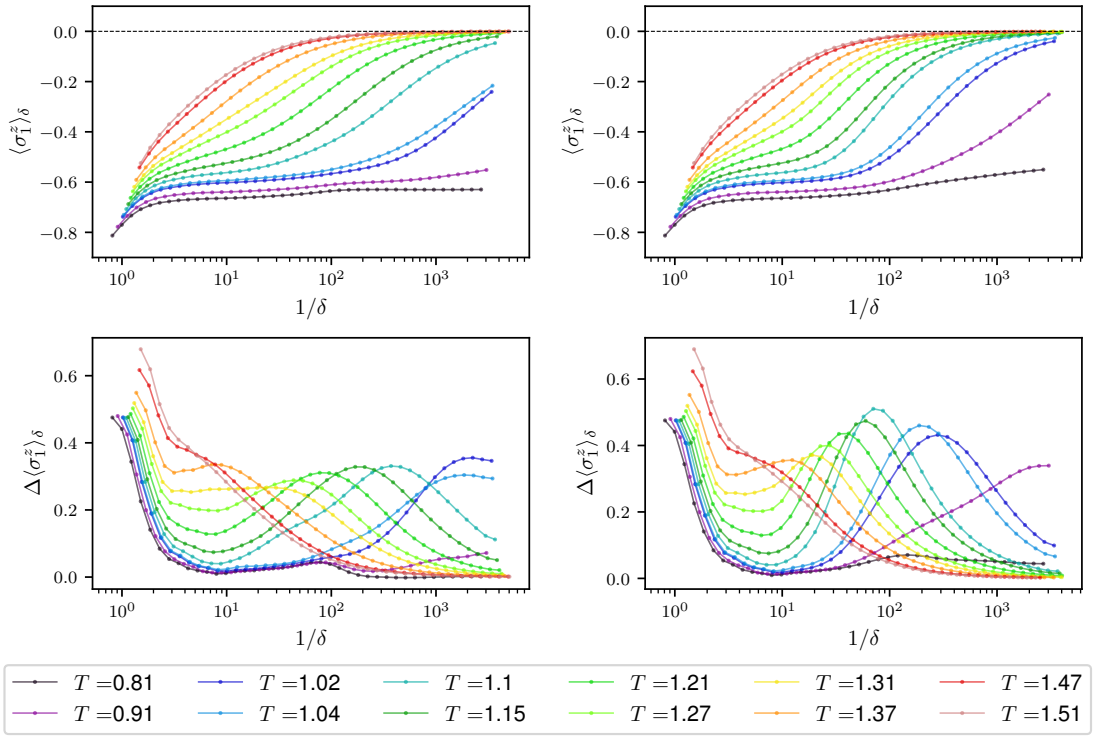

Figure 6.3: Expectation value of local observable σ_1^z based on the filter calculations as a function of inverse width for system sizes $N = 20$ (left column, computed by the Arnoldi method) and $N = 50$ (right column, MPS simulations with $D = 400$) for time periods from $T = 0.81$ to $T = 1.51$ and initial state $|Z-\rangle = |1\rangle^{\otimes N}$. Top row indicates expectation value of σ_1^z in the state produced by the periodic Gaussian filter as a function of inverse width δ, in which we observe slowly changing plateaus in the convergence curves for time periods between $T = 1.02$ to $T = 1.21$ that are the signatures of prethermalization. Bottom row shows finite difference gradient of the Gaussian filtered expectation value. For time same periods between $T = 1.02$ to $T = 1.21$, the appearance of a plateau followed by a peak in the gradient with decreasing filter width signals prethermalization which confirms the sensitivity of our filtering procedure to intermediate dynamical behaviours.

the filtered expectation value does not approach zero as the width decreases.

Furthermore, we observe from the plots in the top row that the convergence behavior to the diagonal ensemble varies with the time period. For smaller time periods (e.g. $T = 1.02$) the filtered expectation value plateaus initially before increasing to the infinite temperature value as the filter width decreases. In contrast, for larger time periods (e.g. $T = 1.15$), the plateau is absent. We attribute this effect to prethermalization occurring at smaller time periods. Prethermalization in this model occurs because, if the period T is small enough, the dynamics produced by the Floquet propagator U_T is well approximated by a propagator generated from a time-independent, local effective Hamiltonian that can be obtained from truncating the Magnus expansion (see Eq. (3.7)) for the Floquet Hamiltonian after a few terms as described in Chapter 3.2. For a total time mT the error of the

truncated Magnus expansion can be bounded as [155, 158, 232],

$$\|U_T^m - U_{\text{eff}}^m\| \leq \kappa m N T e^{-c/T}, \tag{6.19}$$

where $U_{\text{eff}} = e^{-iH_{\text{eff}}T}$, H_{eff} is the effective local Hamiltonian, and c is a constant independent from N and T. Thus, in finite size systems and for a time that scales exponentially with the driving frequency, the effect of the evolution is approximately that of the local Hamiltonian and, correspondingly, the expectation values of observables can be well approximated by the ones that would be obtained evolving with the latter, with an error that scales with m, N, T as in Eq. (6.19). The filtered expectation values Eq. (6.12) are computed from stroboscopic observations at times up to $O(1/\delta)$. For a period T that exhibits prethermalization, when δ is not too small, the filtered expectation value Eq. (6.12) is mostly decided by the dynamics generated by the effective Hamiltonian, and hence, tends to converge, in the generic case and in the limit of small δ, to a thermal value at a certain inverse temperature β determined by the energy (w.r.t. H_{eff}) of the initial state. Thus, the slowly changing plateaus at intermediate δ in the convergence of the filtered expectation value in the top row of Fig. 6.3 arise from the combination of prethermalization, i.e. the convergence to the thermal value w.r.t. H_{eff}, with an additional error that grows (at most) linearly in the stroboscopic time index m.

A possibly clearer signature of prethermalization can also be found by looking at the rate of change of the filtered expectation with the filter width. The lower row in Fig. 6.3 shows the finite difference gradient of the filtered expectation value as the filter width changes. For time periods between $T = 1.02$ to $T = 1.21$ for which prethermalization occurs, (the magnitude of the) gradient drops after the initial relaxation and plateaus to a small value corresponding to the prethermal regime, then it increases, signifying the start of relaxation to the infinite temperature ensemble, and finally it drops to zero as the relaxation to infinite temperature becomes complete.

Although we have considered a Gaussian filter function so far, the method of defining a periodic filter function and using its Fourier decomposition can be generalized to any other functional form. An example is stroboscopic-time averaging, defined by $c_m = 1/(R+1)$ for $0 \leq m \leq R$ and $c_m = 0$ otherwise, which corresponds to the filter function

$$f_{\text{avg}}(x; R) = \frac{e^{iRTx/2}}{R+1} \frac{\sin((R+1)Tx/2)}{\sin(Tx/2)}, \tag{6.20}$$

where we plot the result of this average in Fig. 6.4 and its convergence to the diagonal ensemble with increasing averaging window length parameter R. We observe that this stroboscopic-time average also exhibits prethermal plateaus, but they are noisier in comparison to the Gaussian filtered expectation value— we attribute this to the oscillations in the corresponding filter function $f_{\text{avg}}(x; R)$ as opposed to the more monotonic nature of the Gaussian filter function.

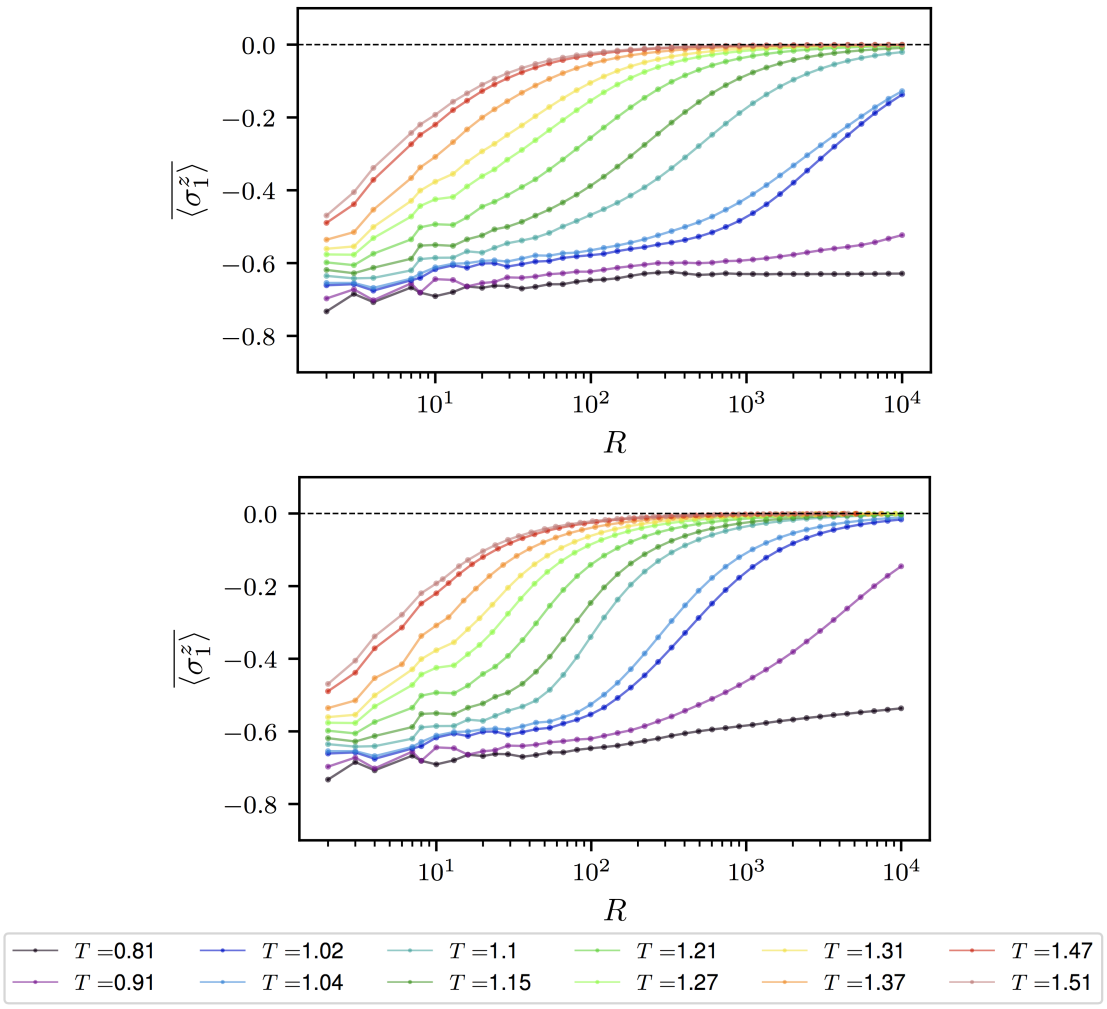

Figure 6.4: Convergence of the stroboscopic-time average of local observable σ_1^z with increasing averaging window length parameter R as given in Eq. (6.20), for system sizes $N = 20$ (left plot, computed by the Arnoldi method) and $N = 50$ (right plot, MPS simulations), time periods from $T = 0.81$ to $T = 1.51$, and initial state $|Z-\rangle = |1\rangle^{\otimes N}$. Prethermal plateaus are also visible in this case, but are noisier compared to the Gaussian filter.

6.3 Discussion

We have shown how the filtering algorithms that we presented in Chapter 4 and Chapter 5 can be applied to systems with a time-periodic Hamiltonian in order to approximate expectation values in the Floquet diagonal ensemble. By formulating the filter as a function of the Floquet operator, we obtain a periodic version of a Gaussian filter operator, that can produce the Floquet diagonal ensemble in the limit of vanishing Gaussian width. As in Chapter 5, expectation values of observables in the filtered state can be calculated from measurements of the expectation value of the observable at periodic time instances, i.e. without explicitly constructing the filtered state.

We numerically demonstrated the filtering technique using tensor network dynamical simulations of a non-integrable spin-chain model exhibiting Floquet ETH and prethermalization. We observed that as the filtered expectation value of an observable converges to the infinite temperature value with decreasing filter width, it displays signals of prethermalization at intermediate widths. The Gaussian filtering technique can be considered as an alternative to taking the stroboscopic time-average to obtain the long-time limit of Floquet dynamics in which we observed in our comparison of these approaches that the signature of prethermalization is clearer (less noisy) in the results of filtering technique.

Interesting directions for future work include studying the behavior of our filtering approach in systems which approximate emergent symmetries even when an effective Hamiltonian approximation cannot be made [241] or the initial state is at a high or infinite temperature [242].

While our calculations are done with classical (tensor network) methods, which limits the minimal filter width that can be reached, a quantum version of the algorithm, analogous to [289, 290], would be capable of exploring narrower filters or higher dimensional problems in the future.

The periodic filter construction Eq. (6.6) can also be modified to work directly with Floquet eigenstates (instead of the diagonal ensemble) as its argument. Filtering Floquet eigenstates with arbitrarily small quasienergy variance is similar to an approach for time-independent systems [288]. We expect that restricting the stroboscopic observations required in this direct filtering approach to the prethermal window could enable the study of ground state or thermal properties of the prethermal effective Hamiltonian through the Floquet dynamics — another interesting avenue for future inquiry.

Finally, we point out again that the periodic filter construction method can be adapted to study other functions, besides Gaussians, of the Floquet Hamiltonian and its commutator. We hope that this encourages the search for other interesting filters for Floquet quantum systems.

Part IV

Thermodynamic Ensembles

Chapter 7

Alternative Ensembles for Tensor Networks

Most of the content of this part is contained in:

- *"Variational Approximations of Thermal States for Tensor Networks"* Giacomo Giudice, Aslı Çakan, J. Ignacio Cirac and Mari Carmen Bañuls **Phys. Rev. B 103, 205128 (2021)**

In this chapter, we turned our attention to dynamics in thermal equilibrium for which we aim to construct alternative ensembles that respect the same constraints as the Gibbs ensemble. We analyze the properties of such ensembles, in particular how they approximate the thermal properties, and present several variational algorithms which can be used to compute them.

More explicitly, the Gibbs state, $\rho_G = \frac{1}{\mathcal{Z}_G} e^{-\beta H}$, describes the thermal equilibrium at a given temperature. It is the ensemble that maximizes the von Neumann entropy, $S(\rho) = -\mathrm{tr}(\rho \log \rho)$, at a given energy, which can equivalently be expressed by the minimization of the free energy,

$$F(\rho) = \mathrm{tr}(H\rho) - \frac{1}{\beta} S(\rho). \tag{7.1}$$

Here, the alternative thermodynamic ensembles that we study, instead of the von Neumann entropy, maximize the α-Rényi entropy [296],

$$S_\alpha(\rho) = \frac{1}{1-\alpha} \log \mathrm{tr}\rho^\alpha \tag{7.2}$$

at a fixed energy. In the limit of $\alpha \to 1$, S_α reduces to the von Neumann entropy. By replacing the von Neumann entropy in Eq. (7.1) by a Rényi entropy, we define a *Rényi free energy*:

$$F_\alpha(\rho) = \mathrm{tr}(H\rho) - \frac{1}{\beta_\alpha} S_\alpha(\rho). \tag{7.3}$$

In the first part of this chapter, we demonstrate how this new ensemble, which minimizes the Rényi free energy in Eq. (7.3), reproduces all local expectation values in the thermodynamic limit although in general the extremizer ρ_α of this

function is not the thermal ensemble. The parameter β_α is not, in general, related to the conventional inverse temperature β, but should be treated as a constant for the optimization. We discuss from a TN perspective that the definition in Eq. (7.3) offers the possibility of directly performing a minimization, since the Rényi entropies in Eq. (7.2) are efficiently computable—at least for small integer values of α. Accordingly, we consider the most convenient case $\alpha = 2$, for which Eq. (7.3) becomes

$$\rho_R := \arg\min_{\rho \succeq 0} F_R, \quad F_R(\rho) = \mathrm{tr}(H\rho) + \frac{1}{\beta_R} \log \mathrm{tr}\rho^2, \tag{7.4}$$

where the subscript R represents $\alpha = 2$. In other words, optimizing Eq. (7.4) is equivalent to finding the most mixed state at a chosen energy.

In the second part of this chapter, we discuss the difficulties of the optimization of such a function as given in Eq. (7.3) in many-body quantum physics since the dimension of ρ increases exponentially with the system size which makes such approaches impractical for large systems. We introduce an optimization strategy based on uniform MPS, in order to approximate the purification of ρ_R directly in the thermodynamic limit. This non-linear optimization can be accelerated using state-of-the-art techniques [297] by restricting it to the Grassmann manifold. This is discussed in detail in Sec. 7.2.1, and accompanying numerical experiments to benchmark the algorithm are presented. Moreover, we present an alternative technique, based on a non-linear evolution of the density operator in Sec. 7.2.2, which flows towards the desired ensemble. To conclude, we finalize this chapter by discussing possible developments.

7.1 Ensemble with Maximal 2-Renyi Entropy

Here we start by introducing the analytical form of the extremizer of Eq. (7.3), which has been previously derived for classical distributions [298–300]. We can use this result in the quantum case noticing that the state that minimizes Eq. (7.3) must be diagonal in the energy eigenbasis $\{|E_k\rangle\}$ and thus its eigenvalues are equivalent to a probability distribution.

In order to find the coefficients $\{p_k\}$ in the density operator $\rho = \sum_k p_k |E_k\rangle \langle E_k|$, $\rho \succeq 0$ which maximizes the Rényi entropy Eq. (7.2) under the constraints $\mathrm{tr}\rho = 1$ and $\mathrm{tr}(H\rho) = \bar{E}$, we introduce the Lagrange multipliers β_α and γ_α. The functional $\mathcal{L}$ is then

$$\mathcal{L}(\rho) \;=\; \frac{1}{1-\alpha} \log \sum_k p_k^\alpha \;-\; \gamma_\alpha \left(\sum_k p_k - 1 \right) \;-\; \beta_\alpha \left(\sum_k E_k p_k - \bar{E} \right). \tag{7.5}$$

At the stationary point, the parameter γ_α can be eliminated [298], and we obtain the *maximal Rényi ensemble* (MRE):

$$\rho_\alpha = \frac{1}{\mathcal{Z}_\alpha} \Pi_{E_\perp} \left(1 - \beta_\alpha \frac{\alpha - 1}{\alpha} (H - \bar{E}) \right)^{\frac{1}{\alpha - 1}} \Pi_{E_\perp}, \tag{7.6}$$

where $\mathcal{Z}_\alpha$ is a normalization factor and $\Pi_{E_\perp}$ is a projector onto the eigenvalues below a cutoff energy $E_\perp := \frac{\alpha}{\beta(\alpha-1)} + \bar{E}$:

$$\begin{aligned} \Pi_{E_\perp} &= \Theta(E_\perp - H), \\ \mathcal{Z}_\alpha &= \mathrm{tr}\left[\Pi_{E_\perp}\left(1 - \beta_\alpha \frac{\alpha-1}{\alpha}(H-\bar{E})\right)^{\frac{1}{\alpha-1}}\right], \end{aligned} \tag{7.7}$$

where $\Theta(\cdot)$ is the Heaviside function. Symmetrically, there is also a solution with a projector onto energies above the cutoff energy: $E > E_\perp$ which represents the Rényi-equivalent of negative temperatures as we will illustrate this region for a comparison in the following.

Initial test and benchmarks: Here, we focus on 2-Rényi case for our tests and benchmarking. Therefore, we take $\alpha = 2$ in the expression Eq. (7.6) and we obtain the maximal 2-Rényi ensemble as,

$$\rho_R = \frac{1}{\mathcal{Z}_R}\Pi_{E_\perp}\left(1 - \frac{\beta_R}{2}(H-\bar{E})\right)\Pi_{E_\perp}. \tag{7.8}$$

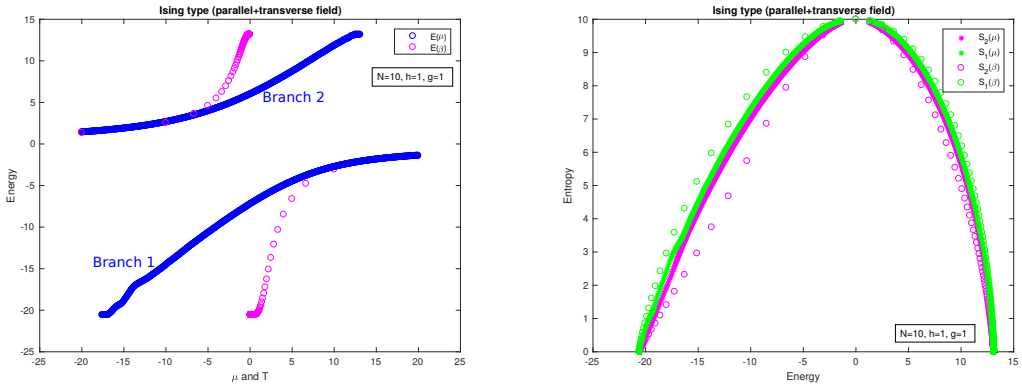

Figure 7.1: Left figure indicates the relation between the energy $\bar{E}$ and the parameters T (temperature in Gibbs ensemble) and μ ($E_\perp$) for a non-integrable Ising model with parameters $(J, g, h) = (1, 1, 1)$ in Eq. (7.15) and system size $N = 10$. Pink colors indicate the exact results computed by the Gibbs ensemble while blue colors showing the results of the exact calculations based on the 2-Rényi ensemble given in Eq. (7.8). Branch 1 indicates the case where the eigenvalues are below the cutoff energy $\mu > E$, while Branch 2 represents the region above the cutoff energy $\mu < E$, which corresponds to the negative temperatures in Gibbs ensemble. Right figure shows the behaviour of entropy as a function of energy for the same case. We illustrate both von Neumann (green) and 2-Rényi entropy (pink) calculations based on both ensembles. Circles belong to the Gibbs ensemble based results and stars represent the 2-Rényi ensemble based ones.

Here we again consider a non-integrable instance of the Ising model as we have studied in the previous chapters and also present the model here in Eq. (7.15), in which we choose the parameters as $(J, g, h) = (1, 1, 1)$ for our comparisons.

In Fig. 7.1, we indicate $E_\perp = \mu$ and provide our comparative results based on the exact calculation of both Gibbs and 2-Rényi ensembles for system size $N = 10$. In the left figure, we present the relation between the energy and the parameters, T and μ, where T is the temperature in Gibbs ensemble. Pink circles indicate the calculations based on the Gibbs ensemble, while blue circles belong to the calculations based on the 2-Rényi ensemble.

Branch 1 indicates the case where the eigenvalues are below the cutoff energy $E < E_\perp$, while Branch 2 represents the region above the cutoff energy $E > E_\perp$, which is equivalent of negative temperatures as illustrated in Fig. 7.1. We observe that T and μ become equivalent for the same energy when $\bar{E} \to 0$, while they differ very much for the same energy values when $\bar{E} \to E_{\max}(E_{\min})$.

We also analyze the relation between the energy and entropies which can be seen in the right panel in Fig. 7.1. Starred data points belong to the calculations based on the 2-Rényi ensemble while the circles are based on the Gibbs ensemble. Green ones represent the von Neumann entropy which we labelled as S_1 and the pink ones are 2-Renyi entropy labelled as S_2. We observe that both ensembles concide in the limits when $\bar{E} = E_{\min}$ and $\bar{E} = E_{\max}$, and the curves behave qualitatively similar.

Further tests together with larger system sizes: To visualize the behavior of Eq. 7.6, we demonstrate some characteristcs of the different ensembles in a particular finite case in Fig. 7.2. In panels $(a$–$b)$ we illustrate the distribution of ρ relative to the eigenbasis. The MRE has a distinctive cutoff energy, beyond which the distribution is zero and therefore quite different from the case of the canonical ensemble. However, in a many-body system, we need to take into account that the density of states is non-uniform, but becomes increasingly peaked in the middle of the spectrum. Then the distributions which are weighted by the density of states, become much more similar, as seen in panel (b).

In Fig. 7.2$(a$–$b)$ we explicitly demonstrate, the comparison of von Neumann and 2-Rényi entropies for the ensembles that maximize each of them over the whole energy range for a small system size. As observed in the initial test given in Fig. 7.1, while the behavior is qualitatively similar, both ensembles only agree in the limiting cases $\bar{E} = 0$, when the state is maximally mixed (corresponding to the Gibbs ensemble at infinite temperature $\beta = 0$) and $\bar{E} = E_{\min}$ $(E_{\max})$, when the ensemble reduces to the ground (maximally excited) state, corresponding to $\beta \to +\infty$ $(-\infty)$.

In order to explore the behavior at large system sizes, we consider an exactly solvable case of Ising model given in Eq. (7.15) with the parameter choice as $(J, g, h) = (1, 0, 0.5)$. We present the corresponding results in Fig. 7.3, in which only the largest size $N = 500$ is demonstrated for the Gibbs ensemble since there is no visible difference in the curves for ρ_G.

In panels (a) and (b) of Fig. 7.3, we observe that, as the system size increases, the von Neumann entropy density of the Rényi ensemble approaches that of the

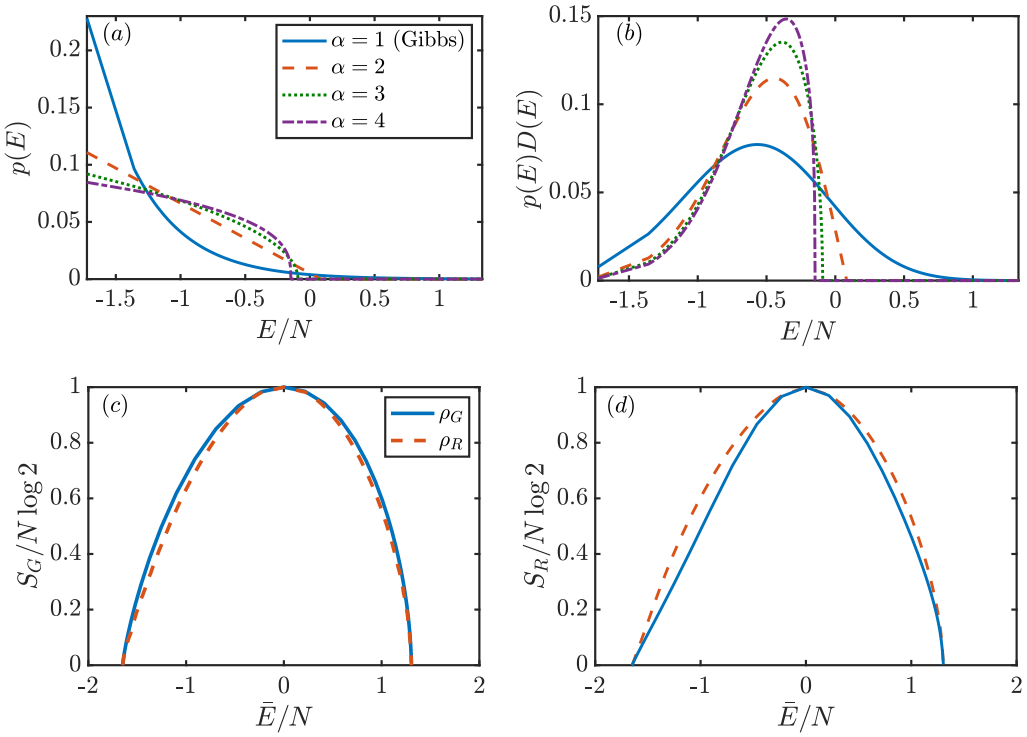

Figure 7.2: (a) Distribution $p(E)$ of the Maximal Rényi and Gibbs ensembles for different values of α for the Ising model in Eq. (7.15), with longitudinal and transverse fields $(J, g, h) = (1, -1.05, 0.5)$ and system size $N = 10$ (PBC). The mean energy $\bar{E}$ is fixed at $-1/4$ of the width of the spectrum. (b) The same distributions weighted with the corresponding density of states $D(E)$, from the approximation in Ref. [301]. Below, the von Neumann (c) and 2-Rényi (d) entropies for the canonical (solid line) and 2-Rényi (dashed line) ensembles are compared at a given mean energy density, for the same system size and Hamiltonian. In both cases, the asymptotic behaviors $\lim_{\beta\to 0} S = \lim_{\beta_R\to 0} S_R = N \log 2$ and $\lim_{\beta\to\pm\infty} S = \lim_{\beta_R\to\pm\infty} S_R = 0$ are recovered. The branch with negative (positive) mean energy density corresponds to a $\beta > 0$ ($\beta < 0$), corresponding to a solution with a projector onto energies below (above) the cutoff energy $E_\perp$.

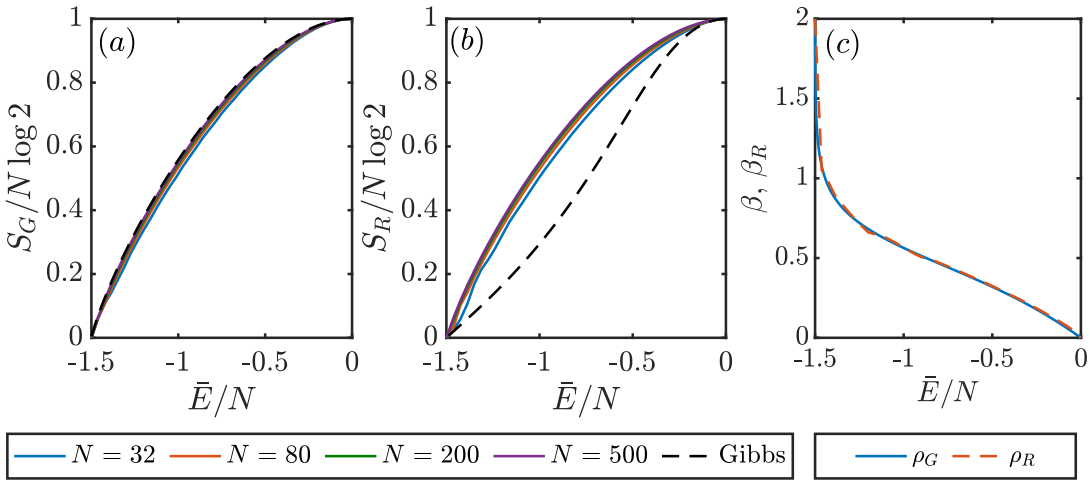

Figure 7.3: $(a$–$b)$ Von Neumann and 2-Rényi entropies compared to the mean energy density, for the (classical) Ising model with $(J, g, h) = (1, 0, 0.5)$. (c) Comparison of β and β_R as a function of the mean energy density for the largest size $N = 500$.

Gibbs ensemble [1]. The Rényi entropy difference Δs_R instead increases with system size.

For this choice of parameters, the density of states becomes Gaussian, and it is interesting to see that the Rényi ensemble has a von Neumann entropy which approaches the Gibbs state, and hence will have a free energy (see Eq. (7.1)) which increasingly approaches its maximal value. However, the same cannot be said for the Rényi free energy introduced in Eq. (7.3).

In Fig. 7.3 (c), we show the behaviour of β and β_R as a function of the mean energy density in which they agree well, and we will be further discussing in Sec. 7.2.1.

7.1.1 Equivalence of local observables

We consider a one-dimensional quantum system described by a local Hamiltonian H, an operator in the complex Hilbert space $\mathcal{H}$. This total Hilbert space is formed by the tensor product of N local Hilbert spaces

$$\mathcal{H} = \bigotimes_{n=1}^{N} \mathcal{H}_n \,. \tag{7.9}$$

The Hamiltonian is restricted to be ℓ-local, i.e. it can then be written in the form

$$H = \sum_{n=1}^{N} h_n, \tag{7.10}$$

[1] Since the eigenvalues correspond to only a number of discrete energies, oscillations occur at finite sizes.

where each h_n acts non-trivially only on sites $n, \ldots, n+\ell-1$, and has finite operator norm. In addition, we will assume that almost all local terms satisfy $\|h_n\|_{\text{op}} > 0$, such that the spectrum of H is extensive. We mostly consider infinitely-large systems, but when considering finite systems, we specify either open boundary conditions (OBC) or periodic boundary conditions (PBC).

In this setting, it is straightforward to see that the *density of states*

$$D(E) = \text{tr}[\delta(H - E)] \tag{7.11}$$

has a variance which scales as $\mathcal{O}(\sqrt{N})$. It can be shown that $D(E)$ becomes Gaussian in the thermodynamic limit for specific models, such as strictly 1-local Hamiltonians. Under the assumption of a Gaussian density of states, we can then compute the variance of the energy when we take into account the energy distribution of the ensemble. In the case of the 2-Rényi entropy, it turns out that this can be computed exactly. As described in Appendix of ref. [302], in both cases the variances scale as $\mathcal{O}(N)$. Hence, if we think about the normalized energy spectrum, both distributions will be increasingly peaked around the same $\bar{E} = \langle H \rangle$ with a standard deviation $\mathcal{O}(1/\sqrt{N})$ for large N. Hence, the expectation values of local observables become equivalent in the thermodynamic limit. This derives from the correspondence between microcanonical and canonical ensembles [303]. While there exist counterexamples to this correspondence, a sufficient condition for it to hold is that the energy per site converges to a constant [304, 305]. Note that while this argument has been carried out for a Gaussian density of states, we believe that it can be extended to the general case as long as the Hamiltonian is local.

A couple of final remarks are in order. First, we obtain a correspondence $\beta_R \to \beta$ which holds in the thermodynamic limit, at least in the case of $\alpha = 2$. This holds asymptotically for large β_R and the range of validity of this approximation increases with system size. Hence, the β_R for which the Rényi ensemble has the same energy density $\bar{E}$ as a Gibbs ensemble turns out to be the same as the inverse temperature β. Second, this can be shown in the case of a Gaussian density of states (see Appendix of ref. [302]), and we numerically observe in both integrable and non-integrable models as we will be discussing in the following Sec. 7.2.1. This is somewhat surprising, since there is no connection between the parameters describing the two different ensembles. However this correspondence is convenient to approximate a thermal ensemble, since we may as well take β_R to be the inverse temperature.

7.2 Variational algorithms for approximating the Rényi ensemble

In this Section, we introduce two different possibilities to obtain numerically the Rényi ensemble in Eq. (7.6). Although we have a closed form for the exact solution, its use in a many-body setting is impractical because it would require knowledge of the full energy eigenbasis or of the projector in Eq. (7.6). This motivates the formulation of methods compatible with tensor network techniques.

In the first part of this section, we study how uniform matrix product states can be used to form a purification which represents the density matrix, and its

individual tensors can be optimized directly by using techniques from Riemannian optimization. In the second part of this section, we introduce a non-linear evolution which has Eq. (7.6) as a fixed point, so that any arbitrary state can be brought to the desired one by simulating this evolution for a sufficient amount of time.

7.2.1 Minimization on the MPS manifold

The optimization problem in Eq. (7.4) can be restricted to the manifold of states described by some class of tensor networks. In particular MPS are arguably the most effective ansatz to represent ground states of local, gapped Hamiltonians in one dimension [77, 81, 93, 306]. We consider a uniform MPS [2]:

$$|\Psi(A)\rangle = \sum_{\vec{s}} \mathrm{tr}\left(\dots A^{s_{n-1}} A^{s_n} A^{s_{n+1}} \dots\right) |\vec{s}\rangle\,, \tag{7.12}$$

where $|\vec{s}\rangle = |s_1, \dots, s_N\rangle$.

As discussed in Chapter 2.1.1, quantum-mechanical operators can be cast into MPO form [42, 43, 307], which is composed of rank-4 tensors contracted sequentially for which the graphical representation is given in Fig. 2.1.1. The key point of the construction is that it is difficult to ensure positivity, which is a necessary condition for objects like density operators. The issue is that positivity is a global property, which cannot be captured in the local tensors [308–310]. Even though the stationary points of dissipative dynamics [311, 312] has been successfully approximated with the use of an MPO ansatz, it is challenging for a variational method since there is no way to vary the local tensors without compromising positivity.

An alternative way is to introduce a *locally purified state* [42, 308, 313], which ensures the positivity of the operator for any local tensor. The idea of the construction is as follows: one considers a pure state, where each site has twice the degrees of freedom, which we call *system* and *ancilla*. We find a ladder-like tensor network by tracing out the ancillary degrees of freedom, which represents the density matrix $\rho = \mathrm{tr}_{\mathrm{anc}} |\Psi\rangle \langle\Psi|$. Even if the objective function is quadratic in ρ, as in Eq. (7.4), it will be quartic in the local tensors due to the fact that we have introduced a non-linearity in ρ with respect to the local tensors A^s. Thus we cannot use linear algebra to iteratively optimize the local tensors, as in the case of DMRG [33]. However, we can consider the problem in Eq. (7.4) as a non-linear optimization over the tensors of an MPS.

In order to optimize a generic function $f(A)$ using any gradient-based optimization, we must be able to compute the gradient with respect to the parameters in A and project it onto the tangent space of the Grassmann manifold. The optimization of differentiable functions on Riemannian manifolds has been the object of extensive studies in mathematics and recently these techniques have been applied to tensor networks [297]. The key ingredients of this optimization can be found in Appendix of Ref. [302].

[2] In this Section we focus on uniform MPS for simplicity, but the method can be applied to finite MPS as well.

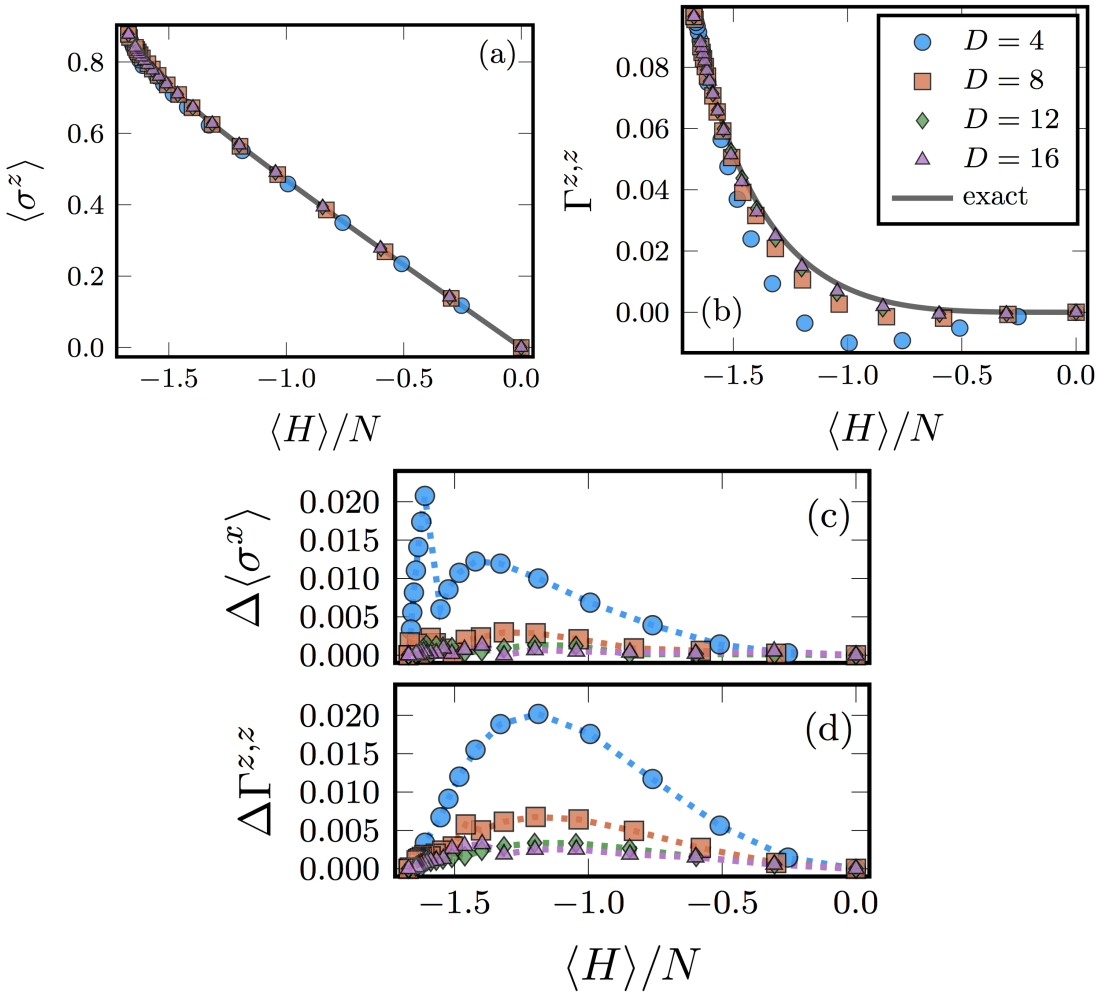

Figure 7.4: Expectation values of local observables σ^z in panel (a) and next-neighbor correlation $\Gamma^{z,z}$ in panel (b) as a function of the mean energy per particle for the Ising model with parameters $(J, g, h) = (1, 1.5, 0)$ based on exact (dotted black lines) and MPS calculations with different bond dimensions $D = 4, 8, 12, 16$. In $(c–d)$, comparison of the absolute errors and the exact solution is illustrated. No spontaneous symmetry breaking can occur at finite temperature in one-dimensional systems with local interactions—we therefore explicitly enforce the $\mathbb{Z}_2$ symmetry in the tensors.

For our application, the objective function is given by Eq. (7.4). For the uniform MPS of Eq. (7.12), it reduces to

$$f_R := \frac{F_R}{N} = \varepsilon + \frac{1}{\beta_R} \log \eta, \tag{7.13}$$

where $\varepsilon = \mathrm{tr}(H\rho)/N$ is the energy per site and $\eta = (\mathrm{tr}\rho^2)^{1/N}$ is the purity per site. Both these terms are computable with standard tensor network routines in polynomial time, for uniform MPS as well as finite MPS. The gradient of Eq. 7.13 with respect to A is

$$\frac{\partial f_R}{\partial A} = \frac{\partial \varepsilon}{\partial A} + \frac{1}{\beta_R \eta} \frac{\partial \eta}{\partial A}. \tag{7.14}$$

We thus use this gradient information to perform the optimization on the Riemannian manifold using the l-BFGS algorithm [314, 315].

To conclude, we note that gradient methods are not expected to ensure in any way convergence towards the global minimum, but only some local minimum. While Eq. (7.4) has a unique solution in the cone of the positive operators, the same is not expected to happen on a uniform MPS manifold of fixed bond dimension.

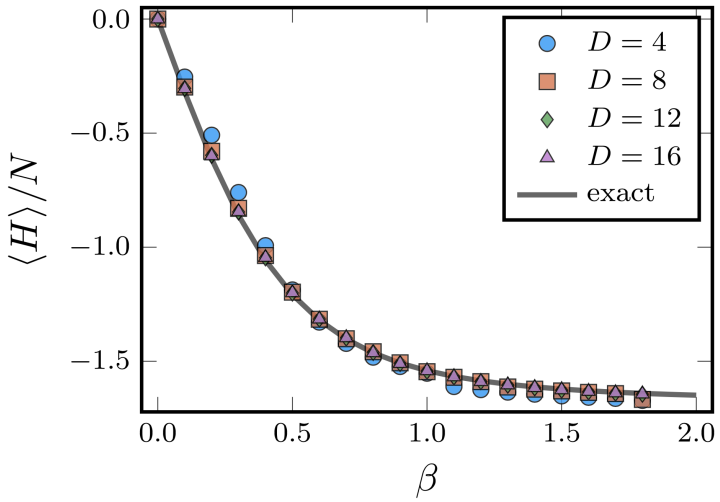

Figure 7.5: Average energy from Fig. 7.4 with the choice of $\beta_R = \beta$.

Numerical experiments

For our numerical experiments, we consider the Ising model as in the previous chapters,

$$H_{\text{Ising}} = J \sum_i \sigma_z^{[i]} \sigma_z^{[i+1]} + g \sum_i \sigma_x^{[i]} + h \sum_i \sigma_z^{[i]}. \tag{7.15}$$

In the case of absence of the longitudinal field ($h = 0$), the model is integrable, and local observables and correlations have a closed form [316, 317]. We use this model to perform the optimization of Eq. (7.4) as described in Sec. 7.2.1. The parameter β_R is fixed to different values in the interval $\beta_R \in [0, 2]$, and the uniform MPS is optimized until the gradient is small enough [3].

In Fig. 7.4, we have shown the results of the optimization, plotting some local observables such as the expectation value of $\langle \sigma_i^z \rangle$ and next-neighbor correlation $\Gamma^{a,b} = \langle \sigma_i^a \sigma_{i+1}^b \rangle - \langle \sigma_i^a \rangle \langle \sigma_{i+1}^b \rangle$ as a function of the mean energy density of the ensemble. We increase the number of the free parameters by increasing the bond dimension, and we observe that the numerical results converge towards the thermal ones. In addition to that, we have shown the comparison of the thermal observables by setting $\beta_R = \beta$ in Fig. 7.5. Up to $\beta_R \lesssim 2$, we observe that there is a correspondence between the two ensembles at $\beta_R = \beta$. For $\beta_R \gtrsim 2$ the optimization

[3] The optimization halts after the norm of the gradient vector in tangent space is smaller than 10^{-6}.

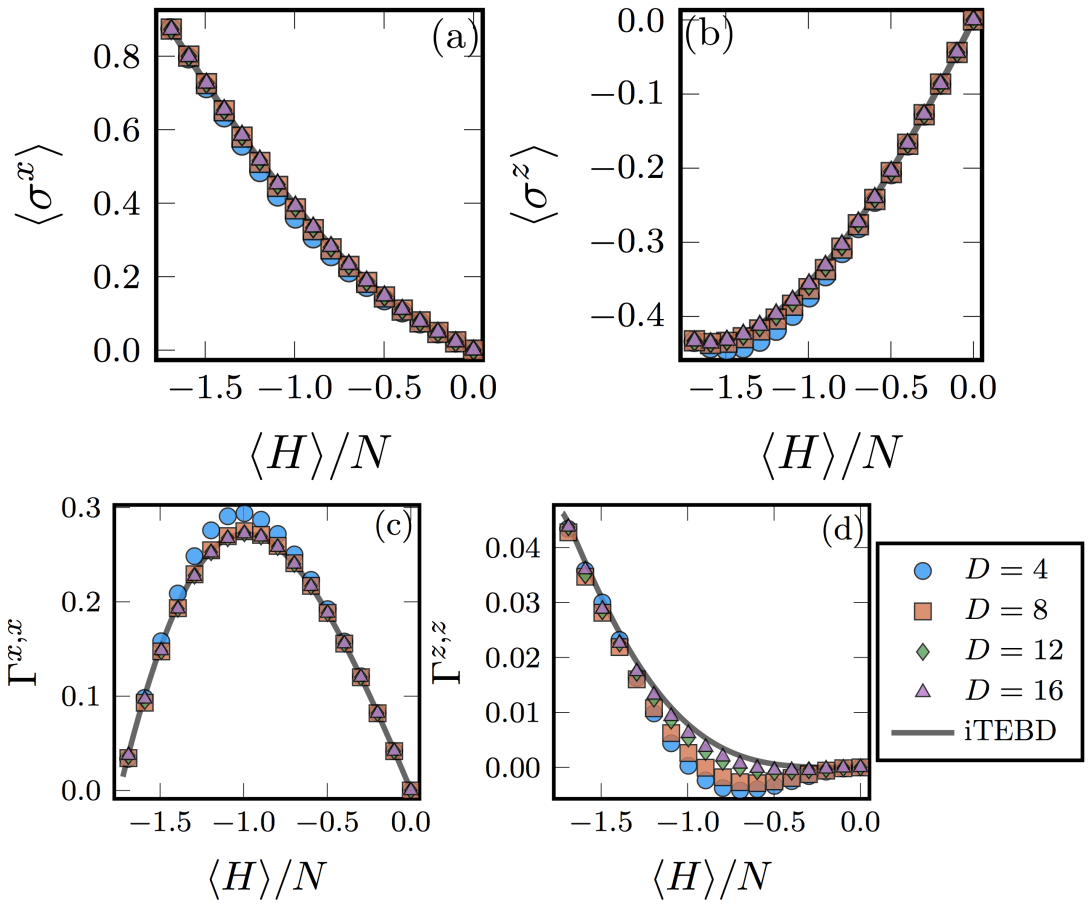

Figure 7.6: Expectation value of local observable σ^x in panel (a), σ^z in panel (b) and nearest-neighbor correlations $\Gamma^{x,x}$ in panel (c) and $\Gamma^{z,z}$ in panel (d) are given as a function of the mean energy density for the non-integrable case with $(J, g, h) = (1, -1.05, 0.5)$. The dotted line corresponds to the results given by the iTEBD algorithm.

of Eq. (7.13) converges to the ground state exactly, in particular at small bond dimensions.

In order to explore the physics of finite temperatures, it is therefore more convenient to reexpress the optimization problem in Eq. (7.4) by introducing a Lagrange multiplier

$$\rho^* = \arg\min_{\rho \succeq 0} \left\{ \mathrm{tr}\rho^2 + \frac{\lambda^2}{2} \left(\mathrm{tr}(H\rho) - \bar{E} \right)^2 \right\}. \tag{7.16}$$

The gradient can be modified accordingly, and the non-linear optimization can be performed in a similar way. This new objective function gets rid of the dependence on β_R, and one can directly choose an energy to target, since $\lim_{\lambda \to \infty} \mathrm{tr}(H\rho^*) = \bar{E}$. However, if one wishes to explore the behavior of some observable with respect to $\bar{E}$, it is not necessary to perform the extrapolation with $\lambda \to \infty$, but a finite λ is adequate to find an energy in the vicinity of the desired value [4].

[4] In our simulations, we set $\lambda = 10$. Since the purity per site $0.5 \leq \eta \leq 1$ is order 1, we expect

We also would like to note here that the method is general and independent of whether the system is integrable or not. To complete our benchmarks, we consider a non-integrable instance as well, introducing a longitudinal field and present our results in Fig. 7.6. In this case exact results are not known, but our results are compared to those of an MPS approximation to the Gibbs state purification obtained with a traditional imaginary time-evolution method [42, 49]. Since the model does not have a finite-temperature phase transition, the method will behave similarly for any value of the fields. In the case of $(J, g, h) = (1, 1, 0)$, the required bond dimension is expected to increase when $\beta \to \infty$, as the critical ground state is approached [318–321]. In this regime, the cost function in Eq. (7.4) will be dominated by the energy term. Hence the algorithm is reduced to an energy minimization, and we expect it to behave equivalently to other variational methods, such as the one proposed in Ref. [297].

7.2.2 Non-linear evolution

In Ref. [322], a non-linear evolution was introduced with the purpose of approximating the thermal ensemble with Gaussian states. Following the same idea, here we generalize this non-linear evolution for the Rényi entropies, which leads us to an evolution that is efficiently computable with tensor network techniques.

Let us start by considering a non-linear evolution of a density operator ρ_τ which depends on a real parameter τ

$$\dot{\rho}_\tau := \frac{\partial \rho_\tau}{\partial \tau} = -\frac{1}{2} \left\{ \mathbb{J}_\tau - \langle \mathbb{J}_\tau \rangle , \rho_\tau \right\} . \tag{7.17}$$

The operator $\mathbb{J}_\tau$ can be chosen such that the fixed point of this evolution leads to the MRE. For instance, the choice

$$\mathbb{J}_\tau \rho_\tau = \beta_R H + \frac{2}{\mathrm{tr}\rho_\tau^2} \rho_\tau \tag{7.18}$$

ends up with the same density operator as Eq. (7.4). The similar proof given in Ref. [322] can be followed, and it is sufficient to demonstrate that the operator $\mathbb{J}_\tau$ in Eq. (7.18) satisfies the following criteria:

$$\mathrm{tr}\rho_\tau = 1, \ \forall \tau \in \mathbb{R} \qquad \text{Trace conservation} \tag{7.19a}$$

$$\rho_\tau \succeq 0, \ \forall \tau \in \mathbb{R} \qquad \text{Positivity conservation} \tag{7.19b}$$

$$\partial f_R(\rho_\tau)/\partial \tau \leq 0 \qquad \text{Free energy decrease} \tag{7.19c}$$

Hence, choosing an appropriate density operator ρ_0 and integrating Eq. (7.17) over a sufficiently long interval, we find the solution to Eq. (7.4), since its value can only decrease with time. It is not ensured that one can reach the global minimum—and indeed any eigenstate of H does not evolve under Eq. (7.17)—but a random choice of the initial state should be sufficient in most cases.

We illustrate some numerical experiments performed on small system sizes in Fig. 7.7, where the energy eigenbasis is available. In all cases the numerically

deviations in energy density around $\mathcal{O}(1/\lambda^2)$.

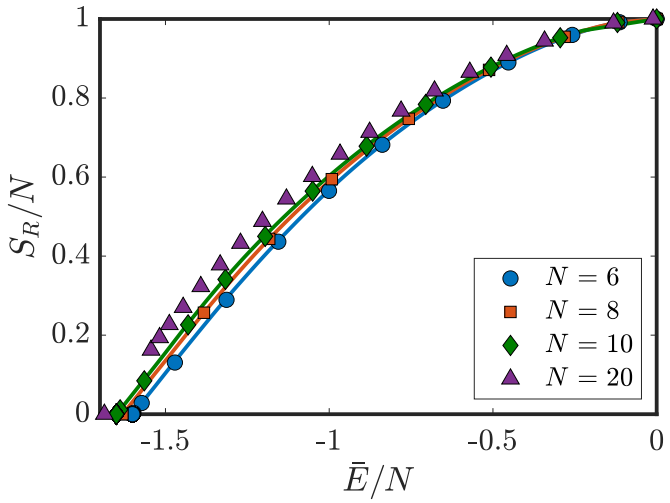

Figure 7.7: 2-Rényi entropy of the maximal Rényi ensemble results based on the analytic solution (solid lines) and nonlinear evolution (points). Results are obtained for the Ising model (OBC) in Eq. (7.15) with longitudinal and transverse fields $(J, g, h) = (1, -1.05, 0.5)$. We also show numerical results for $N = 20$ (triangles) based on the non-linear evolution with MPS.

integrated density operator converges to the ensemble in Eq. (7.6). The evolution is discretized by expanding Eq. (7.17) to first order,

$$\rho_{\tau+\delta\tau} \approx e^{-\frac{\delta\tau}{2}(\mathbb{J}_\tau - \langle \mathbb{J}_\tau \rangle)} \rho_\tau e^{-\frac{\delta\tau}{2}(\mathbb{J}_\tau - \langle \mathbb{J}_\tau \rangle)}. \tag{7.20}$$

If the time step is chosen to be sufficiently small, then this evolution will converge to the desired fixed point. This is witnessed by the fact that the Rényi entropy reaches the theoretical maximum for each mean energy, as shown in Fig. 7.7. As a proof of concept, we also perform the integration using MPS, in particular using the TDVP scheme [323, 324] to update the state at each time step. However, in practice, we experience that the time step required to achieve accurate results scales unfavourably with the system size, and we have yet to fully understand if the evolution becomes ill-conditioned for large system sizes. Nonetheless, it might be possible to treat it by different integration schemes which allow for large time steps without compromising the stability of the evolution. We leave more detailed analyses for future works.

7.3 Discussion

We have presented a new approach to compute thermal expectation values instead of simulating the conventional imaginary time-evolution based on the Gibbs state purification. Here, we construct an alternative ensemble which maximizes the 2-Rényi entropy for the same mean energy, and is expected to reproduce local observables of the corresponding Gibbs ensemble in the thermodynamic limit.

We have demonstrated that this ensemble can be efficiently approximated using MPS techniques. To this end, we have presented variational algorithms to find such an approximation, in which it is possible to work directly in the thermodynamic limit and use an MPS representation of the ensemble that optimizes the Rényi free energy in Eq. (7.4). Although this function seems to have a simple form, the optimization is non-linear and one possible way to tackle it is to approach by gradient-based methods. Since the positivity constraint in tensor networks is highly non-local, one needs to consider additional tools to treat it: one possible way of enforcing it is by means of a purification. The convergence can be improved with techniques based on manifold optimization, but suffers from a fundamental limitation, having the high contraction cost. Indeed, for a purification of bond dimension D, the time-complexity occurred by the computation of the purity is $\mathcal{O}(D^5)$, which is significantly higher than the typical $\mathcal{O}(D^3)$ for other popular MPS algorithms, such as time evolution or ground state search. Incidentally, the former is the same leading cost of the original formulation of DMRG with periodic boundary conditions [61]. Further, we observe that moderate bond dimensions are sufficient to study the ensemble and its local properties both in integrable and non-integrable models in spite of the higher time-complexity.

Alternatively, we have also adapted a method based on a non-linear evolution of the density operator. Under this evolution, we observe that the Rényi free energy is monotonically decreasing, and hence flows to the maximal Rényi ensemble.

The ideas outlined here could be applied to other wave-function ansätze. Recently, variational Monte Carlo techniques have been used to optimize neural networks to describe the steady state of dissipative dynamics [325–328]. Such techniques could also be adapted here to perform the optimization described in this chapter, which can be an option for further inquries.

Part V

Conclusions

Chapter 8

Summary and outlook

Throughout this dissertation, we have studied the application of novel tools to challenging problems in quantum many-body physics using tensor network methods. Our studies are focused around thermalization, equilibration and prethermalization problems of isolated quantum many-body systems in one dimension, and tensor networks provided powerful approximations to those problems with desirable properties that allow to probe moderately large systems.

On the one hand, we have shown that the standard MPS techniques when combined with sensible methods are adequate tools to explore the thermalization and equilibration concepts in one-dimensional isolated systems. To this end, by constructing a filtering method which includes a Gaussian operator of Hamiltonian commutator with the purpose of suppressing the off-diagonal components of the density operator, first we have examined a non-integrable spin chain for which we approximated the diagonal ensemble as a MPO. By assisting our numerics in MPS simulations with the use of a Chebyshev polynomial series which approximates the Gaussian filter, we have shown that expectation values of local observables converge towards their thermal values polynomially with the inverse width of the Gaussian filter. Our results show that simulating larger systems with moderate off-diagonal width is possible although the results of small systems indicated the scaling of the operator space entanglement entropy of the diagonal ensemble as a volume law, which limits the system sizes for which we can have a reliable MPO approximation.

Moreover, taking the advantage of the fact that the filtering procedure we have proposed is not limited to the generic cases since it does not directly target the diagonal ensemble but the time-average limit, we have also explored the feasibility of this method on an integrable spin chain where we have explicitly demonstrated that local observables converge to considerably different values from the thermal equilibrium ones as expected. Furthermore, we have observed a similar convergence behaviour for both non-integrable and integrable models, in which the curves for all system sizes fall on top of each other, i.e., the convergence behaviour is independent of the system size. These findings from our studies provide in this way insight beyond exact diagonalization even for moderate filter widths.

On the other hand, we have alternatively studied by the way of replacing the previous approximation of Gaussian filter by Chebyshev polynomial series

with the Cosine filter for the purpose of approximating the expectation values in the diagonal ensemble, and concluded that it allows us directly to compute the expectation value of observables in diagonal ensemble without constructing the diagonal ensemble as an MPO. In addition, when the expectation value of local observables is the point in question, our comparative results based on both approaches for similar models show that we can simulate further regimes reaching much narrower widths due to the considerable reduction of computational cost in the latter procedure.

Based on our findings, which give evidence that the proposed filtering procedure is reliable enough to explore different dynamics of different kinds of models, we have studied further questions which have been related to characterizing diagonal ensembles and capturing interesting intermediate-time behaviours such as prethermalization and quantum scars. By introducing incoherent and coherent averages using the filter which target to distinguish between the cases with and without degeneracies in the spectrum, we have examined two specific models; near-integrable and PXP models. Results of our simulations on these different scenarios have given remarkable clues that our filtering procedure is indeed capable of detecting distinctive dynamical behaviours in different models. Moreover, numerical implementation with standard MPS techniques is fairly straightforward by this method, thus makes it possible to treat and perform efficient simulations for larger systems.

Since our construction is quite general and could be performed for different kinds of systems, we have shown that extending the success of combining MPS tools with the filtering technique to time-periodic systems is also possible for which interesting dynamical properties have been characterized. By formulating the filter as a function of the Floquet operator, we have shown without explicitly constructing the Floquet Hamiltonian, the filter gives access to study its properties.

We have numerically simulated a non-integrable spin chain model in a periodically driven system which exhibits Floquet ETH and prethermalization, and monitored that, as the filtered expectation value of an observable converges to the diagonal ensemble value with decreasing filter width, it reveals a clear signature of prethermalization at intermediate widths. Furthermore, our comparative results of the Gaussian filtering technique with directly stroboscopic time-average have shown that the filtering approach provides clearer picture of prethermalization while the results of stroboscopic time-average show noiser behaviours. Our findings provide clear evidences that the filtering procedure is sensitive enough to capture interesting intermediate-time dynamics besides exploring the long-time dynamics.

In all of our simulations with the filtering technique for different models in both time-independent and time-periodic settings, we have performed our calculations with classical tensor network methods, in which we have obtained desirable results to explore the dynamics out of equilibrium. Additionally, our numerical results can also serve as benchmarking data that could help to test and validate future quantum version of algorithms, which would be capable of investigating narrower filters or higher dimensional problems in the future. Although the computational cost for higher dimensions is expected to be much higher, combination of tensor networks and the filtering methods might be helpful to reach possible solutions as

the filter construction does not make any assumption on spatial dimension.

In the last part of this dissertation, we turned our attention to the expectation values in thermal equilibrium, in which we have studied an alternative ensemble that minimizes the free energy with 2-Rényi entropy as an alternative to Gibbs state. We have shown that this ensemble can be efficiently approximated using MPS tools by optmizing the Rényi free energy, which has a non-local structure. Based on the gradient-based methods, we have demostrated that it is possible to tackle the non-linear optimization, and observed that a moderate bond dimension captures well the ensemble and its local properties, both in integrable and non-integrable models.

In addition to gradient-based optimization, we have performed our simulations based on a non-linear evolution of the density operator, in which Rényi free energy is monotonically decreasing, and thus flows to the maximal Rényi ensemble. An interesting further inquiry would be to adapt different techniques to perform this optimization such as variational Monte Carlo as used in recent works [325–328] to optimize neural networks.

Altogether these works contribute to the growing interest of connecting tensor networks with new ideas to improve the understanding on dynamical properties of systems in and out of equilibrium. In guidance of tensor networks and their robust mathematical formulation, our understanding on the behaviour of quantum mechanical wave functions has been improved. Further, assisting them with clever approaches might provide ground for developing more rigorous results in the field of quantum statistical mechanics.

Bibliography

[1] Lev Davidovič Landau and Evgenij Mikhailovich Lifshitz. *Statistical physics.* Number Vol. 5 in Course of Theoretical Physics. Butterworth Heinemann, Oxford, 3. ed edition, 1980.

[2] Gibbs J W. *Elementary principles in statistical mechanics.* New York: C. Scribner, 1902.

[3] E. T. Jaynes. Information theory and statistical mechanics. *Phys. Rev.*, 106:620–630, May 1957.

[4] E. T. Jaynes. Information theory and statistical mechanics. ii. *Phys. Rev.*, 108:171–190, Oct 1957.

[5] J. M. Deutsch. Quantum statistical mechanics in a closed system. *Phys. Rev. A*, 43:2046–2049, Feb 1991.

[6] Mark Srednicki. Chaos and quantum thermalization. *Phys. Rev. E*, 50:888–901, Aug 1994.

[7] Mark Srednicki. The approach to thermal equilibrium in quantized chaotic systems. *Journal of Physics A: Mathematical and General*, 32(7):1163–1175, Jan 1999.

[8] Jürgen Berges and Jürgen Cox. Thermalization of quantum fields from time-reversal invariant evolution equations. *Physics Letters B*, 517(3-4):369–374, Oct 2001.

[9] Marcos Rigol, Vanja Dunjko, and Maxim Olshanii. Thermalization and its mechanism for generic isolated quantum systems. *Nature*, 452(7189):854–858, Apr 2008.

[10] Lluís Masanes, Augusto J. Roncaglia, and Antonio Acín. Complexity of energy eigenstates as a mechanism for equilibration. *Phys. Rev. E*, 87:032137, Mar 2013.

[11] Christian Gogolin and Jens Eisert. Equilibration, thermalisation, and the emergence of statistical mechanics in closed quantum systems. *Reports on Progress in Physics*, 79(5):056001, Apr 2016.

[12] Corinna Kollath, Andreas M. Läuchli, and Ehud Altman. Quench dynamics and nonequilibrium phase diagram of the bose-hubbard model. *Phys. Rev. Lett.*, 98:180601, Apr 2007.

[13] S. R. Manmana, S. Wessel, R. M. Noack, and A. Muramatsu. Strongly correlated fermions after a quantum quench. *Phys. Rev. Lett.*, 98:210405, May 2007.

[14] A. Flesch, M. Cramer, I. P. McCulloch, U. Schollwöck, and J. Eisert. Probing local relaxation of cold atoms in optical superlattices. *Phys. Rev. A*, 78:033608, Sep 2008.

[15] Michael Moeckel and Stefan Kehrein. Interaction quench in the hubbard model. *Phys. Rev. Lett.*, 100:175702, May 2008.

[16] Marcos Rigol. Breakdown of thermalization in finite one-dimensional systems. *Phys. Rev. Lett.*, 103:100403, Sep 2009.

[17] Marcos Rigol, Vanja Dunjko, Vladimir Yurovsky, and Maxim Olshanii. Relaxation in a completely integrable many-body quantum system: An ab initio study of the dynamics of the highly excited states of 1d lattice hard-core bosons. *Phys. Rev. Lett.*, 98:050405, Feb 2007.

[18] M. Cramer, C. M. Dawson, J. Eisert, and T. J. Osborne. Exact relaxation in a class of nonequilibrium quantum lattice systems. *Phys. Rev. Lett.*, 100:030602, Jan 2008.

[19] Luca D'Alessio, Yariv Kafri, Anatoli Polkovnikov, and Marcos Rigol. From quantum chaos and eigenstate thermalization to statistical mechanics and thermodynamics. *Advances in Physics*, 65(3):239–362, May 2016.

[20] M. Greiner, O. Mandel, T.W. Hänsch, and I. Bloch. Collapse and revival of the matter wave field of a bose-einstein condensate. *Nature*, 419(51-54), 2002.

[21] Sebastian Will, Thorsten Best, Ulrich Schneider, Lucia Hackermüller, Dirk-Sören Lühmann, and Immanuel Bloch. Time-resolved observation of coherent multi-body interactions in quantum phase revivals. *Nature*, 465(7295):197–201, May 2010.

[22] Sebastian Will, Thorsten Best, Simon Braun, Ulrich Schneider, and Immanuel Bloch. Coherent interaction of a single fermion with a small bosonic field. *Phys. Rev. Lett.*, 106:115305, Mar 2011.

[23] Sebastian Will, Deepak Iyer, and Marcos Rigol. Observation of coherent quench dynamics in a metallic many-body state of fermionic atoms. *Nature Communications*, 6(1):6009, Jan 2015.

[24] S. Trotzky, Y.-A. Chen, A. Flesch, I. P. McCulloch, U. Schollwöck, J. Eisert, and I. Bloch. Probing the relaxation towards equilibrium in an isolated strongly correlated one-dimensional bose gas. *Nature Physics*, 8(4):325–330, Apr 2012.

[25] H. Ott, E. de Mirandes, F. Ferlaino, G. Roati, G. Modugno, and M. Inguscio. Collisionally induced transport in periodic potentials. *Phys. Rev. Lett.*, 92:160601, Apr 2004.

[26] C. D. Fertig, K. M. O'Hara, J. H. Huckans, S. L. Rolston, W. D. Phillips, and J. V. Porto. Strongly inhibited transport of a degenerate 1d bose gas in a lattice. *Phys. Rev. Lett.*, 94:120403, Apr 2005.

[27] Niels Strohmaier, Yosuke Takasu, Kenneth Günter, Robert Jördens, Michael Köhl, Henning Moritz, and Tilman Esslinger. Interaction-controlled transport of an ultracold fermi gas. *Phys. Rev. Lett.*, 99:220601, Nov 2007.

[28] Lin Xia, Laura A. Zundel, Juan Carrasquilla, Aaron Reinhard, Joshua M. Wilson, Marcos Rigol, and David S. Weiss. Quantum distillation and confinement of vacancies in a doublon sea. *Nature Physics*, 11(4):316–320, Apr 2015.

[29] Ulrich Schneider, Lucia Hackermüller, Jens Philipp Ronzheimer, Sebastian Will, Simon Braun, Thorsten Best, Immanuel Bloch, Eugene Demler, Stephan Mandt, David Rasch, and Achim Rosch. Fermionic transport and out-of-equilibrium dynamics in a homogeneous hubbard model with ultracold atoms. *Nature Physics*, 8(3):213–218, Mar 2012.

[30] J. P. Ronzheimer, M. Schreiber, S. Braun, S. S. Hodgman, S. Langer, I. P. McCulloch, F. Heidrich-Meisner, I. Bloch, and U. Schneider. Expansion dynamics of interacting bosons in homogeneous lattices in one and two dimensions. *Phys. Rev. Lett.*, 110:205301, May 2013.

[31] L. Faddeev. Algebraic aspects of the bethe ansatz. *Int. J. Mod. Phys. A*, 10:1845–1878, 1995.

[32] Román Orús. A practical introduction to tensor networks: Matrix product states and projected entangled pair states. *Annals of Physics*, 349:117–158, 2014.

[33] Ulrich Schollwöck. The density-matrix renormalization group in the age of matrix product states. *Annals of Physics*, 326(1):96 – 192, 2011. January 2011 Special Issue.

[34] David J. Luitz, Nicolas Laflorencie, and Fabien Alet. Many-body localization edge in the random-field heisenberg chain. *Phys. Rev. B*, 91:081103, Feb 2015.

[35] W. M. C. Foulkes, L. Mitas, R. J. Needs, and G. Rajagopal. Quantum monte carlo simulations of solids. *Rev. Mod. Phys.*, 73:33–83, Jan 2001.

[36] Matthias Troyer and Uwe-Jens Wiese. Computational complexity and fundamental limitations to fermionic quantum monte carlo simulations. *Phys. Rev. Lett.*, 94:170201, May 2005.

[37] Florian Goth and Fakher F. Assaad. Time and spatially resolved quench of the fermionic hubbard model showing restricted equilibration. *Phys. Rev. B*, 85:085129, Feb 2012.

[38] Steven R. White. Density-matrix algorithms for quantum renormalization groups. *Phys. Rev. B*, 48:10345–10356, Oct 1993.

[39] F. Verstraete, V. Murg, and J.I. Cirac. Matrix product states, projected entangled pair states, and variational renormalization group methods for quantum spin systems. *Advances in Physics*, 57(2):143–224, Mar 2008.

[40] Norbert Schuch and J. Ignacio Cirac. Matrix product state and mean-field solutions for one-dimensional systems can be found efficiently. *Phys. Rev. A*, 82:012314, Jul 2010.

[41] Zeph Landau, Umesh Vazirani, and Thomas Vidick. A polynomial time algorithm for the ground state of one-dimensional gapped local hamiltonians. *Nature Physics*, 11:566–569, 2015.

[42] F. Verstraete, J. J. García-Ripoll, and J. I. Cirac. Matrix product density operators: Simulation of finite-temperature and dissipative systems. *Phys. Rev. Lett.*, 93:207204, Nov 2004.

[43] Michael Zwolak and Guifré Vidal. Mixed-state dynamics in one-dimensional quantum lattice systems: A time-dependent superoperator renormalization algorithm. *Physical Review Letters*, 93(20):207205, November 2004.

[44] Adrian E. Feiguin and Steven R. White. Finite-temperature density matrix renormalization using an enlarged hilbert space. *Phys. Rev. B*, 72:220401, Dec 2005.

[45] Michael M. Wolf, Frank Verstraete, Matthew B. Hastings, and J. Ignacio Cirac. Area laws in quantum systems: Mutual information and correlations. *Phys. Rev. Lett.*, 100:070502, Feb 2008.

[46] Bin-Bin Chen, Yun-Jing Liu, Ziyu Chen, and Wei Li. Series-expansion thermal tensor network approach for quantum lattice models. *Physical Review B*, 95(16):161104, April 2017.

[47] Bin-Bin Chen, Lei Chen, Ziyu Chen, Wei Li, and Andreas Weichselbaum. Exponential Thermal Tensor Network Approach for Quantum Lattice Models. *Physical Review X*, 8(3):031082, September 2018.

[48] Ulrich Schollwöck. The density-matrix renormalization group in the age of matrix product states. *Annals of Physics*, 326(1):96 – 192, 2011. January 2011 Special Issue.

[49] Guifré Vidal. Efficient classical simulation of slightly entangled quantum computations. *Phys. Rev. Lett.*, 91:147902, Oct 2003.

[50] Guifré Vidal. Efficient simulation of one-dimensional quantum many-body systems. *Phys. Rev. Lett.*, 93:040502, Jul 2004.

[51] F. Verstraete, J. J. García-Ripoll, and J. I. Cirac. Matrix product density operators: Simulation of finite-temperature and dissipative systems. *Phys. Rev. Lett.*, 93:207204, Nov 2004.

[52] Juan José García-Ripoll. Time evolution of matrix product states. *New Journal of Physics*, 8(12):305–305, dec 2006.

[53] Jutho Haegeman, J. Ignacio Cirac, Tobias J. Osborne, Iztok Pižorn, Henri Verschelde, and Frank Verstraete. Time-dependent variational principle for quantum lattices. *Phys. Rev. Lett.*, 107:070601, Aug 2011.

[54] Pasquale Calabrese and John Cardy. Evolution of entanglement entropy in one-dimensional systems. *Journal of Statistical Mechanics: Theory and Experiment*, 2005(04):P04010, apr 2005.

[55] Tobias J. Osborne. Efficient approximation of the dynamics of one-dimensional quantum spin systems. *Phys. Rev. Lett.*, 97:157202, Oct 2006.

[56] N Schuch, M M Wolf, K G H Vollbrecht, and J I Cirac. On entropy growth and the hardness of simulating time evolution. *New Journal of Physics*, 10(3):033032, Mar 2008.

[57] Sebastian Paeckel, Thomas Köhler, Andreas Swoboda, Salvatore R. Manmana, Ulrich Schollwöck, and Claudius Hubig. Time-evolution methods for matrix-product states. *Annals of Physics*, 411:167998, 2019.

[58] Tobias J Osborne. Hamiltonian complexity. *Reports on Progress in Physics*, 75(2):022001, jan 2012.

[59] Lev Vidmar, Lucas Hackl, Eugenio Bianchi, and Marcos Rigol. Entanglement entropy of eigenstates of quadratic fermionic hamiltonians. *Physical Review Letters*, 119(2), jul 2017.

[60] Steven R. White and Adrian E. Feiguin. Real-time evolution using the density matrix renormalization group. *Phys. Rev. Lett.*, 93:076401, Aug 2004.

[61] F. Verstraete, D. Porras, and J. I. Cirac. Density Matrix Renormalization Group and Periodic Boundary Conditions: A Quantum Information Perspective. *Physical Review Letters*, 93(22):227205, November 2004.

[62] G. Vidal. Classical simulation of infinite-size quantum lattice systems in one spatial dimension. *Phys. Rev. Lett.*, 98:070201, Feb 2007.

[63] G. Vidal. Entanglement renormalization. *Phys. Rev. Lett.*, 99:220405, Nov 2007.

[64] G. Vidal. Class of quantum many-body states that can be efficiently simulated. *Phys. Rev. Lett.*, 101:110501, Sep 2008.

[65] J. Jordan, R. Orús, G. Vidal, F. Verstraete, and J. I. Cirac. Classical simulation of infinite-size quantum lattice systems in two spatial dimensions. *Phys. Rev. Lett.*, 101:250602, Dec 2008.

[66] Christina V. Kraus, Norbert Schuch, Frank Verstraete, and J. Ignacio Cirac. Fermionic projected entangled pair states. *Phys. Rev. A*, 81:052338, May 2010.

[67] Iztok Pižorn and Frank Verstraete. Fermionic implementation of projected entangled pair states algorithm. *Phys. Rev. B*, 81:245110, Jun 2010.

[68] Thomas Barthel, Ulrich Schollwöck, and Steven R. White. Spectral functions in one-dimensional quantum systems at finite temperature using the density matrix renormalization group. *Phys. Rev. B*, 79:245101, Jun 2009.

[69] Carlos Pineda, Thomas Barthel, and Jens Eisert. Unitary circuits for strongly correlated fermions. *Phys. Rev. A*, 81:050303, May 2010.

[70] Philippe Corboz, Román Orús, Bela Bauer, and Guifré Vidal. Simulation of strongly correlated fermions in two spatial dimensions with fermionic projected entangled-pair states. *Phys. Rev. B*, 81:165104, Apr 2010.

[71] Philippe Corboz, Jacob Jordan, and Guifré Vidal. Simulation of fermionic lattice models in two dimensions with projected entangled-pair states: Next-nearest neighbor hamiltonians. *Phys. Rev. B*, 82:245119, Dec 2010.

[72] J. Ignacio Cirac, David Pérez-García, Norbert Schuch, and Frank Verstraete. Matrix product states and projected entangled pair states: Concepts, symmetries, theorems. *Rev. Mod. Phys.*, 93:045003, Dec 2021.

[73] Román Orús. A practical introduction to tensor networks: Matrix product states and projected entangled pair states. *Annals of Physics*, 349:117 – 158, 2014.

[74] F. Verstraete, V. Murg, and J.I. Cirac. Matrix product states, projected entangled pair states, and variational renormalization group methods for quantum spin systems. *Advances in Physics*, 57(2):143–224, 2008.

[75] D. Perez-Garcia, F. Verstraete, M. M. Wolf, and J. I. Cirac. Matrix product state representations. *Quantum Info. Comput.*, 7(5):401–430, July 2007.

[76] N. de Beaudrap, M. Ohliger, T. J. Osborne, and J. Eisert. Solving frustration-free spin systems. *Phys. Rev. Lett.*, 105:060504, Aug 2010.

[77] M. B. Hastings. An area law for one-dimensional quantum systems. *Journal of Statistical Mechanics: Theory and Experiment*, 2007(08):P08024–P08024, aug 2007.

[78] M. B. Hastings. Entropy and entanglement in quantum ground states. *Phys. Rev. B*, 76:035114, Jul 2007.

[79] M. B. Plenio, J. Eisert, J. Dreißig, and M. Cramer. Entropy, entanglement, and area: Analytical results for harmonic lattice systems. *Phys. Rev. Lett.*, 94:060503, Feb 2005.

[80] M Cramer and J Eisert. Correlations, spectral gap and entanglement in harmonic quantum systems on generic lattices. *New Journal of Physics*, 8(5):71–71, may 2006.

[81] F. Verstraete and J. I. Cirac. Matrix product states represent ground states faithfully. *Phys. Rev. B*, 73:094423, Mar 2006.

[82] Pasquale Calabrese and John Cardy. Entanglement entropy and quantum field theory. *Journal of Statistical Mechanics: Theory and Experiment*, 2004(06):P06002, jun 2004.

[83] Michael M. Wolf. Violation of the entropic area law for fermions. *Phys. Rev. Lett.*, 96:010404, Jan 2006.

[84] B Pirvu, V Murg, J I Cirac, and F Verstraete. Matrix product operator representations. *New Journal of Physics*, 12(2):025012, feb 2010.

[85] Ian P McCulloch. From density-matrix renormalization group to matrix product states. *Journal of Statistical Mechanics: Theory and Experiment*, 2007(10):P10014–P10014, oct 2007.

[86] Gregory M. Crosswhite and Dave Bacon. Finite automata for caching in matrix product algorithms. *Phys. Rev. A*, 78:012356, Jul 2008.

[87] E M Stoudenmire and Steven R White. Minimally entangled typical thermal state algorithms. *New Journal of Physics*, 12(5):055026, May 2010.

[88] Michael Zwolak and Guifré Vidal. Mixed-state dynamics in one-dimensional quantum lattice systems: A time-dependent superoperator renormalization algorithm. *Phys. Rev. Lett.*, 93:207205, Nov 2004.

[89] A J Daley, C Kollath, U Schollwöck, and G Vidal. Time-dependent density-matrix renormalization-group using adaptive effective hilbert spaces. *Journal of Statistical Mechanics: Theory and Experiment*, 2004(04):P04005, apr 2004.

[90] U. Schollwöck. The density-matrix renormalization group. *Rev. Mod. Phys.*, 77:259–315, Apr 2005.

[91] Jacob C Bridgeman and Christopher T Chubb. Hand-waving and interpretive dance: an introductory course on tensor networks. *Journal of Physics A: Mathematical and Theoretical*, 50(22):223001, may 2017.

[92] Mari Carmen Bañuls. Tensor network algorithms: a route map, 2022.

[93] M. B. Hastings. Solving gapped hamiltonians locally. *Phys. Rev. B*, 73:085115, Feb 2006.

[94] Matthew B. Hastings and Tohru Koma. Spectral Gap and Exponential Decay of Correlations. *Communications in Mathematical Physics*, 265(3):781–804, August 2006.

[95] Andras Molnar, Norbert Schuch, Frank Verstraete, and J. Ignacio Cirac. Approximating gibbs states of local hamiltonians efficiently with projected entangled pair states. *Phys. Rev. B*, 91:045138, Jan 2015.

[96] Jiří Guth Jarkovský, András Molnár, Norbert Schuch, and J. Ignacio Cirac. Efficient Description of Many-Body Systems with Matrix Product Density Operators. *PRX Quantum*, 1(1):010304, September 2020.

[97] Tomotaka Kuwahara, Álvaro M. Alhambra, and Anurag Anshu. Improved thermal area law and quasi-linear time algorithm for quantum gibbs states, 2020.

[98] Michael A. Nielsen and Isaac L. Chuang. *Quantum Computation and Quantum Information*. Cambridge University Press, 2000.

[99] Masuo SUZUKI. General decomposition theory of ordered exponentials. *Proceedings of the Japan Academy, Series B*, 69(7):161–166, 1993.

[100] Tomohiro Hashizume, Ian P. McCulloch, and Jad C. Halimeh. Dynamical phase transitions in the two-dimensional transverse-field ising model. *Phys. Rev. Research*, 4:013250, Mar 2022.

[101] Michael P. Zaletel, Roger S. K. Mong, Christoph Karrasch, Joel E. Moore, and Frank Pollmann. Time-evolving a matrix product state with long-ranged interactions. *Phys. Rev. B*, 91:165112, Apr 2015.

[102] M. C. Bañuls, M. B. Hastings, F. Verstraete, and J. I. Cirac. Matrix product states for dynamical simulation of infinite chains. *Phys. Rev. Lett.*, 102:240603, Jun 2009.

[103] Hyungwon Kim and David A. Huse. Ballistic spreading of entanglement in a diffusive nonintegrable system. *Phys. Rev. Lett.*, 111:127205, Sep 2013.

[104] Alexander Weiße, Gerhard Wellein, Andreas Alvermann, and Holger Fehske. The kernel polynomial method. *Rev. Mod. Phys.*, 78:275–306, Mar 2006.

[105] Andreas Alvermann and Holger Fehske. Chebyshev approach to quantum systems coupled to a bath. *Phys. Rev. B*, 77:045125, Jan 2008.

[106] A. Alvermann and H. Fehske. Sparse polynomial space approach to dissipative quantum systems: Application to the sub-ohmic spin-boson model. *Phys. Rev. Lett.*, 102:150601, Apr 2009.

[107] Alexander Weiße. Green-function-based monte carlo method for classical fields coupled to fermions. *Phys. Rev. Lett.*, 102:150604, Apr 2009.

[108] Andreas Holzner, Andreas Weichselbaum, Ian P. McCulloch, Ulrich Schollwöck, and Jan von Delft. Chebyshev matrix product state approach for spectral functions. *Phys. Rev. B*, 83:195115, May 2011.

[109] Jad C. Halimeh, Fabian Kolley, and Ian P. McCulloch. Chebyshev matrix product state approach for time evolution. *Phys. Rev. B*, 92:115130, Sep 2015.

[110] F. Alexander Wolf, Jorge A. Justiniano, Ian P. McCulloch, and Ulrich Schollwöck. Spectral functions and time evolution from the chebyshev recursion. *Phys. Rev. B*, 91:115144, Mar 2015.

[111] Andrew M. Childs, Robin Kothari, and Rolando D. Somma. Quantum algorithm for systems of linear equations with exponentially improved dependence on precision. *SIAM Journal on Computing*, 46(6):1920–1950, Jan 2017.

[112] H. D. Xie, R. Z. Huang, X. J. Han, X. Yan, H. H. Zhao, Z. Y. Xie, H. J. Liao, and T. Xiang. Reorthonormalization of chebyshev matrix product states for dynamical correlation functions. *Phys. Rev. B*, 97:075111, Feb 2018.

[113] Yimin Ge, Jordi Tura Brugués, and J. Cirac. Faster ground state preparation and high-precision ground energy estimation with fewer qubits. *Journal of Mathematical Physics*, 60:022202, 02 2019.

[114] Yilun Yang, Sofyan Iblisdir, J. Ignacio Cirac, and Mari Carmen Bañuls. Probing thermalization through spectral analysis with matrix product operators. *Phys. Rev. Lett.*, 124:100602, Mar 2020.

[115] Mari Carmen Bañuls, David A. Huse, and J. Ignacio Cirac. Entanglement and its relation to energy variance for local one-dimensional hamiltonians. *Phys. Rev. B*, 101:144305, Apr 2020.

[116] Alexander Weiße, Gerhard Wellein, Andreas Alvermann, and Holger Fehske. The kernel polynomial method. *Rev. Mod. Phys.*, 78:275–306, Mar 2006.

[117] Marcos Rigol. Quantum quenches in the thermodynamic limit. ii. initial ground states. *Phys. Rev. E*, 90:031301, Sep 2014.

[118] M. Rigol. Quantum quenches in the thermodynamic limit. *Phys. Rev. Lett.*, 112:170601, Apr 2014.

[119] Krishnanand Mallayya and Marcos Rigol. Numerical linked cluster expansions for quantum quenches in one-dimensional lattices. *Phys. Rev. E*, 95:033302, Mar 2017.

[120] Amy C. Cassidy, Douglas Mason, Vanja Dunjko, and Maxim Olshanii. Threshold for chaos and thermalization in the one-dimensional mean-field bose-hubbard model. *Phys. Rev. Lett.*, 102:025302, Jan 2009.

[121] Lea F. Santos and Marcos Rigol. Onset of quantum chaos in one-dimensional bosonic and fermionic systems and its relation to thermalization. *Phys. Rev. E*, 81:036206, Mar 2010.

[122] Dmitry A. Abanin, Ehud Altman, Immanuel Bloch, and Maksym Serbyn. Colloquium: Many-body localization, thermalization, and entanglement. *Rev. Mod. Phys.*, 91:021001, May 2019.

[123] C. J. Turner, A. A. Michailidis, D. A. Abanin, M. Serbyn, and Z. Papić. Quantum scarred eigenstates in a rydberg atom chain: Entanglement, breakdown of thermalization, and stability to perturbations. *Phys. Rev. B*, 98:155134, Oct 2018.

[124] Z. Papić, E. Miles Stoudenmire, and Dmitry A. Abanin. Many-body localization in disorder-free systems: The importance of finite-size constraints. *Annals of Physics*, 362:714 – 725, 2015.

[125] A. Smith, J. Knolle, D. L. Kovrizhin, and R. Moessner. Disorder-free localization. *Phys. Rev. Lett.*, 118:266601, Jun 2017.

[126] M. Schulz, C. A. Hooley, R. Moessner, and F. Pollmann. Stark many-body localization. *Phys. Rev. Lett.*, 122:040606, Jan 2019.

[127] Yilun Yang, J. Ignacio Cirac, and Mari Carmen Bañuls. Classical algorithms for many-body quantum systems at finite energies. *Phys. Rev. B*, 106:024307, Jul 2022.

[128] Sirui Lu, Mari Carmen Bañuls, and J. Ignacio Cirac. Algorithms for quantum simulation at finite energies. *PRX Quantum*, 2:020321, May 2021.

[129] Jon H. Shirley. Solution of the Schr\"odinger Equation with a Hamiltonian Periodic in Time. *Phys. Rev.*, 138(4B):B979–B987, May 1965.

[130] Hideo Sambe. Steady States and Quasienergies of a Quantum-Mechanical System in an Oscillating Field. *Phys. Rev. A*, 7(6):2203–2213, June 1973.

[131] Shmuel Fishman, D. R. Grempel, and R. E. Prange. Chaos, Quantum Recurrences, and Anderson Localization. *Phys. Rev. Lett.*, 49(8):509–512, August 1982.

[132] M. Matti Maricq. Application of average Hamiltonian theory to the NMR of solids. *Phys. Rev. B*, 25(11):6622–6632, June 1982.

[133] Daniel W. Hone, Roland Ketzmerick, and Walter Kohn. Time-dependent Floquet theory and absence of an adiabatic limit. *Phys. Rev. A*, 56(5):4045–4054, November 1997.

[134] Milena Grifoni and Peter Hänggi. Driven quantum tunneling. *Physics Reports*, 304(5):229–354, October 1998.

[135] André Eckardt, Christoph Weiss, and Martin Holthaus. Superfluid-Insulator Transition in a Periodically Driven Optical Lattice. *Phys. Rev. Lett.*, 95(26):260404, December 2005.

[136] Daniel W. Hone, Roland Ketzmerick, and Walter Kohn. Statistical mechanics of Floquet systems: The pervasive problem of near degeneracies. *Phys. Rev. E*, 79(5):051129, May 2009.

[137] Michal Leskes, P. K. Madhu, and Shimon Vega. Floquet theory in solid-state nuclear magnetic resonance. *Progress in Nuclear Magnetic Resonance Spectroscopy*, 57(4):345–380, November 2010.

[138] Arnab Das. Exotic freezing of response in a quantum many-body system. *Phys. Rev. B*, 82(17):172402, November 2010.

[139] Angelo Russomanno, Alessandro Silva, and Giuseppe E. Santoro. Periodic Steady Regime and Interference in a Periodically Driven Quantum System. *Phys. Rev. Lett.*, 109(25):257201, December 2012.

[140] Achilleas Lazarides, Arnab Das, and Roderich Moessner. Periodic Thermodynamics of Isolated Quantum Systems. *Phys. Rev. Lett.*, 112(15):150401, April 2014.

[141] Asmi Haldar and Arnab Das. Statistical mechanics of floquet quantum matter: exact and emergent conservation laws. *Journal of Physics: Condensed Matter*, 34(23):234001, apr 2022.

[142] Vedika Khemani, Achilleas Lazarides, Roderich Moessner, and S. L. Sondhi. Phase Structure of Driven Quantum Systems. *Phys. Rev. Lett.*, 116(25):250401, June 2016.

[143] Marin Bukov, Luca D'Alessio, and Anatoli Polkovnikov. Universal High-Frequency Behavior of Periodically Driven Systems: From Dynamical Stabilization to Floquet Engineering. *Advances in Physics*, 64(2):139–226, March 2015.

[144] C. W. von Keyserlingk and S. L. Sondhi. Phase structure of one-dimensional interacting Floquet systems. I. Abelian symmetry-protected topological phases. *Phys. Rev. B*, 93(24):245145, June 2016.

[145] C. W. von Keyserlingk and S. L. Sondhi. Phase structure of one-dimensional interacting Floquet systems. II. Symmetry-broken phases. *Phys. Rev. B*, 93(24):245146, June 2016.

[146] R. Moessner and S. L. Sondhi. Equilibration and order in quantum Floquet matter. *Nature Phys*, 13(5):424–428, May 2017.

[147] Jon H. Shirley. Solution of the schrödinger equation with a hamiltonian periodic in time. *Phys. Rev.*, 138:B979–B987, May 1965.

[148] Hideo Sambe. Steady states and quasienergies of a quantum-mechanical system in an oscillating field. *Phys. Rev. A*, 7:2203–2213, Jun 1973.

[149] Marin Bukov, Sarang Gopalakrishnan, Michael Knap, and Eugene Demler. Prethermal Floquet Steady States and Instabilities in the Periodically Driven, Weakly Interacting Bose-Hubbard Model. *Phys. Rev. Lett.*, 115(20):205301, November 2015.

[150] Saar Rahav, Ido Gilary, and Shmuel Fishman. Effective Hamiltonians for periodically driven systems. *Phys. Rev. A*, 68(1):013820, July 2003.

[151] André Eckardt, Christoph Weiss, and Martin Holthaus. Superfluid-insulator transition in a periodically driven optical lattice. *Phys. Rev. Lett.*, 95:260404, Dec 2005.

[152] A. P. Itin and M. I. Katsnelson. Effective Hamiltonians for Rapidly Driven Many-Body Lattice Systems: Induced Exchange Interactions and Density-Dependent Hoppings. *Phys. Rev. Lett.*, 115(7):075301, August 2015.

[153] Wilhelm Magnus. On the exponential solution of differential equations for a linear operator. *Communications on Pure and Applied Mathematics*, 7(4):649–673, 1954.

[154] S. Blanes, F. Casas, J.A. Oteo, and J. Ros. The magnus expansion and some of its applications. *Physics Reports*, 470(5):151–238, 2009.

[155] Tomotaka Kuwahara, Takashi Mori, and Keiji Saito. Floquet–Magnus theory and generic transient dynamics in periodically driven many-body quantum systems. *Annals of Physics*, 367:96–124, April 2016.

[156] Takashi Mori, Tomotaka Kuwahara, and Keiji Saito. Rigorous bound on energy absorption and generic relaxation in periodically driven quantum systems. *Phys. Rev. Lett.*, 116:120401, Mar 2016.

[157] Takashi Mori. Floquet resonant states and validity of the floquet-magnus expansion in the periodically driven friedrichs models. *Phys. Rev. A*, 91:020101, Feb 2015.

[158] Dmitry A. Abanin, Wojciech De Roeck, Wen Wei Ho, and François Huveneers. Effective Hamiltonians, prethermalization, and slow energy absorption in periodically driven many-body systems. *Phys. Rev. B*, 95(1):014112, January 2017.

[159] Dmitry A. Abanin and Zlatko Papić. Recent progress in many-body localization. *Annalen der Physik*, 529(7):1700169, 2017.

[160] H. Lignier, C. Sias, D. Ciampini, Y. Singh, A. Zenesini, O. Morsch, and E. Arimondo. Dynamical Control of Matter-Wave Tunneling in Periodic Potentials. *Phys. Rev. Lett.*, 99(22):220403, November 2007.

[161] C. Sias, H. Lignier, Y. P. Singh, A. Zenesini, D. Ciampini, O. Morsch, and E. Arimondo. Observation of Photon-Assisted Tunneling in Optical Lattices. *Phys. Rev. Lett.*, 100(4):040404, February 2008.

[162] Lih-King Lim, C. Morais Smith, and Andreas Hemmerich. Staggered-Vortex Superfluid of Ultracold Bosons in an Optical Lattice. *Phys. Rev. Lett.*, 100(13):130402, April 2008.

[163] André Eckardt. Colloquium: Atomic quantum gases in periodically driven optical lattices. *Rev. Mod. Phys.*, 89(1):011004, March 2017.

[164] Alessandro Zenesini, Hans Lignier, Donatella Ciampini, Oliver Morsch, and Ennio Arimondo. Coherent Control of Dressed Matter Waves. *Phys. Rev. Lett.*, 102(10):100403, March 2009.

[165] Marin Bukov, Michael Kolodrubetz, and Anatoli Polkovnikov. Schrieffer-Wolff Transformation for Periodically Driven Systems: Strongly Correlated Systems with Artificial Gauge Fields. *Phys. Rev. Lett.*, 116(12):125301, March 2016.

[166] Colin V. Parker, Li-Chung Ha, and Cheng Chin. Direct observation of effective ferromagnetic domains of cold atoms in a shaken optical lattice. *Nature Phys*, 9(12):769–774, December 2013.

[167] Gregor Jotzu, Michael Messer, Rémi Desbuquois, Martin Lebrat, Thomas Uehlinger, Daniel Greif, and Tilman Esslinger. Experimental realization of the topological Haldane model with ultracold fermions. *Nature*, 515(7526):237–240, November 2014.

[168] Li-Chung Ha, Logan W. Clark, Colin V. Parker, Brandon M. Anderson, and Cheng Chin. Roton-Maxon Excitation Spectrum of Bose Condensates in a Shaken Optical Lattice. *Phys. Rev. Lett.*, 114(5):055301, February 2015.

[169] F. Meinert, M. J. Mark, K. Lauber, A. J. Daley, and H.-C. Nägerl. Floquet Engineering of Correlated Tunneling in the Bose-Hubbard Model with Ultracold Atoms. *Phys. Rev. Lett.*, 116(20):205301, May 2016.

[170] D. M. Kennes, A. de la Torre, A. Ron, D. Hsieh, and A. J. Millis. Floquet Engineering in Quantum Chains. *Phys. Rev. Lett.*, 120(12):127601, March 2018.

[171] Benjamin M. Fregoso, Y. H. Wang, N. Gedik, and Victor Galitski. Driven electronic states at the surface of a topological insulator. *Phys. Rev. B*, 88(15):155129, October 2013.

[172] Martin Reitter, Jakob Näger, Karen Wintersperger, Christoph Sträter, Immanuel Bloch, André Eckardt, and Ulrich Schneider. Interaction Dependent Heating and Atom Loss in a Periodically Driven Optical Lattice. *Phys. Rev. Lett.*, 119(20):200402, November 2017.

[173] Christoph Sträter and André Eckardt. Interband heating processes in a periodically driven optical lattice. *Zeitschrift für Naturforschung A*, 71(10):909–920, October 2016.

[174] Dario Poletti and Corinna Kollath. Slow quench dynamics of periodically driven quantum gases. *Phys. Rev. A*, 84(1):013615, July 2011.

[175] Markus Heyl, Philipp Hauke, and Peter Zoller. Quantum localization bounds trotter errors in digital quantum simulation. *Science Advances*, 5(4):eaau8342, 2019.

[176] Lukas M. Sieberer, Tobias Olsacher, Andreas Elben, Markus Heyl, Philipp Hauke, Fritz Haake, and Peter Zoller. Digital quantum simulation, Trotter errors, and quantum chaos of the kicked top. *npj Quantum Inf*, 5(1):1–11, September 2019.

[177] Dominic V. Else, Bela Bauer, and Chetan Nayak. Floquet Time Crystals. *Phys. Rev. Lett.*, 117(9):090402, August 2016.

[178] N. Y. Yao, A. C. Potter, I.-D. Potirniche, and A. Vishwanath. Discrete Time Crystals: Rigidity, Criticality, and Realizations. *Phys. Rev. Lett.*, 118(3):030401, January 2017.

[179] J. Randall, C. E. Bradley, F. V. van der Gronden, A. Galicia, M. H. Abobeih, M. Markham, D. J. Twitchen, F. Machado, N. Y. Yao, and T. H. Taminiau. Many-body-localized discrete time crystal with a programmable spin-based quantum simulator. *Science*, 0(0):eabk0603.

[180] William Berdanier, Michael Kolodrubetz, S. A. Parameswaran, and Romain Vasseur. Floquet quantum criticality. *PNAS*, 115(38):9491–9496, September 2018.

[181] Kaoru Mizuta, Kazuaki Takasan, and Norio Kawakami. High-frequency expansion for Floquet prethermal phases with emergent symmetries: Application to time crystals and Floquet engineering. *Phys. Rev. B*, 100(2):020301, July 2019.

[182] Francisco Machado, Dominic V. Else, Gregory D. Kahanamoku-Meyer, Chetan Nayak, and Norman Y. Yao. Long-Range Prethermal Phases of Nonequilibrium Matter. *Phys. Rev. X*, 10(1):011043, February 2020.

[183] Dominic V. Else, Bela Bauer, and Chetan Nayak. Prethermal Phases of Matter Protected by Time-Translation Symmetry. *Phys. Rev. X*, 7(1):011026, March 2017.

[184] J. Zhang, P. W. Hess, A. Kyprianidis, P. Becker, A. Lee, J. Smith, G. Pagano, I.-D. Potirniche, A. C. Potter, A. Vishwanath, N. Y. Yao, and C. Monroe. Observation of a discrete time crystal. *Nature*, 543(7644):217–220, March 2017.

[185] Soonwon Choi, Joonhee Choi, Renate Landig, Georg Kucsko, Hengyun Zhou, Junichi Isoya, Fedor Jelezko, Shinobu Onoda, Hitoshi Sumiya, Vedika Khemani, Curt von Keyserlingk, Norman Y. Yao, Eugene Demler, and Mikhail D. Lukin. Observation of discrete time-crystalline order in a disordered dipolar many-body system. *Nature*, 543(7644):221–225, March 2017.

[186] Netanel H. Lindner, Gil Refael, and Victor Galitski. Floquet topological insulator in semiconductor quantum wells. *Nature Phys*, 7(6):490–495, June 2011.

[187] Mark S. Rudner and Netanel H. Lindner. Band structure engineering and non-equilibrium dynamics in Floquet topological insulators. *Nat Rev Phys*, 2(5):229–244, May 2020.

[188] Adolfo G. Grushin, Álvaro Gómez-León, and Titus Neupert. Floquet Fractional Chern Insulators. *Phys. Rev. Lett.*, 112(15):156801, April 2014.

[189] Dominic V. Else and Chetan Nayak. Classification of topological phases in periodically driven interacting systems. *Phys. Rev. B*, 93(20):201103, May 2016.

[190] Andrew C. Potter, Takahiro Morimoto, and Ashvin Vishwanath. Classification of Interacting Topological Floquet Phases in One Dimension. *Phys. Rev. X*, 6(4):041001, October 2016.

[191] I.-D. Potirniche, A. C. Potter, M. Schleier-Smith, A. Vishwanath, and N. Y. Yao. Floquet Symmetry-Protected Topological Phases in Cold-Atom Systems. *Phys. Rev. Lett.*, 119(12):123601, September 2017.

[192] Martin Claassen, Hong-Chen Jiang, Brian Moritz, and Thomas P. Devereaux. Dynamical time-reversal symmetry breaking and photo-induced chiral spin liquids in frustrated Mott insulators. *Nat Commun*, 8(1):1192, December 2017.

[193] Takashi Oka and Hideo Aoki. Photovoltaic Hall effect in graphene. *Phys. Rev. B*, 79(8):081406, February 2009.

[194] Takuya Kitagawa, Takashi Oka, Arne Brataas, Liang Fu, and Eugene Demler. Transport properties of nonequilibrium systems under the application of light: Photoinduced quantum Hall insulators without Landau levels. *Phys. Rev. B*, 84(23):235108, December 2011.

[195] Thomas Iadecola, David Campbell, Claudio Chamon, Chang-Yu Hou, Roman Jackiw, So-Young Pi, and Silvia Viola Kusminskiy. Materials Design from Nonequilibrium Steady States: Driven Graphene as a Tunable Semiconductor with Topological Properties. *Phys. Rev. Lett.*, 110(17):176603, April 2013.

[196] Jianpeng Liu, Kasra Hejazi, and Leon Balents. Floquet Engineering of Multiorbital Mott Insulators: Applications to Orthorhombic Titanates. *Phys. Rev. Lett.*, 121(10):107201, September 2018.

[197] J. H. Mentink, K. Balzer, and M. Eckstein. Ultrafast and reversible control of the exchange interaction in Mott insulators. *Nat Commun*, 6(1):6708, March 2015.

[198] R. V. Mikhaylovskiy, E. Hendry, A. Secchi, J. H. Mentink, M. Eckstein, A. Wu, R. V. Pisarev, V. V. Kruglyak, M. I. Katsnelson, Th Rasing, and A. V. Kimel. Ultrafast optical modification of exchange interactions in iron oxides. *Nat Commun*, 6(1):8190, September 2015.

[199] Juan Jose Mendoza-Arenas, Fernando Javier Gómez-Ruiz, Martin Eckstein, Dieter Jaksch, and Stephen R. Clark. Ultra-Fast Control of Magnetic Relaxation in a Periodically Driven Hubbard Model. *Annalen der Physik*, 529(10):1700024, 2017.

[200] N. Goldman and J. Dalibard. Periodically Driven Quantum Systems: Effective Hamiltonians and Engineered Gauge Fields. *Phys. Rev. X*, 4(3):031027, August 2014.

[201] J. Struck, C. Ölschläger, M. Weinberg, P. Hauke, J. Simonet, A. Eckardt, M. Lewenstein, K. Sengstock, and P. Windpassinger. Tunable Gauge Potential for Neutral and Spinless Particles in Driven Optical Lattices. *Phys. Rev. Lett.*, 108(22):225304, May 2012.

[202] W. Hu, S. Kaiser, D. Nicoletti, C. R. Hunt, I. Gierz, M. C. Hoffmann, M. Le Tacon, T. Loew, B. Keimer, and A. Cavalleri. Optically enhanced coherent transport in YBa2Cu3O6.5 by ultrafast redistribution of interlayer coupling. *Nature Mater*, 13(7):705–711, July 2014.

[203] D. Fausti, R. I. Tobey, N. Dean, S. Kaiser, A. Dienst, M. C. Hoffmann, S. Pyon, T. Takayama, H. Takagi, and A. Cavalleri. Light-Induced Superconductivity in a Stripe-Ordered Cuprate. *Science*, 331(6014):189–191, January 2011.

[204] M. Mitrano, A. Cantaluppi, D. Nicoletti, S. Kaiser, A. Perucchi, S. Lupi, P. Di Pietro, D. Pontiroli, M. Riccò, S. R. Clark, D. Jaksch, and A. Cavalleri. Possible light-induced superconductivity in K3C60 at high temperature. *Nature*, 530(7591):461–464, February 2016.

[205] Peter Reimann. Foundation of Statistical Mechanics under Experimentally Realistic Conditions. *Phys. Rev. Lett.*, 101(19):190403, November 2008.

[206] Peter Reimann and Michael Kastner. Equilibration of isolated macroscopic quantum systems. *New J. Phys.*, 14(4):043020, April 2012.

[207] Pedro Ponte, Z. Papić, François Huveneers, and Dmitry A. Abanin. Many-Body Localization in Periodically Driven Systems. *Phys. Rev. Lett.*, 114(14):140401, April 2015.

[208] Shankar Iyer, Vadim Oganesyan, Gil Refael, and David A. Huse. Many-body localization in a quasiperiodic system. *Phys. Rev. B*, 87(13):134202, April 2013.

[209] Pedro Ponte, Anushya Chandran, Z. Papić, and Dmitry A. Abanin. Periodically driven ergodic and many-body localized quantum systems. *Annals of Physics*, 353:196–204, February 2015.

[210] Analabha Roy and Arnab Das. Fate of dynamical many-body localization in the presence of disorder. *Phys. Rev. B*, 91(12):121106, March 2015.

[211] Dmitry A. Abanin, Wojciech De Roeck, and François Huveneers. Theory of many-body localization in periodically driven systems. *Annals of Physics*, 372:1–11, September 2016.

[212] Achilleas Lazarides, Arnab Das, and Roderich Moessner. Fate of Many-Body Localization Under Periodic Driving. *Phys. Rev. Lett.*, 115(3):030402, July 2015.

[213] Liangsheng Zhang, Vedika Khemani, and David A. Huse. A Floquet model for the many-body localization transition. *Phys. Rev. B*, 94(22):224202, December 2016.

[214] Hoi Chun Po, Lukasz Fidkowski, Takahiro Morimoto, Andrew C. Potter, and Ashvin Vishwanath. Chiral Floquet Phases of Many-Body Localized Bosons. *Phys. Rev. X*, 6(4):041070, December 2016.

[215] Pranjal Bordia, Henrik Lüschen, Ulrich Schneider, Michael Knap, and Immanuel Bloch. Periodically driving a many-body localized quantum system. *Nature Phys*, 13(5):460–464, May 2017.

[216] Tomaz Prosen. Quantum invariants of motion in a generic many-body system. *J. Phys. A: Math. Gen.*, 31(37):L645–L653, September 1998.

[217] Tomaž Prosen. Time Evolution of a Quantum Many-Body System: Transition from Integrability to Ergodicity in the Thermodynamic Limit. *Phys. Rev. Lett.*, 80(9):1808–1811, March 1998.

[218] Tomaž Prosen. Ergodic properties of a generic nonintegrable quantum many-body system in the thermodynamic limit. *Phys. Rev. E*, 60(4):3949–3968, October 1999.

[219] Luca D'Alessio and Anatoli Polkovnikov. Many-body energy localization transition in periodically driven systems. *Annals of Physics*, 333:19–33, June 2013.

[220] Tomaž Prosen. General relation between quantum ergodicity and fidelity of quantum dynamics. *Phys. Rev. E*, 65(3):036208, February 2002.

[221] Roberta Citro, Emanuele G. Dalla Torre, Luca DÁlessio, Anatoli Polkovnikov, Mehrtash Babadi, Takashi Oka, and Eugene Demler. Dynamical Stability of a Many-body Kapitza Pendulum. *Annals of Physics*, 360:694–710, September 2015.

[222] Anushya Chandran and S. L. Sondhi. Interaction-stabilized steady states in the driven O (N) model. *Phys. Rev. B*, 93(17):174305, May 2016.

[223] Asmi Haldar, Diptiman Sen, Roderich Moessner, and Arnab Das. Dynamical Freezing and Scar Points in Strongly Driven Floquet Matter: Resonance vs Emergent Conservation Laws. *Phys. Rev. X*, 11(2):021008, April 2021.

[224] Asmi Haldar, Roderich Moessner, and Arnab Das. Onset of Floquet thermalization. *Phys. Rev. B*, 97(24):245122, June 2018.

[225] Luca D'Alessio and Marcos Rigol. Long-time Behavior of Isolated Periodically Driven Interacting Lattice Systems. *Phys. Rev. X*, 4(4):041048, December 2014.

[226] Achilleas Lazarides, Arnab Das, and Roderich Moessner. Equilibrium states of generic quantum systems subject to periodic driving. *Phys. Rev. E*, 90(1):012110, July 2014.

[227] Hyungwon Kim, Tatsuhiko N. Ikeda, and David A. Huse. Testing whether all eigenstates obey the eigenstate thermalization hypothesis. *Phys. Rev. E*, 90(5):052105, November 2014.

[228] Marin Bukov, Markus Heyl, David A. Huse, and Anatoli Polkovnikov. Heating and many-body resonances in a periodically driven two-band system. *Phys. Rev. B*, 93(15):155132, April 2016.

[229] Maximilian Genske and Achim Rosch. Floquet-Boltzmann equation for periodically driven Fermi systems. *Phys. Rev. A*, 92(6):062108, December 2015.

[230] Angelo Russomanno, Rosario Fazio, and Giuseppe E. Santoro. Thermalization in a periodically driven fully connected quantum Ising ferromagnet. *EPL*, 110(3):37005, May 2015.

[231] Takashi Mori, Tomotaka Kuwahara, and Keiji Saito. Rigorous Bound on Energy Absorption and Generic Relaxation in Periodically Driven Quantum Systems. *Phys. Rev. Lett.*, 116(12):120401, March 2016.

[232] Dmitry Abanin, Wojciech De Roeck, Wen Wei Ho, and François Huveneers. A Rigorous Theory of Many-Body Prethermalization for Periodically Driven and Closed Quantum Systems. *Commun. Math. Phys.*, 354(3):809–827, September 2017.

[233] Simon A. Weidinger and Michael Knap. Floquet prethermalization and regimes of heating in a periodically driven, interacting quantum system. *Sci Rep*, 7(1):45382, April 2017.

[234] Netanel H. Lindner, Erez Berg, and Mark S. Rudner. Universal Chiral Quasisteady States in Periodically Driven Many-Body Systems. *Phys. Rev. X*, 7(1):011018, February 2017.

[235] Elena Canovi, Marcus Kollar, and Martin Eckstein. Stroboscopic prethermalization in weakly interacting periodically driven systems. *Phys. Rev. E*, 93(1):012130, January 2016.

[236] Dmitry A. Abanin, Wojciech De Roeck, and François Huveneers. Exponentially Slow Heating in Periodically Driven Many-Body Systems. *Phys. Rev. Lett.*, 115(25):256803, December 2015.

[237] Andreas Herrmann, Yuta Murakami, Martin Eckstein, and Philipp Werner. Floquet prethermalization in the resonantly driven Hubbard model. *EPL*, 120(5):57001, December 2017.

[238] Francesco Peronaci, Marco Schiró, and Olivier Parcollet. Resonant Thermalization of Periodically Driven Strongly Correlated Electrons. *Phys. Rev. Lett.*, 120(19):197601, May 2018.

[239] Alan Morningstar, Markus Hauru, Jackson Beall, Martin Ganahl, Adam G.M. Lewis, Vedika Khemani, and Guifre Vidal. Simulation of Quantum Many-Body Dynamics with Tensor Processing Units: Floquet Prethermalization. *PRX Quantum*, 3(2):020331, May 2022.

[240] Ken Xuan Wei, Pai Peng, Oles Shtanko, Iman Marvian, Seth Lloyd, Chandrasekhar Ramanathan, and Paola Cappellaro. Emergent Prethermalization Signatures in Out-of-Time Ordered Correlations. *Phys. Rev. Lett.*, 123(9):090605, August 2019.

[241] Wen Wei Ho and Wojciech De Roeck. A Rigorous Theory of Prethermalization without Temperature. *arXiv:2011.14583 [cond-mat, physics:math-ph, physics:quant-ph]*, December 2020.

[242] David J. Luitz, Roderich Moessner, S. L. Sondhi, and Vedika Khemani. Prethermalization without Temperature. *Physical Review X*, 10(2):021046, May 2020.

[243] M. Gring, M. Kuhnert, T. Langen, T. Kitagawa, B. Rauer, M. Schreitl, I. Mazets, D. Adu Smith, E. Demler, and J. Schmiedmayer. Relaxation and prethermalization in an isolated quantum system. *Science*, 337(6100):1318–1322, 2012.

[244] Marcus Kollar, F. Alexander Wolf, and Martin Eckstein. Generalized gibbs ensemble prediction of prethermalization plateaus and their relation to nonthermal steady states in integrable systems. *Phys. Rev. B*, 84:054304, Aug 2011.

[245] Michael Vogl, Pontus Laurell, Aaron D. Barr, and Gregory A. Fiete. Flow Equation Approach to Periodically Driven Quantum Systems. *Phys. Rev. X*, 9(2):021037, May 2019.

[246] André Eckardt and Egidijus Anisimovas. High-frequency approximation for periodically driven quantum systems from a Floquet-space perspective. *New J. Phys.*, 17(9):093039, September 2015.

[247] N. Goldman, J. Dalibard, M. Aidelsburger, and N. R. Cooper. Periodically driven quantum matter: The case of resonant modulations. *Phys. Rev. A*, 91(3):033632, March 2015.

[248] Man-Duen Choi. Completely positive linear maps on complex matrices. *Linear Algebra and its Applications*, 10(3):285 – 290, 1975.

[249] Sirui Lu, Mari Carmen Bañuls, and J. Ignacio Cirac. Algorithms for quantum simulation at finite energies, 2020.

[250] Jad C. Halimeh, Fabian Kolley, and Ian P. McCulloch. Chebyshev matrix product state approach for time evolution. *Phys. Rev. B*, 92:115130, Sep 2015.

[251] H. D. Xie, R. Z. Huang, X. J. Han, X. Yan, H. H. Zhao, Z. Y. Xie, H. J. Liao, and T. Xiang. Reorthonormalization of chebyshev matrix product states for dynamical correlation functions. *Phys. Rev. B*, 97:075111, Feb 2018.

[252] B. Pirvu, F. Verstraete, and G. Vidal. Exploiting translational invariance in matrix product state simulations of spin chains with periodic boundary conditions. *Phys. Rev. B*, 83:125104, Mar 2011.

[253] Toma ž Prosen and Iztok Pižorn. Operator space entanglement entropy in a transverse ising chain. *Phys. Rev. A*, 76:032316, Sep 2007.

[254] Michael Hartmann, Günter mahler, and Ortwin Hess. Gaussian quantum fluctuations in interacting many particle systems. *Letters in Mathematical Physics*, 68(2):103–112, May 2004.

[255] J. P. Keating, N. Linden, and H. J. Wells. Spectra and eigenstates of spin chain hamiltonians. *Communications in Mathematical Physics*, 338(1):81–102, May 2015.

[256] Pietro Silvi, Ferdinand Tschirsich, Matthias Gerster, Johannes Jünemann, Daniel Jaschke, Matteo Rizzi, and Simone Montangero. The Tensor Networks Anthology: Simulation techniques for many-body quantum lattice systems. *SciPost Phys. Lect. Notes*, page 8, 2019.

[257] Anatoly Dymarsky and Hong Liu. New characteristic of quantum many-body chaotic systems. *Phys. Rev. E*, 99:010102, Jan 2019.

[258] Adrian E. Feiguin and Steven R. White. Time-step targeting methods for real-time dynamics using the density matrix renormalization group. *Phys. Rev. B*, 72:020404, Jul 2005.

[259] Cheng-Ju Lin and Olexei I. Motrunich. Exact quantum many-body scar states in the rydberg-blockaded atom chain. *Phys. Rev. Lett.*, 122:173401, Apr 2019.

[260] Karel Van Acoleyen, Michaël Mariën, and Frank Verstraete. Entanglement rates and area laws. *Phys. Rev. Lett.*, 111:170501, Oct 2013.

[261] B. Wouters, J. De Nardis, M. Brockmann, D. Fioretto, M. Rigol, and J.-S. Caux. Quenching the anisotropic heisenberg chain: Exact solution and generalized gibbs ensemble predictions. *Phys. Rev. Lett.*, 113:117202, Sep 2014.

[262] Aslı Çakan, J. Ignacio Cirac, and Mari Carmen Bañuls. Approximating the long time average of the density operator: Diagonal ensemble. *Physical Review B*, 103(11), Mar 2021.

[263] Lorenzo Piroli, Eric Vernier, Pasquale Calabrese, and Marcos Rigol. Correlations and diagonal entropy after quantum quenches in xxz chains. *Phys. Rev. B*, 95:054308, Feb 2017.

[264] Hannes Bernien, Sylvain Schwartz, Alexander Keesling, Harry Levine, Ahmed Omran, Hannes Pichler, Soonwon Choi, Alexander S Zibrov, Manuel Endres, Markus Greiner, Vladan Vuletić, and Mikhail D Lukin. Probing many-body dynamics on a 51-atom quantum simulator. *Nature*, 551(7682):579–584, November 2017.

[265] B. Olmos, R. González-Férez, and I. Lesanovsky. Collective rydberg excitations of an atomic gas confined in a ring lattice. *Phys. Rev. A*, 79:043419, Apr 2009.

[266] B Sun and F Robicheaux. Numerical study of two-body correlation in a 1d lattice with perfect blockade. *New Journal of Physics*, 10(4):045032, apr 2008.

[267] C. J. Turner, A. A. Michailidis, D. A. Abanin, M. Serbyn, and Z. Papić. Weak ergodicity breaking from quantum many-body scars. *Nature Physics*, 14(7):745–749, Jul 2018.

[268] J. Berges, Sz. Borsányi, and C. Wetterich. Prethermalization. *Phys. Rev. Lett.*, 93:142002, Sep 2004.

[269] Toshiya Kinoshita, Trevor Wenger, and David S. Weiss. A quantum newton's cradle. *Nature*, 440(7086):900–903, Apr 2006.

[270] Tim Langen, Michael Gring, Maximilian Kuhnert, Bernhard Rauer, Remi Geiger, David Adu Smith, Igor E. Mazets, and Jörg Schmiedmayer. Prethermalization in one-dimensional bose gases: Description by a stochastic ornstein-uhlenbeck process. *The European Physical Journal Special Topics*, 217(1):43–53, Feb 2013.

[271] R Geiger, T Langen, I E Mazets, and J Schmiedmayer. Local relaxation and light-cone-like propagation of correlations in a trapped one-dimensional bose gas. *New Journal of Physics*, 16(5):053034, may 2014.

[272] Tim Langen, Sebastian Erne, Remi Geiger, Bernhard Rauer, Thomas Schweigler, Maximilian Kuhnert, Wolfgang Rohringer, Igor E. Mazets, Thomas Gasenzer, and Jörg Schmiedmayer. Experimental observation of a generalized gibbs ensemble. *Science*, 348(6231):207–211, 2015.

[273] Tim Langen, Thomas Gasenzer, and Jörg Schmiedmayer. Prethermalization and universal dynamics in near-integrable quantum systems. *Journal of Statistical Mechanics: Theory and Experiment*, 2016(6):064009, jun 2016.

[274] Yijun Tang, Wil Kao, Kuan-Yu Li, Sangwon Seo, Krishnanand Mallayya, Marcos Rigol, Sarang Gopalakrishnan, and Benjamin L. Lev. Thermalization near integrability in a dipolar quantum newton's cradle. *Phys. Rev. X*, 8:021030, May 2018.

[275] Achim Rosch, David Rasch, Benedikt Binz, and Matthias Vojta. Metastable superfluidity of repulsive fermionic atoms in optical lattices. *Phys. Rev. Lett.*, 101:265301, Dec 2008.

[276] F. H. L. Essler, S. Kehrein, S. R. Manmana, and N. J. Robinson. Quench dynamics in a model with tuneable integrability breaking. *Phys. Rev. B*, 89:165104, Apr 2014.

[277] G. P. Brandino, J.-S. Caux, and R. M. Konik. Glimmers of a quantum kam theorem: Insights from quantum quenches in one-dimensional bose gases. *Phys. Rev. X*, 5:041043, Dec 2015.

[278] G. P. Brandino, J.-S. Caux, and R. M. Konik. Glimmers of a quantum kam theorem: Insights from quantum quenches in one-dimensional bose gases. *Phys. Rev. X*, 5:041043, Dec 2015.

[279] Michael Buchhold, Markus Heyl, and Sebastian Diehl. Prethermalization and thermalization of a quenched interacting luttinger liquid. *Phys. Rev. A*, 94:013601, Jul 2016.

[280] Michael Stark and Marcus Kollar. Kinetic description of thermalization dynamics in weakly interacting quantum systems, 2013.

[281] Bruno Bertini, Fabian H. L. Essler, Stefan Groha, and Neil J. Robinson. Prethermalization and thermalization in models with weak integrability breaking. *Phys. Rev. Lett.*, 115:180601, Oct 2015.

[282] Pasquale Calabrese, Fabian H. L. Essler, and Maurizio Fagotti. Quantum quench in the transverse-field ising chain. *Phys. Rev. Lett.*, 106:227203, Jun 2011.

[283] Stefan Birnkammer, Alvise Bastianello, and Michael Knap. Prethermalization in confined spin chains, 2022.

[284] Krishnanand Mallayya and Marcos Rigol. Quantum quenches and relaxation dynamics in the thermodynamic limit. *Phys. Rev. Lett.*, 120:070603, Feb 2018.

[285] Oleksandr Kyriienko. Quantum inverse iteration algorithm for programmable quantum simulators. *npj Quantum Inf*, 6(1):1–8, January 2020.

[286] Pei Zeng, Jinzhao Sun, and Xiao Yuan. Universal quantum algorithmic cooling on a quantum computer, 2021.

[287] Min-Quan He, Dan-Bo Zhang, and Z. D. Wang. Quantum gaussian filter for exploring ground-state properties, 2021.

[288] Mari Carmen Bañuls, David A. Huse, and J. Ignacio Cirac. Entanglement and its relation to energy variance for local one-dimensional Hamiltonians. *Phys. Rev. B*, 101(14):144305, April 2020.

[289] Sirui Lu, Mari Carmen Bañuls, and J. Ignacio Cirac. Algorithms for quantum simulation at finite energies. *PRX Quantum*, 2(2):020321, May 2021.

[290] Yilun Yang, J. Ignacio Cirac, and Mari Carmen Bañuls. Classical algorithms for many-body quantum systems at finite energies, April 2022.

[291] Tomaž Prosen. Exact Time-Correlation Functions of Quantum Ising Chain in a Kicking Transversal Magnetic Field: Spectral Analysis of the Adjoint Propagator in Heisenberg Picture. *Progress of Theoretical Physics Supplement*, 139:191–203, 05 2000.

[292] Marlis Hochbruck and Christian Lubich. On Krylov Subspace Approximations to the Matrix Exponential Operator. *SIAM J. Numer. Anal.*, 34(5):1911–1925, October 1997.

[293] J. W. Daniel, W. B. Gragg, L. Kaufman, and G. W. Stewart. Reorthogonalization and Stable Algorithms for Updating the Gram-Schmidt QR Factorization. *Mathematics of Computation*, 30(136):772, October 1976.

[294] Y. Saad. Analysis of Some Krylov Subspace Approximations to the Matrix Exponential Operator. *SIAM J. Numer. Anal.*, 29(1):209–228, February 1992.

[295] Karthik Seetharam, Paraj Titum, Michael Kolodrubetz, and Gil Refael. Absence of thermalization in finite isolated interacting Floquet systems. *Phys. Rev. B*, 97(1):014311, January 2018.

[296] Alfréd Rényi. On measures of entropy and information. In *Proceedings of the Fourth Berkeley Symposium on Mathematical Statistics and Probability, Volume 1: Contributions to the Theory of Statistics*. The Regents of the University of California, 1961.

[297] Markus Hauru, Maarten Van Damme, and Jutho Haegeman. Riemannian optimization of isometric tensor networks. July 2020.

[298] AG Bashkirov. Maximum Rényi entropy principle for systems with power-law Hamiltonians. *Physical Review Letters*, 93(13):130601, 2004.

[299] Dorje C Brody, Ian RC Buckley, and Irene C Constantinou. Option price Calibration from Rényi entropy. *Physics Letters A*, 366(4-5):298–307, 2007.

[300] Christoph Bunte and Amos Lapidoth. Maximizing Rényi entropy rate. In *2014 IEEE 28th Convention of Electrical & Electronics Engineers in Israel (IEEEI)*, pages 1–4. IEEE, 2014.

[301] Y Y Atas and E Bogomolny. Spectral density of a one-dimensional quantum Ising model: Gaussian and multi-Gaussian approximations. *Journal of Physics A: Mathematical and Theoretical*, 47(33):335201, August 2014.

[302] Giacomo Giudice, Aslı Çakan, J. Ignacio Cirac, and Mari Carmen Bañuls. Rényi free energy and variational approximations to thermal states. *Phys. Rev. B*, 103:205128, May 2021.

[303] Lev Davidovič Landau and Evgenij Mikhailovich Lifshitz. *Statistical Physics, Part 1.* Number Vol. 5 in Course of Theoretical Physics. Butterworth Heinemann, Oxford, 3. ed edition, 1991.

[304] Hugo Touchette. *Equivalence and Nonequivalence of the Microcanonical and Canonical Ensembles: A Large Deviations Study.* PhD Thesis, 2003.

[305] Richard S. Ellis, Hugo Touchette, and Bruce Turkington. Thermodynamic versus statistical nonequivalence of ensembles for the mean-field Blume–Emery–Griffiths model. *Physica A: Statistical Mechanics and its Applications*, 335(3-4):518–538, April 2004.

[306] Yichen Huang. Computing energy density in one dimension. May 2015.

[307] B Pirvu, V Murg, J I Cirac, and F Verstraete. Matrix product operator representations. *New Journal of Physics*, 12(2):025012, 2010.

[308] Gemma De Las Cuevas, Norbert Schuch, David Pérez-García, and J Ignacio Cirac. Purifications of multipartite states: Limitations and constructive methods. *New Journal of Physics*, 15(12):123021, December 2013.

[309] M. Kliesch, C. Gogolin, M. J. Kastoryano, A. Riera, and J. Eisert. Locality of Temperature. *Physical Review X*, 4(3):031019, July 2014.

[310] G. De las Cuevas, T. S. Cubitt, J. I. Cirac, M. M. Wolf, and D. Pérez-García. Fundamental limitations in the purifications of tensor networks. *Journal of Mathematical Physics*, 57(7):071902, 2016.

[311] Jian Cui, J. Ignacio Cirac, and Mari Carmen Bañuls. Variational Matrix Product Operators for the Steady State of Dissipative Quantum Systems. *Physical Review Letters*, 114(22):220601, June 2015.

[312] Eduardo Mascarenhas, Hugo Flayac, and Vincenzo Savona. Matrix-product-operator approach to the nonequilibrium steady state of driven-dissipative quantum arrays. *Physical Review A*, 92(2):022116, August 2015.

[313] A. H. Werner, D. Jaschke, P. Silvi, M. Kliesch, T. Calarco, J. Eisert, and S. Montangero. Positive Tensor Network Approach for Simulating Open Quantum Many-Body Systems. *Physical Review Letters*, 116(23):237201, June 2016.

[314] Dong C. Liu and Jorge Nocedal. On the limited memory BFGS method for large scale optimization. *Mathematical Programming*, 45(1-3):503–528, August 1989.

[315] Jorge Nocedal and Stephen J. Wright, editors. *Numerical Optimization*. Springer Series in Operations Research and Financial Engineering. Springer-Verlag, New York, 1999.

[316] Shigetoshi Katsura. Statistical Mechanics of the Anisotropic Linear Heisenberg Model. *Physical Review*, 127(5):1508–1518, September 1962.

[317] Th. Niemeijer. Some exact calculations on a chain of spins. *Physica*, 36(3):377–419, January 1967.

[318] L. Tagliacozzo, Thiago. R. de Oliveira, S. Iblisdir, and J. I. Latorre. Scaling of entanglement support for matrix product states. *Physical Review B*, 78(2):024410, July 2008.

[319] Frank Pollmann, Subroto Mukerjee, Ari M. Turner, and Joel E. Moore. Theory of Finite-Entanglement Scaling at One-Dimensional Quantum Critical Points. *Physical Review Letters*, 102(25):255701, June 2009.

[320] B. Pirvu, G. Vidal, F. Verstraete, and L. Tagliacozzo. Matrix product states for critical spin chains: Finite-size versus finite-entanglement scaling. *Physical Review B*, 86(7):075117, August 2012.

[321] Andreas M. Läuchli. Operator content of real-space entanglement spectra at conformal critical points. March 2013.

[322] Tao Shi, Eugene Demler, and J. Ignacio Cirac. Variational Approach for Many-Body Systems at Finite Temperature. *Physical Review Letters*, 125(18):180602, October 2020.

[323] Jutho Haegeman, Christian Lubich, Ivan Oseledets, Bart Vandereycken, and Frank Verstraete. Unifying time evolution and optimization with matrix product states. *Physical Review B*, 94(16):165116, October 2016.

[324] Laurens Vanderstraeten, Jutho Haegeman, and Frank Verstraete. Tangent-space methods for uniform matrix product states. *SciPost Physics Lecture Notes*, page 7, January 2019.

[325] Nobuyuki Yoshioka and Ryusuke Hamazaki. Constructing neural stationary states for open quantum many-body systems. *Physical Review B*, 99(21):214306, June 2019.

[326] Michael J. Hartmann and Giuseppe Carleo. Neural-Network Approach to Dissipative Quantum Many-Body Dynamics. *Physical Review Letters*, 122(25):250502, June 2019.

[327] Alexandra Nagy and Vincenzo Savona. Variational Quantum Monte Carlo Method with a Neural-Network Ansatz for Open Quantum Systems. *Physical Review Letters*, 122(25):250501, June 2019.

[328] Filippo Vicentini, Alberto Biella, Nicolas Regnault, and Cristiano Ciuti. Variational Neural-Network Ansatz for Steady States in Open Quantum Systems. *Physical Review Letters*, 122(25):250503, June 2019.